AN ABSTRACT OF THE THESIS OF

Peter Ruggiero for the degree of Doctor of Philosophy in Civil Engineering presented on April 11, 1997.

Title: Wave Runup on High Energy Dissipative Beaches and the Prediction of Coastal Erosion

Redacted for Privacy

Abstract approved: _____
William G. McDougal

Wave runup has been investigated on the high energy dissipative beaches typical of the Pacific Northwest of the United States. This has been accomplished through field investigations on the central Oregon coast utilizing video image processing techniques. Extreme runup statistics have been found to linearly depend on the deep-water significant wave height. This relationship and other potential runup models have been used to develop a methodology which evaluates the susceptibility of coastal properties to erosion. Extreme water elevations, including water elevations measured by tide gauges as well as elevations achieved by wave runup, are compared with measured elevations of the beach face junction on a variety of beaches. The model, valid for conditions when the beach face junction is landward of the mean water line, predicts susceptibilities to erosion that agree well with observations.

A more detailed investigation into the frequency response and frequency-wave number structure of swash motions is also presented. Overlap in the coverage of 3 video cameras allowed for runup elevations to be analyzed at any longshore position over a 1600 m reach of beach. Runup spectra show a large saturated region with an f^{-4} dependence extending to lower frequencies than previously reported.

Runup motions are coherent over very large alongshore distances, O(1 km), at the extremely low frequencies, O(0.005 Hz), that dominate the swash zone. Due to the low frequency nature of the swash, the array length was too short to resolve between leaky modes and higher edge wave modes.

Finally, an analytic model is presented which predicts longshore currents and sediment transport on beaches backed by vertical structures with toes seaward of the mean water line. A partial standing wave develops in front of the structures causing modulations of the bottom stress, radiation stresses and the resulting setup, longshore current and longshore sediment transport. Model results suggest that the magnitudes of these processes can be either greater or less than on a similar beach without a structure, depending on the position of the structure across the surf zone, the beach slope and the wave conditions.

Wave Runup on High Energy Dissipative Beaches and the Prediction of Coastal Erosion

by

Peter Ruggiero

A THESIS

submitted to

Oregon State University

in partial fulfillment of
the requirements for the
degree of

Doctor of Philosophy

Completed April 11, 1997
Commencment June 1997

Doctor of Philosopy thesis of Peter Ruggiero presented on April, 11 1997

APPROVED:

Redacted for Privacy

Major Professor representing Civil Engineering

Redacted for Privacy

Chair of the Department of Civil, Construction, and Environmental Engineering

Redacted for Privacy

Dean of the Graduate School

I understand that my thesis will become part of the permanent collection of Oregon State University libraries. My signature below authorizes release of my thesis to any reader upon request.

Redacted for Privacy

Peter Ruggiero, Author

ACKNOWLEDGMENTS

I would first like to thank my major advisor, Bill McDougal, for guiding me through the research presented in this dissertation. His insight, energy (and then some) and friendship have continuously been inspirational. Secondly, thanks go to Paul Komar who has served as my co-advisor and an alter-ego to McDougal. Much of the knowledge I have of the beautiful Oregon coast, and its many fine restaurants, comes from Paul. I would also like to thank the rest of my committee, Dr. Charles Sollitt who served as my major advisor during my masters degree and saw me through the lean times, Dr. Ron Guenther who graciously agreed to a last minute committee switch and Dr. Charles Rosenfeld. Not satisfied with only two primary advisors, I owe many thanks to Rob Holman and Reg Beach who have also served as scientific mentors. Through Rob and Reg I have had the opportunity to participate in several stimulating field experiments and have been welcomed into a second academic home.

The most important part of my time at Oregon State University has been knowing such an incredible group of people. In particular, the students and staff of the Ocean Engineering group and more recently the students and staff of the Coastal Imaging Lab, have always been unparalleled as both colleagues and friends. I would like to thank each of those who touched my life, making OSU, and Corvallis as a whole, such a wonderful community to be a part of. Finally, I would like to thank my family, without who's foundation I have always been able to stand on, none of this would have been possible.

This dissertation has been funded by the NOAA Office of Sea Grant, Department of Commerce, the Oregon State Department of Land Conservation and Development and the Office of Naval Research, Coastal Sciences Program Grant # N000-14-94-11196.

TABLE OF CONTENTS

LIST OF FIGURES

List of Figures, Continued

List of Figures, Continued

List of Figures, Continued

LIST OF TABLES

LIST OF APPENDICES

LIST OF APPENDIX FIGURES

LIST OF APPENDIX TABLES

WAVE RUNUP ON HIGH ENERGY, DISSIPATIVE BEACHES AND THE PREDICTION OF COASTAL EROSION

CHAPTER ONE: GENERAL INTRODUCTION

Erosion has been common along the Oregon coast due to the high energy nature of the wave climate and the dynamic behavior of its beaches. Erosion has occurred in areas where either sea cliffs or foredunes back the beaches. The erosion has been episodic, associated with the occurrence of extreme storms, and it also has been spatially variable. This spatial variation is due in part to the tectonic setting of Oregon, which has resulted in different rates of coastal uplift (Komar and Shih, 1993). In general, the southern part of the coast and the northern-most part near the Columbia River are rising faster than the present rate of sea level rise, while the north-central stretch has minimal uplift and therefore is experiencing a sea level transgression due to the global rise in sea level. This coast wide pattern of relative sea-level change is reflected in the degree of sea cliff and dune erosion. However, there also are more local controls, which include the volume of sand on the fronting beach and the corresponding ability of the beach to act as a buffer between the sea cliffs or sand dunes and storm waves (Shih and Komar, 1994). The north-central portion of the Oregon coast, where erosion has been greatest, is segmented into a series of littoral cells by large headlands, which effectively isolate the stretches of beach within each cell. Sources and losses of sand to the series of littoral cells are highly variable, and this has controlled the amount of sand on the beach and the elevation of the junction between the beach face and the backing feature, be it a sea cliff, sand dune or shore protection structure. As a result, there tends to be differences in the susceptibilities of properties to erosion between the series of littoral cells. It is this highly spatial as well as temporal variation that has made it important to develop analysis techniques that can assist in rationally evaluating potential erosion. One such methodology (developed in this thesis) examines the

extreme total water levels experienced on Oregon beaches relative to the elevation of the beach face junction. This analysis requires the capability to predict both the extreme water levels measured by tide gauges as well as extreme wave runup levels during large storm events.

Many beaches in the Pacific Northwest of the United States can be classified as dissipative. They exhibit behavior which is very different than beaches on the more heavily populated, and more heavily studied, intermediate to reflective beaches common on the east coast of the U.S. Beaches in general can be morphologically classified as ranging from fully dissipative, corresponding to low sloping beaches, to highly reflective steep beaches (Wright and Short, 1983). Dissipative beaches are characterized by spilling breakers and wide saturated surf zones, while on more reflective beaches, nearshore processes occur over a narrower region. As incident waves propagate shoreward and become significantly affected by the shallowing bathymetry, wave energy is transferred through non-linear processes to both higher and lower frequencies (Longuet-Higgens and Stewart, 1962). On steep beaches, this evolution of the incident spectrum occurs over only a few wave lengths. On very mild sloped beaches, the evolution occurs over many wavelengths, in which case the incident waves can be strongly dissipated and the inner surf zone can be dominated by low frequency (infragravity) energy. In particular, fluid motions over the swash zone, defined as the section of intermittently wetted profile between the landward most runup of ocean waves and the furthest offshore rundown, can be of extremely low frequency on dissipative beaches.

Nearshore field studies in the U.S. have, until recently, been limited to a relatively narrow range of beach types and offshore wave conditions, primarily focusing on intermediate to reflective beaches subject to relatively low wave heights. Holman and Sallenger (1985) and Holman (1986), using an extensive data set taken from the intermediate beach of the Field Research Facility in Duck, North Carolina, showed that swash on natural beaches depends strongly on a non-dimensional surf similarity parameter known as the Iribarren number. Other field studies of wave

runup have taken place on relatively low energy dissipative beaches in southern California (Guza and Thornton, 1984 and Raubenheimer and Guza, 1996). These studies have shown wave runup to be linearly dependent simply on the offshore wave height, rather than the Iribarren number. Incident band energy in the swash zone of these dissipative beaches is typically saturated, and it is the infragravity energy that increases with increasing offshore wave height. A recent field experiment on the central Oregon coast (described in this thesis) investigated the dynamics of a high energy dissipative beach. Video image processing techniques were employed to make accurate measurements of the swash zone during the experiment (Holman and Guza, 1984; Holland *et al.*, 1997).

This thesis has three primary objectives. The first is to characterize wave runup on the high energy dissipative beaches typical of the Pacific Northwest of the U.S. This objective is addressed in both Chapters 2, "Wave runup, extreme water levels and the erosion of properties backing beaches," and 3, "Longshore variability of wave runup on a high energy dissipative beach." In Chapter 2 it is shown that extreme runup statistics are linearly related to the offshore wave height, consistent with the observations of Guza and Thornton (1982). Portions of this chapter, co-authored by Dr. Paul Komar, Dr. William McDougal and Dr. Reginald Beach, were presented at the 25th Conference on Coastal Engineering and will appear in the conference proceedings (Ruggiero *et al.*, in press). The chapter in full will be submitted to the Journal of Coastal Research. Swash dynamics on dissipative beaches are more closely examined in Chapter 3. This chapter extends the extreme statistical analysis of Chapter 2 to an investigation of the frequency response of swash motions, as well as to the frequency wavenumber structure of these motions. Runup is found to be coherent over very large alongshore distances, O(1 km), at the extremely low frequencies, O(0.005 Hz), that dominate the swash zone. Chapter 3 is co-authored by Dr. Rob Holman and Dr. Reginald Beach and will be submitted to the Journal of Geophysical Research.

The second objective of this thesis is to develop a quantitative methodology for determining the susceptibility of coastal properties to wave induced erosion. This objective is addressed in Chapter 2, where we report on analyses of extreme water levels measured by a tide gauge, on predicted extreme total water levels including wave runup, on efforts to document the beach morphology variations that affect wave runup and determine beach face junction levels, and on efforts to apply the analyses in coastal-zone management decisions. Combining empirical relationships for wave runup with long-term data bases of measured tides and waves, we predict the frequency with which properties backing beaches are subject to potential erosion. The application in this chapter is to the Oregon coast, but the techniques can be used on other coastlines, employing wave and water level data specific to those areas.

The model described in Chapter 2 can predict not only the frequency with which sea cliffs and dunes are impacted by storm wave runup, but also the susceptibility of coastal protection structures to potential failure. The third objective of this thesis extends the analysis of Chapter 2 to vertical structures that are more disruptive to surf zone processes. Vertical structures in this sense can be thought of as either sea cliffs or sea walls. Weggel (1988) proposed a classification scheme for vertical structures, depending on the location of the structure with respect to the shoreline. A Type-1 sea wall (or sea cliff), according to Weggel (1988), has its toe located landward of the level of maximum runup at all times. The toe of a Type-2 sea wall is always above the mean water level but is impacted by wave runup during storm conditions. These are the conditions for which the erosion susceptibility model of Chapter 2 was developed, in order to predict how often the sea wall or sea cliff would be impacted by wave runup. The toe of a Type-3 through a Type-5 sea wall ranges from occasionally submerged under the still water level to always submerged at every tide level but still within the surf zone. Finally, a Type-6 sea wall is located beyond the breaker line. Although the assumptions in the model of Chapter 2 are not applicable above the Type-2 classification, the model described in Chapter 4, "Longshore currents and sediment transport on beaches with seawalls," is

valid for sea wall types 3-5. Therefore, the third objective of this thesis is to predict longshore currents and sediment transport on beaches backed by sea walls. This is accomplished with an analytic model based on the depth and time averaged shallow water equations of motion in the nearshore. Model results suggest that the magnitudes of longshore currents and sediment transport in front of a seawall can be either greater or less than a similar beach without a seawall, depending on the location of the structure within the surf zone, the beach slope and the wave conditions. Chapter 4 is co-authored by Dr. William McDougal and has been submitted to Coastal Engineering.

Conclusions drawn from the investigations into these three objectives are summarized in Chapter 5. Beach morphology data collected for the application of the model described in Chapter 2, as well as for studies of the long term beach response to shore stabilization structures (Hearon, 1995 and Hearon *et al.*, in press) and numerical modelling of foredune erosion on the Oregon coast (Carpenter, 1995), is presented in Appendix A. The appendix, taken from an engineering report submitted to the Oregon Department of Land Conservation and Development, describes beach morphology monitoring on the Oregon coast from 1993 through 1996 with information about the 23 sites in the data base. The actual survey data can be found in Ruggiero (1995).

CHAPTER TWO: WAVE RUNUP, EXTREME WATER LEVELS AND THE EROSION OF PROPERTIES BACKING BEACHES

2.1 Abstract

A model has been developed to evaluate the susceptibilities of coastal properties to wave induced erosion. The model includes analyses of the probabilities of extreme water levels affected by various oceanographic and atmospheric processes, as well as by predicted tides, and the runup elevations of storm waves on beaches. The application is to the Oregon coast, where measured tides often exceed predicted tides by tens of centimeters, especially during the occurrence of an El Niño, and where measurement of the runup on dissipative beaches typical of the Oregon coast have been found to depend on the deep-water significant wave height. Predicted extreme water elevations are compared with the measured elevations of the junctions between the beach face and the toes of foredunes and sea cliffs. The objective is to evaluate the expected number of hours per year water can reach the property, an evaluation of the susceptibility to potential erosion. This assessment is illustrated by an application to the Jump Off Joe Landslide in Newport, Oregon, with the analysis showing that the toe of the slide can expect upwards of 173 hours of wave attack per year, while the adjacent vegetated sea cliff unaffected by landsliding is impacted only 13 hours. The model is applied to the entire littoral cell in the Newport area, demonstrating how this type of analysis can aid in making coastal management decisions. Application is made to other sites along the Oregon coast, revealing differences between the various littoral cells, depending on the quantity of sand on the beach and its capacity to act as a buffer from wave attack.

2.2 Introduction

The overall morphology of a beach can be characterized as ranging from dissipative to reflective (Wright and Short, 1983), depending on the sediment grain size and wave conditions. This classification scheme relates to the dissipation of wave energy, the dynamic response of the beach morphology, and ultimately to the natural capacity of the beach to protect coastal properties. Much of the Oregon coast is characterized by wide, dissipative, sandy beaches, which are backed by either sea cliffs or sand dunes. This dynamic coast typically experiences a very intense winter wave climate, and there have been many documented cases of dramatic, yet episodic, sea cliff and dune erosion (Komar and Shih, 1993). A typical response of property owners following such erosion events is to build large coastal protection structures. Often these structures are built after a single event, which is followed by a long period with no significant wave attack. From a coastal management perspective, it is of interest to be able to predict the expected frequency and intensity of such erosion events to determine if a coastal structure is an appropriate response as well as to rationally determine setback lines for the siting of new developments.

Wave induced erosion of properties backing beaches, whether they be in foredunes or sited atop sea cliffs, depends on the elevation achieved by the water relative to the elevation of the fronting beach. There are two main components, diagrammed in Figure 2.1, which combine to generate total water levels (Shih *et al.*, 1994; Ruggiero *et al.*, 1996). The first is the measured tide elevation, ζ, which consists of the predicted tide and the many oceanographic and atmospheric processes that alter the mean water level from the predicted tidal elevation. These factors include water temperature, the geostrophic effects of offshore currents, the presence of winds, particularly onshore winds that can cause storm surge, and the various processes associated with El Niños which can alter water levels by tens of centimeters (Komar and Enfield, 1987). Superimposed on these many processes that

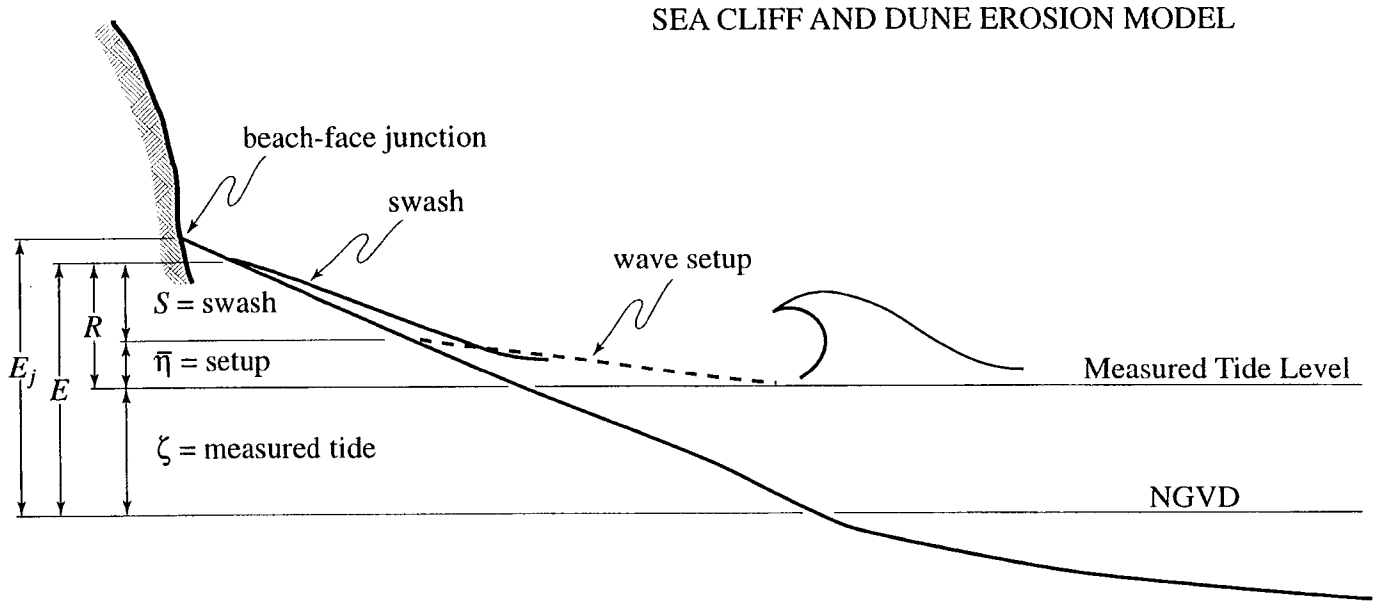

Figure 2.1. The basic model for the quantitative assessment of the susceptibilities of sea cliffs and sand dunes to wave-induced erosion.

affect the mean water level at any given time along the coast, is the vertical component of wave runup, R, which consists of both the wave setup $\bar{\eta}$, that elevates the mean shoreline position, and swash fluctuations, S, about the setup. Wave induced erosion of a sea cliff or dune will occur only when the total elevation of the water at times of maximum runup exceeds the elevation of the beach-face junction ($\zeta + R > E_j$).

This paper reports on a model that has been developed to provide quantitative evaluations of the susceptibilities of coastal properties to erosion by waves. This is achieved through evaluations of the factors discussed above, including examinations of the probabilities of extreme mean water elevations and the runup of storm waves beyond the mean water elevation. The application here is to the central Oregon coast where long-term measurements of tides and deep-water wave conditions make such analyses possible. Other researchers have attempted to determine the risk of coastal properties to erosion using probabilistic techniques. For example, Gares (1990) demonstrates a method for using runup to determine flooding risk on the New Jersey shoreline. Runup is calculated using the composite slope technique presented in the Shore Protection Manual (USACOE, 1984), and probability curves are produced assuming that maximum runup occurs at times of maximum storm surge. In the current work, an attempt is made to characterize extreme runup statistics on the high energy, yet dissipative beaches common in Oregon where the storm surge is relatively small. Experiments have been undertaken on a number of beaches so that runup can be related to the deep-water wave conditions, as well as to the local beach morphology. The application is illustrated for a variety of sites along the coast, sites that differ in the morphologies of the fronting beaches and in their ability to protect foredunes and sea cliffs from erosion. Although the application here is to the Oregon coast, the techniques being illustrated can be used on other coasts to evaluate the susceptibilities of properties to erosion, and thus can serve as the basis for coastal management decisions.

2.3 Analysis of Wave Runup and Extreme Water Levels

The objective of this study is to predict the frequency with which the total water level, E, reaches or exceeds the elevation E_j of the junction between sea cliff, dune or coastal protection structure and the beach face. To achieve this goal, we first examine wave runup on high energy dissipative beaches and then construct extreme value probability distributions (e-v pdf) for the combined total water levels due to wave runup and water levels measured by tide gages.

2.3.1 Wave Runup

The evaluation of wave runup, loosely defined as the time varying location of the shoreward edge of water on the beach face, has been of interest to coastal engineers, oceanographers and coastal planners. Wave runup is a continuous process, but statistics of runup maxima are often the measure of particular interest in engineering and management applications. The symbol R will be used for all statistical representations of wave runup whether concerning the continuous process or simply the maxima. Particular statistics will be denoted by subscripts. Based on laboratory observations of monochromatic waves, Hunt (1959) demonstrated a dependence between the non-dimensional maximum vertical runup elevation, R_{max} (normalized by the deep-water significant wave height H_s) and a "surf similarity" parameter

$$\frac{R_{\max}}{H_s} = c\xi_o \tag{2.1}$$

where c is a dimensionless constant. The Iribarren number, ξ_o, one of several similarity parameters that have been used to explain a variety of surf zone processes (Battjes, 1974), is defined as

$$\xi_o = \frac{\beta}{(H_s/L_o)^{1/2}} \tag{2.2}$$

where β is the beach slope in radians (assumed small, so that $\tan \beta \simeq \sin \beta \simeq \beta$) and L_o is the deep-water wave length given by $L_o=(g/2\pi)T^2$, g is the acceleration due to gravity and T is the wave period. Low values of ξ_o indicate relatively dissipative beaches. Holman and Sallenger (1985) and Holman (1986), using an extensive data set taken from the intermediate sloped beach of the Field Research Facility (FRF) in Duck, North Carolina, showed that broad band swash on natural beaches also strongly depends on the Iribarren number. Similar results have been found by other researchers, including Battjes (1971) and van der Meer and Stam (1992).

Much effort has been spent formulating methods to determine the probability distribution function of irregular wave runup maxima (Saville, 1962; Battjes, 1971; Nielson and Hanslow, 1991; and Walton, 1992). Many of these models have employed the hypothesis of equivalency (Battjes, 1971) in which the distribution of runup of random waves can be found by applying the runup value of a monochromatic wave train to the individual wave in the irregular wave train. Extreme runup statistics can then be derived from these analytical probability density functions, typically Rayleigh, by examining the tails of the distribution. Holland and Holman (1993) note that the zero-crossing definition of runup maxima used in these studies should be restricted to narrow banded spectra. A more generic description of maxima, suitable for both narrow and broad banded spectra, includes all local maxima, both negative and positive. Holman (1986) examined the relationship between extreme runup statistics and the Iribarren number using the above more inclusive definition of runup maxima. Due to relatively short data records, and therefore a limited number of runup maxima, Holman calculated quantile exceedence values from the observed frequency distribution for each data set, rather than fitting the data to a known (Rayleigh) frequency distribution. In particular, Holman (1986) examined the 2% exceedence value of runup maxima,

$R_{2\%}$. From this study, the dimensionless constant of (2.1) was found to be approximately $c = 0.9$. Conditions in which 2% of runup maxima are reaching or exceeding the elevation of the beach face junction are taken in this paper to be a reasonable proxy for potential erosion.

When analyzing a dissipative subset of their data, with Iribarren numbers between 0.5 and 1.0, Holman and Sallenger (1985) found that the incident band swash was saturated while the infragravity band swash increased with increasing offshore wave height. These results were similar to those found by Guza and Thornton (1982), who investigated swash dynamics on low energy dissipative beaches in southern California. Guza and Thornton (1982) suggested a linear relationship between the significant vertical runup elevation, R_s, and the significant wave height, H_s, obtaining

$$R_s\ (m) = 0.71 H_s + 0.035\ (m) \qquad \textbf{(2.3)}$$

R_s is defined as 4σ, where σ^2 is the total variance of the runup elevation time series, and is thus a statistic describing runup as a continuous process. Aagard (1990) also found a linear relationship between runup elevation and wave height on relatively low energy dissipative beaches in Denmark and Australia.

Data bases containing a decade or more of measurements of wave heights and periods are now becoming readily available for use by engineers, scientists and planners. These data coupled with simple relationships, such as those above, between wave runup and deep-water wave and beach morphology characteristics, suggest a straight forward method of determining extreme runup statistics for a variety of conditions. If the interest is in predicting potential erosion, as in this paper, then empirical relationships for statistics such as $R_{2\%}$, which represent actual elevations relative to some vertical datum, are necessary. R_s is a measure of the relative energy in a runup record, but does not indicate a particular elevation

reached by the runup. With a suitable runup model, one can take advantage of measurements of wave characteristics, heights and periods, and a knowledge of beach morphology, to develop extreme value distributions for the particular runup statistic of interest.

2.3.2 Measurements of Wave Runup

Field investigations have been performed on the central Oregon coast in an attempt to determine predictive relationships for extreme runup, and to further our understanding of runup dynamics on the high energy dissipative beaches common in the Pacific Northwest of the U.S. All runup measurements were made employing the video techniques developed at the Coastal Imaging Lab of Oregon State University (Holman and Guza, 1984; Holland *et al.*, in press). Runup elevation time series were extracted from video recordings using the modified "timestack" technique as described by Aagard and Holm (1989) and Holland and Holman (1993), in which the landward most identifiable edge of water is digitized using standard image processing algorithms along with manual refinements. Runup was measured under a wide variety of wave conditions; deep-water wave heights ranged from 1.4 m to 4.6 m, spectral peak periods ranged from 7 s to 17 s, and a variety of nearshore morphologies were included with beach slopes ranging from 0.005 to 0.047. The field program culminated in February, 1996 at Agate Beach in Newport, Oregon with a major investigation into the dynamics of high energy dissipative beaches. During this experiment, three video cameras were used with the overlap in the field of view of the cameras allowing for continuous coverage of runup measurements over a 1.6 km alongshore stretch of beach (Chapter 3).

Table 2.1 lists the locations at which runup data were obtained and the environmental conditions during data collection. For each data record, the tide (measured at the Hatfield Marine Science Center, Oregon State University, in Yaquina Bay at Newport, Oregon) has been removed and extreme runup statistics

Table 2.1. Environmental conditions during runup measurements.

Location	Date	# of Runs	H_s (m)	T (s)	β
Gleneden	02/02/91	1	3.2	11	0.047
21st Street	02/17/91	1	2.2	11	0.033
Beverly Beach	03/17/91	1	3.8	15	0.040
Beverly Beach	03/15/94	3	3.0	17	0.040
Beverly Beach	11/16/94	4	4.6	14	0.047
Nye Beach	11/08/95	1	3.3	9	0.030
Nye Beach	11/21/95	3	2.3	7	0.033
Beverly Beach	11/22/95	2	2.0	9	0.037
Agate Beach	(02/07/96-02/17/96)	58	(1.4-4.1)	(5-17)	(0.005-0.025)

have been computed after identifying the local maxima of the shoreline elevation time series. Although there is a distinction between the processes that force wave setup and swash fluctuations, for most engineering applications the measure of interest is the extreme statistics associated with the total runup. Therefore, all runup statistics presented include both setup and swash. The beach slopes, β, given in Table 2.1 are specifically the foreshore slopes, taken to be the best linear fit of the measured beach surface between plus and minus two standard deviations from the mean raw runup elevation. Beach morphology, as well as ground control points used for solving the geometry of the video images, were typically obtained using standard terrestrial surveying techniques. However, during the Agate Beach field experiment, differential global positioning system (DGPS) surveying techniques were employed. The survey system was installed on a 6-wheeled amphibious "buggy" which, by traveling at approximately 5 m/s, allowed for the dense mapping of the large alongshore beach surface in only a few hours (Plant and Holman, in prep.). All wave height and period information in this paper is taken from the Scripps Institute of Oceanography Coastal Data Information Program (CDIP) buoy offshore from Bandon, Oregon located in approximately 64 m of water.

2.3.3 Observations

Several statistical representations of the Oregon runup data have been calculated. The two percent exceedence elevation of local runup maxima, $R_{2\%}$, non-dimensionalized by the deep-water significant wave height, is shown in Figure 2.2 plotted against the Iribarren number. The pluses in the figure represent the data obtained on Oregon beaches, while the circles are the data of Holman (1986) from the FRF, which are shown for comparison. The Iribarren number clearly distinguishes between the dynamically different nearshore systems from which the data were taken. The Oregon data fall in the extremely dissipative range of Iribarren numbers, while the FRF data range from dissipative to reflective. Although the Oregon data are of the expected order of magnitude, any linear

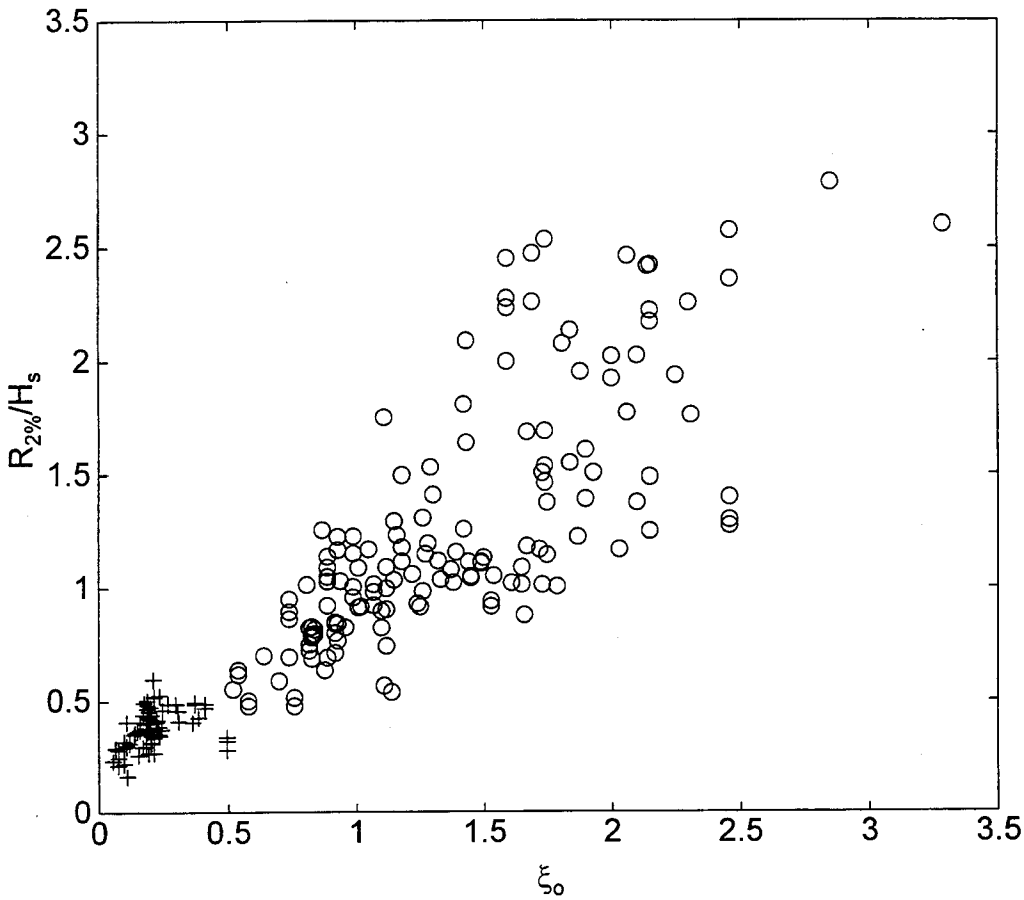

Figure 2.2. Comparison between non-dimensional extreme runup statistics obtained by Holman (1986) from the FRF (circles) and from data collected on Oregon beaches (pluses).

predictive model forced through the origin, such as (2.1) derived from Holman's data, would tend to under-predict $R_{2\%}$ on the flatter Oregon beaches, an observation noted earlier by Shih *et al.* (1994). However, when regressing all of the data (a total of 223 points) against the Iribarren number and calculating an intercept, a linear model does a very good job in explaining the variance of the data. The slope and intercept calculated for Figure 2.2, as well as the subsequent data plots, are listed in Table 2.2.

A close examination of Figure 2.2 reveals that, between Iribarren numbers from approximately 0.25 to 0.75, there may be a flattening in the linear dependence between the normalized extreme runup and the Iribarren number. In fact, Figure 2.3a shows that for the limited and extremely dissipative range of Iribarren numbers of the Oregon data, $0.05 < \xi_o < 0.5$, the non-dimensional $R_{2\%}$ does not strongly depend on this similarity parameter ($r^2 = 0.14$) except at very low ξ_o. Figure 2.3b also reveals little dependence of the non-dimensional Oregon runup data on the foreshore beach slope ($r^2 = 0.18$), again except for at very low values of β. Holman's (1986) data have been re-analyzed by Douglass (1992), who found that removing the beach slope term from (2.1) does not cause any reduction in the ability to predict runup on intermediate beaches. Similarly, by analyzing a wide variety of Australian beaches, Neilsen and Hanslow (1991) found that the relationship proposed by Holman explained results from field experiments on relatively steep beaches with $\beta > 1{:}10$, while for flatter more dissipative beaches with $\beta < 1{:}10$, runup depended only on the wave steepness. In contrast to these results, Figure 2.3c for our Oregon data shows no dependence of $R_{2\%}/H_s$ on the wave steepness ($r^2 = 0.004$). Although not shown, the dimensional extreme runup also does not depend on the wave period, another surprising result as runup has a first order dependence on the wave period in the dimensional form of (2.1).

Similar to the results found by Guza and Thornton (1982) and Aagard (1990), the best simple parameterization of $R_{2\%}$ for the Oregon data alone is a

Table 2.2. Regression coefficients for extreme runup statistics.

Variables	Slope, m	Δ m	Intercept, b	Δ b	r^2
$R_{2\%}/H_s$ vs ξ_o (all data)	0.75	± 0.03	0.22	± 0.29	0.77
$R_{2\%}/H_s$ vs ξ_o (Oregon data only)	0.33	± 0.10	0.32	± 0.08	0.14
$R_{2\%}/H_s$ vs β	3.18	± 0.81	0.32	± 0.07	0.18
$R_{2\%}/H_s$ vs H_s/L_o	0.89	± 1.70	0.37	± 0.09	0.004
$R_{2\%}$ vs H_s (Oregon data)	0.50	± 0.04	-0.22	± 0.21	0.72
$R_{2\%}$ vs H_s (FRF data)	0.42	± 0.03	1.16	± 0.43	0.48
$R_{2\%}$ vs $(\beta H_s L_o)^{1/2}$ (all data)	0.27	± 0.004	0.0	± 0.40	0.67

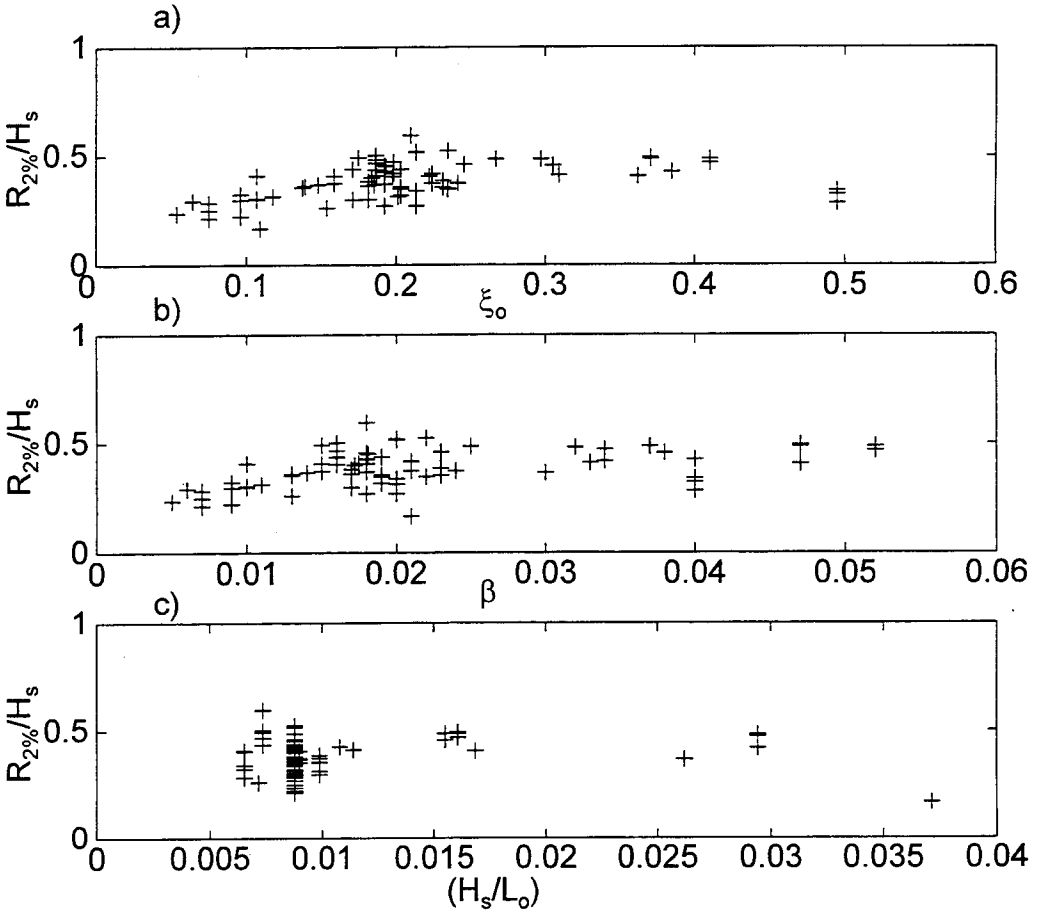

Figure 2.3. Dependence of non-dimensional extreme runup statistics on a) the Iribarren number, b) the foreshore beach slope and c) the wave steepness.

dependence on the deep-water significant wave height as shown in Figure 2.4. The best-fit straight line matched to the Oregon data is

$$R_{2\%}\ (m) = 0.5H_s - 0.22\ (m) \quad (r^2 = 0.72) \tag{2.4}$$

Thirty-three of the data runs from the Agate Beach field experiment listed in Table 2.1 are from an analysis of the longshore variability of wave runup over a 1.6 km distance (Chapter 3). Each of these data runs, from the same 2 hour period, have the same offshore wave conditions and only the foreshore slope is variable. This large alongshore distance has been separated into three regions, based on changes in foreshore slope, and averages of $R_{2\%}$ have been calculated for each region. Including all of the 33 runs in Figure 2.4 simply adds scatter at a single wave height and does not significantly alter the regression coefficients of (2.4) determined when using just the three averages. The FRF data of Holman (1986) are shown again to emphasize the fact that the two data sets are derived from dynamically very different systems, as the Holman data are clearly offset above the Oregon data. Interestingly, within the error estimates of the linear regressions through each individual data sets, the slopes of the dependence on H_s are comparable. Figure 2.5 shows a final parameterization of wave runup, which is slightly different than the dimensional form of the Iribarren number dependence of (2.1). The relationship, shown as the solid line in the figure,

$$R_{2\%} = 0.27\ (\beta H_o L_o)^{1/2} \quad r^2 = 0.67 \tag{2.5}$$

does equally well in explaining the variance of both the Oregon data and the FRF data of Holman (1986). Three predictive runup models, (2.4), (2.1) (using the regression coefficients generated including both data sets) and (2.5), will be used in the subsequent analysis of extreme total water levels.

The extreme runup statistics presented here are monochromatic representations of spectral phenomena. In fact, all of the Oregon runup data, particularly that on the very low sloping Agate Beach, were dominated by

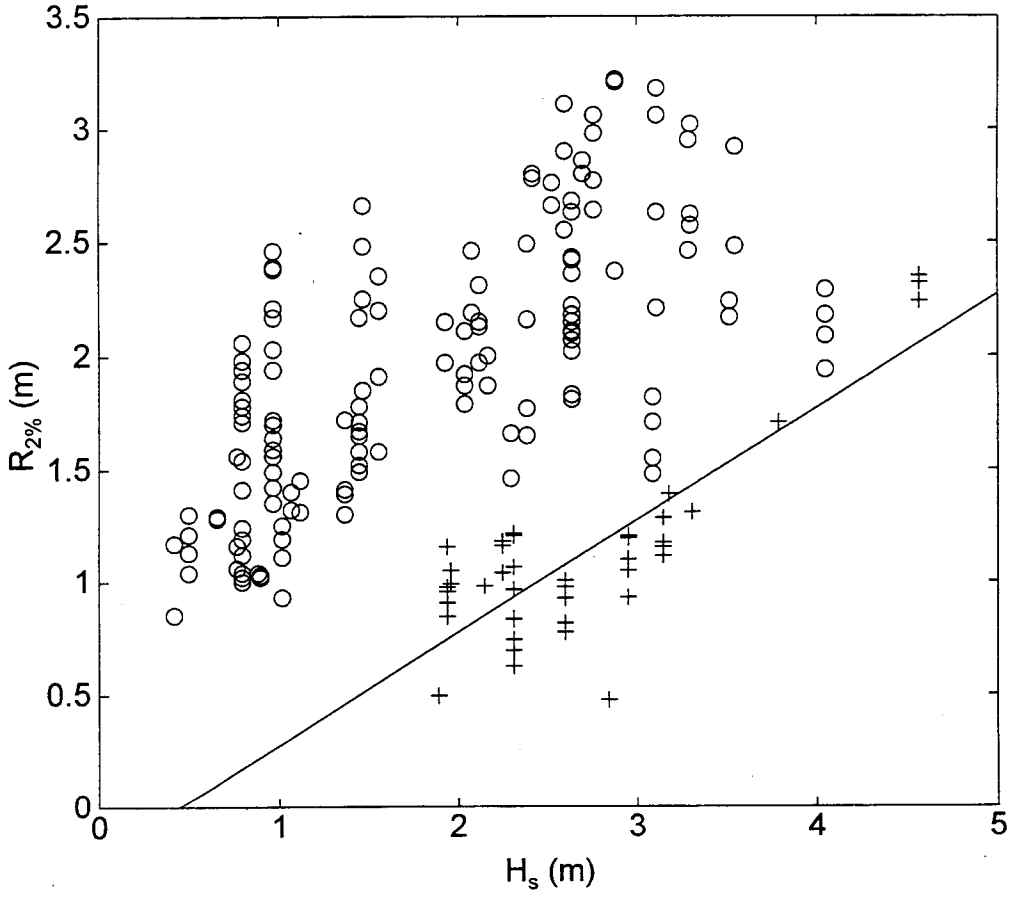

Figure 2.4. Dependence of dimensional extreme runup statistics on the deep water significant wave height for both FRF data (circles) and Oregon data (pluses). The best fit straight line through the Oregon data has a slope and intercept of 0.5 and -0.22 respectively.

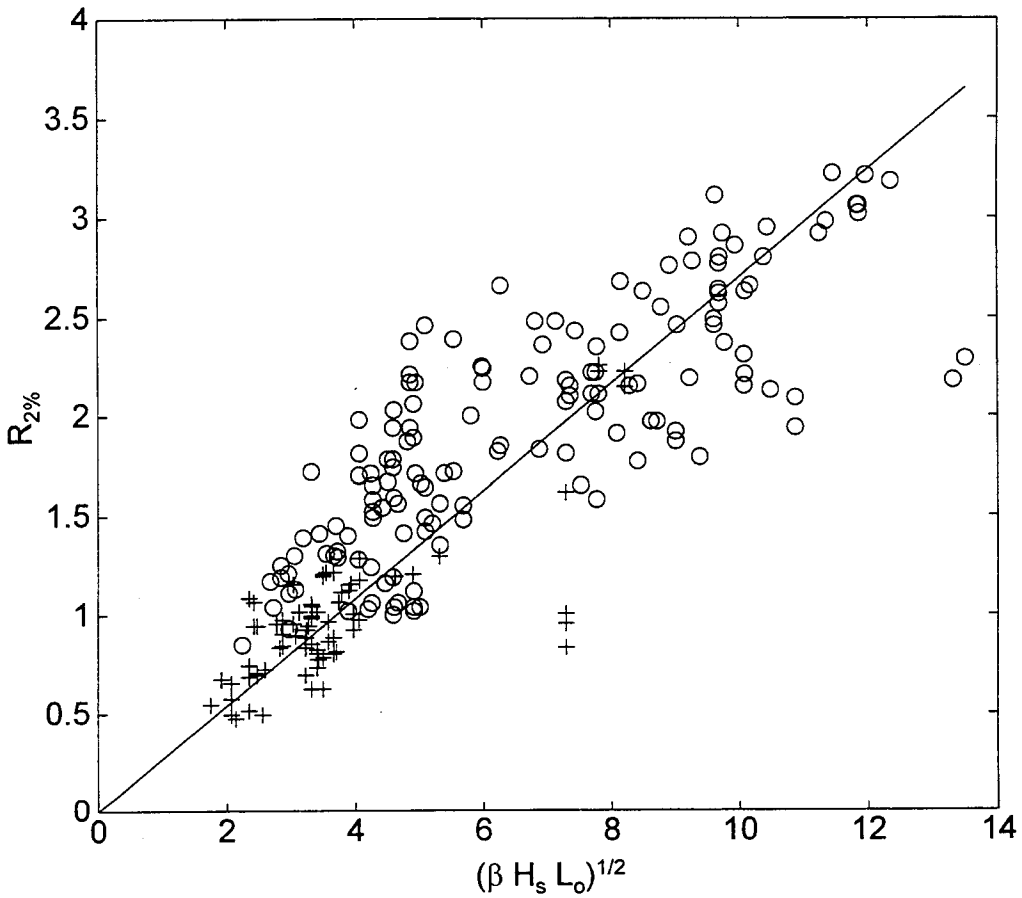

Figure 2.5. Dependence of dimensional extreme runup statistics on $(\beta H_s L_o)^{1/2}$. The slope of the fitted line through the data is 0.27.

infragravity energy ($f < 0.05$ Hz). Spectral peaks typically occurred at periods ranging from approximately 100 seconds to 200 seconds, and usually more than 90% of the runup elevation variance fell in the infragravity band. A representative frequency spectrum from one of the data runs during the Agate Beach field experiment is shown in Figure 2.6, revealing the very low frequency nature of the swash motions. The asterisk in the figure denotes the peak frequency of the incident waves. Note that at this frequency the runup energy density is approximately three orders of magnitude less than at the peak swash frequencies. The broad region in the spectrum with a f^{-4} roll off is an indication that the runup over this frequency band is saturated (Huntley, 1977). The incident band energy was saturated for most data runs, and the dependence on wave height shown in Figure 2.4 can almost entirely be explained by the infragravity band energy and its dependence on the wave height. Again, these results are similar to those found by Guza and Thornton (1982).

2.3.4 Extreme Water Levels

Observed water levels can generally be represented as

$$\zeta(t) = \zeta_o(t) + \zeta_p(t) + \zeta_r(t) \qquad \textbf{(2.6)}$$

in which ζ_o(t) is the mean sea-level, which changes slowly with time, ζ_p(t) is the tidal part of the variation and ζ_r(t) is the non-tidal residual component. Water levels measured by tide gauges are often greater than predicted tidal levels due to the many factors that can make up the residual component, such as the occurrence of a storm surge, the effects of water temperature, currents and atmospheric disturbances such as an El Niño. A 24 year time series of hourly measured tides obtained from the tide gauge in Newport, Oregon has been analyzed to investigate some of these processes. Elevations reported by tide gauges are typically relative to a tidal datum, such as MSL or MLLW, which apply only locally and can vary over time. At the Newport tide gauge, MSL is approximately 10 cm higher than the U.S. National

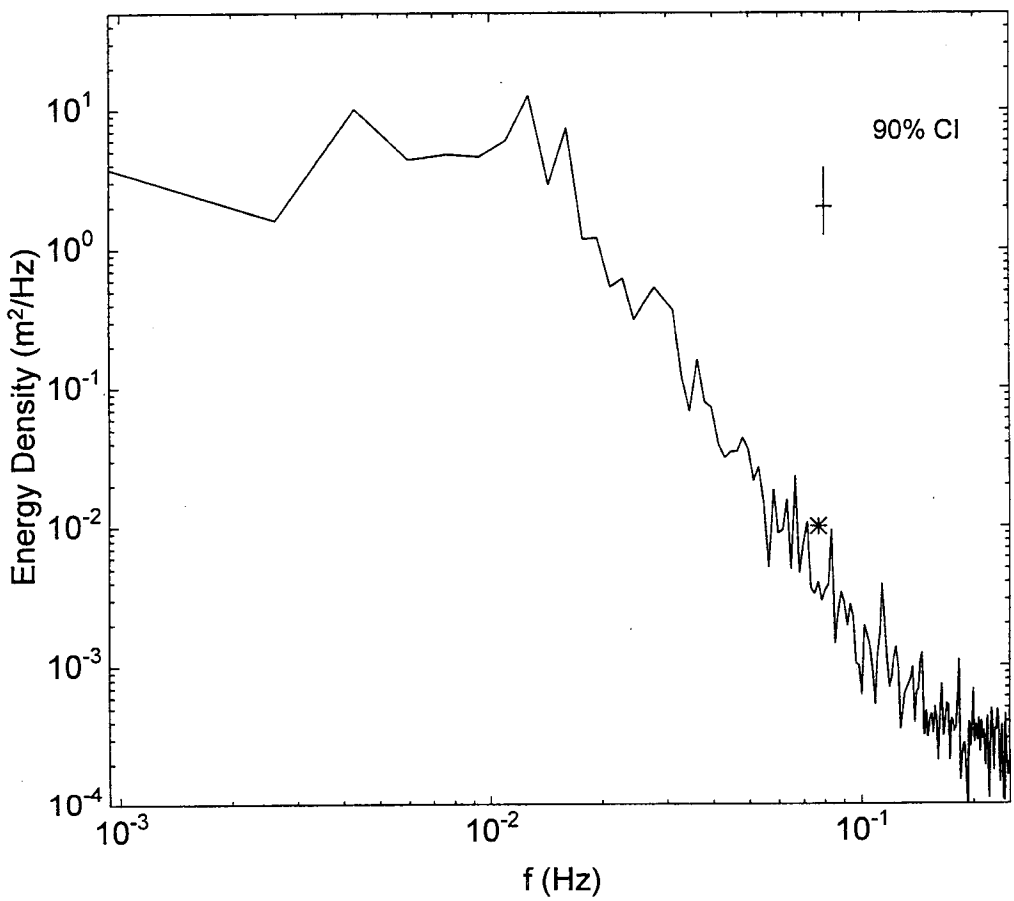

Figure 2.6. Representative energy density spectrum from Oregon runup data, obtained during the High Energy Field Experiment on Agate Beach. The asterisk indicates the peak frequency of the deep-water waves.

Geodetic Vertical Datum (NGVD) of 1929. NGVD has the important advantage of being a nationally fixed reference elevation, therefore most engineering design is relative to this or some other fixed datum. All tidal and land elevations presented in this paper have been adjusted accordingly to NGVD 29. The yearly maxima of the measured tides have been fitted to a Fisher-Tippet Type I extreme-value probability distribution (e-v pdf), commonly known as the Gumbel extreme value distribution, and return intervals have been computed for extreme tides. A predicted tide time series has been generated for the same 24 year period at the same location, using National Ocean Service (NOS) methods, and the predicted yearly maxima have also been fitted to a Gumbel extreme value distribution. Both distributions are shown in Figure 2.7, and as noted by *Shih et al.* (1994), for long return periods there are significant differences, on the order of 0.4 m, between predicted and observed extreme tides.

The difference between measured and predicted tides has been computed for the entire 24 year data set. Although the tectonic setting of the central Oregon coast allows it to feel a relative rise in sea-level, this rise is thought to be quite small (Komar and Shih, 1993), therefore this term is eliminated from the analysis and all differences between measured and predicted tides are lumped into $\zeta_r(t)$. The auto-correlation of this raw residual time series shows a roll off in correlation at a lag of approximately 48 hours. This lag corresponds well with the typical storm duration on the Oregon coast. The raw residuals were then filtered using a 48 hour low pass filter, eliminating measurement noise from the signal. The standard deviation of this low pass filtered residual time series is approximately 13 cm, giving a measure of the typical elevation for storm surge on the Oregon coast (Pugh, 1990). The majority of extreme tidal residuals throughout the 24 year period correspond to times of well-documented El Niño events. For example, the 1982-83 El Niño raised water levels by approximately 15 cm above the previously measured high levels for the winter months, and on the order 35 cm above the average measured levels for those months (Huyer *et al.*, 1983). Although these events are usually associated

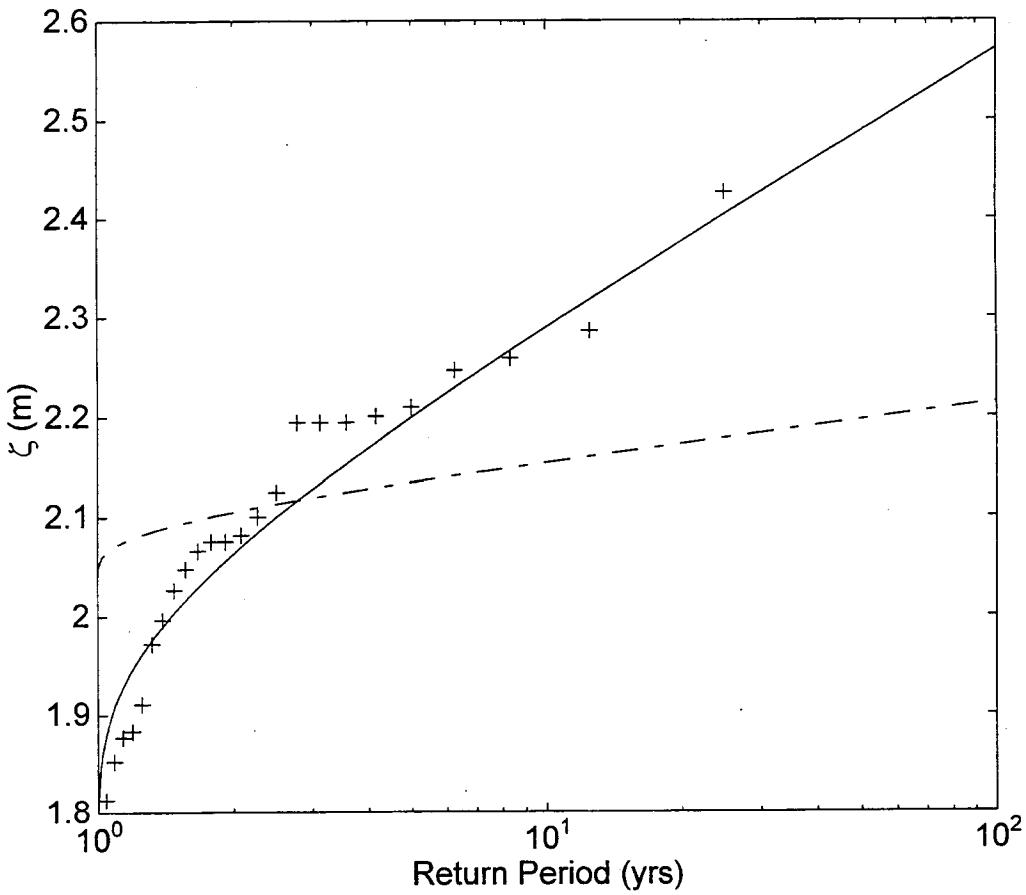

Figure 2.7. Return periods calculated from a Gumbel extreme value distribution of measured (solid line) and predicted tides (dashed-dot line). Pluses indicate binned data through which distribution was fitted.

with increased wave energy, both the residual and the measured tide are not significantly correlated with wave height throughout the period of overlap between the tide and wave data, a period of approximately 15 years. This observation suggests that models such as that proposed by Gares (1990) in which extreme measured water levels and extreme runup occur at the same time, although suited for coastlines which experience hurricanes and Nor' Easters generating significant storm surge, are not generally suitable to the Oregon coast.

2.3.5 Waves and Total Water Levels

In a previous section it was shown that the best simple predictor of extreme runup on dissipative Oregon beaches is the deep-water significant wave height. A 15 year wave data set from the CDIP buoy offshore from Bandon, Oregon has been used to estimate the extreme wave climate of the Oregon coast. Two other data sources could also have been used; a microseismometer system operated by Oregon State University at the Marine Science Center in Newport and a deep-water buoy of the National Data Buoy Center (NDBC) of NOAA offshore from Newport. Although both sources make their measurements closer to the tide gage and the site of the runup experiments, the NDBC buoy has been found to over predict large wave heights by approximately 10% (Tillotsen and Komar, 1997), and the CDIP buoy measurements are of better quality than the microseismometer. The measurements taken in approximately 64 m of water have been shoaled, using linear wave theory, to deep-water. A Gumbel extreme value distribution has been fitted to the yearly maxima of this data, and Figure 2.8 reveals the resulting recurrence intervals for extreme storm waves. Given the relatively short record of wave heights, predictions of very long recurrence intervals have large uncertainties. However, based on the extreme value analyses, the 50 year significant wave height on the central Oregon coast is 8.9 m and the 100 year significant wave height is 9.3 m.

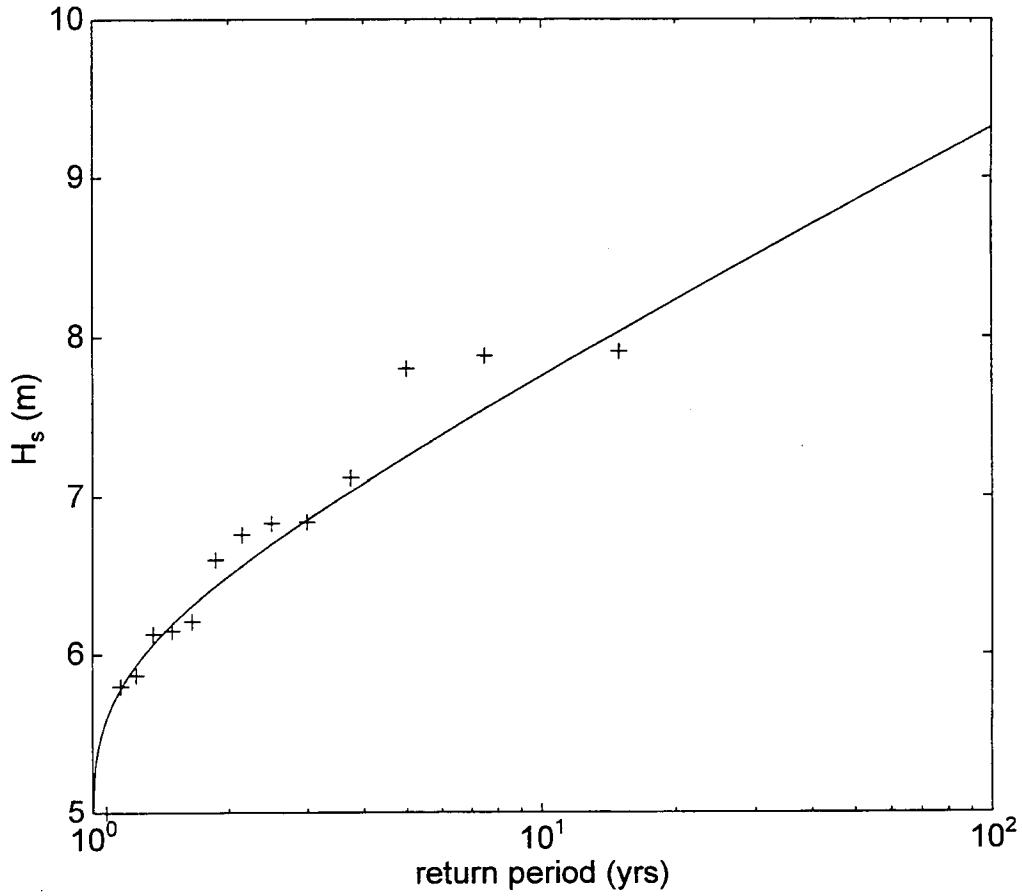

Figure 2.8. Return periods calculated from a Gumbel extreme value distribution of deep-water significant wave heights (solid line) measured by the CDIP buoy off of Bandon, Oregon.

The linear relationship between wave height and extreme runup statistics given in (2.4) can now serve as a transfer function to construct an extreme value distribution for $R_{2\%}$ from the distribution of extreme wave heights. Return periods can again be calculated, shown in Figure 2.9, revealing how often the 2% exceedance elevation of runup maxima reach extreme levels. Analytic probability density functions have now been determined for both extreme measured tides and extreme wave runup, the two components of the sea cliff and dune erosion model shown in Figure 2.1. Assuming that wave runup and measured water levels are statistically independent allows the joint probability of the two components of total water levels to be easily calculated. This exercise has been completed, and contours of equal probability of occurrence have been generated. However, a much more useful and direct method for determining the statistics of extreme total water levels, without making an independence assumption, is to apply the above model for wave runup to the wave component of the joint time series of waves and water levels. This joint time series is constructed from the time periods in which the wave data and tide data overlap. The irregularly spaced wave data have been interpolated to match the hourly measurement interval of the Yaquina Bay tide measurements, and then used to calculate runup at this interval. In doing this we generate a runup time series which can be superimposed on the measured tide to give a simulated total water level time series. Extreme value analysis is then applied to this new time series directly. In this case, however, the extreme value pdf, shown in Figure 2.10a, has been produced using all of the water level data above a threshold of 2.8 m, rather than just the yearly maxima (Muir and El-Shaarawi, 1986). By performing the analysis in this manner, the return intervals shown in Figure 2.10b represent the fraction of time when the 2% exceedence elevation of runup maxima, superimposed on the measured tide, reaches or exceeds any elevation E. Since we have used all of the hourly data above a threshold in constructing the e-v pdf, we can convert return intervals to the more convenient unit of hours of wave runup impact per year which is shown in Figure 2.10c.

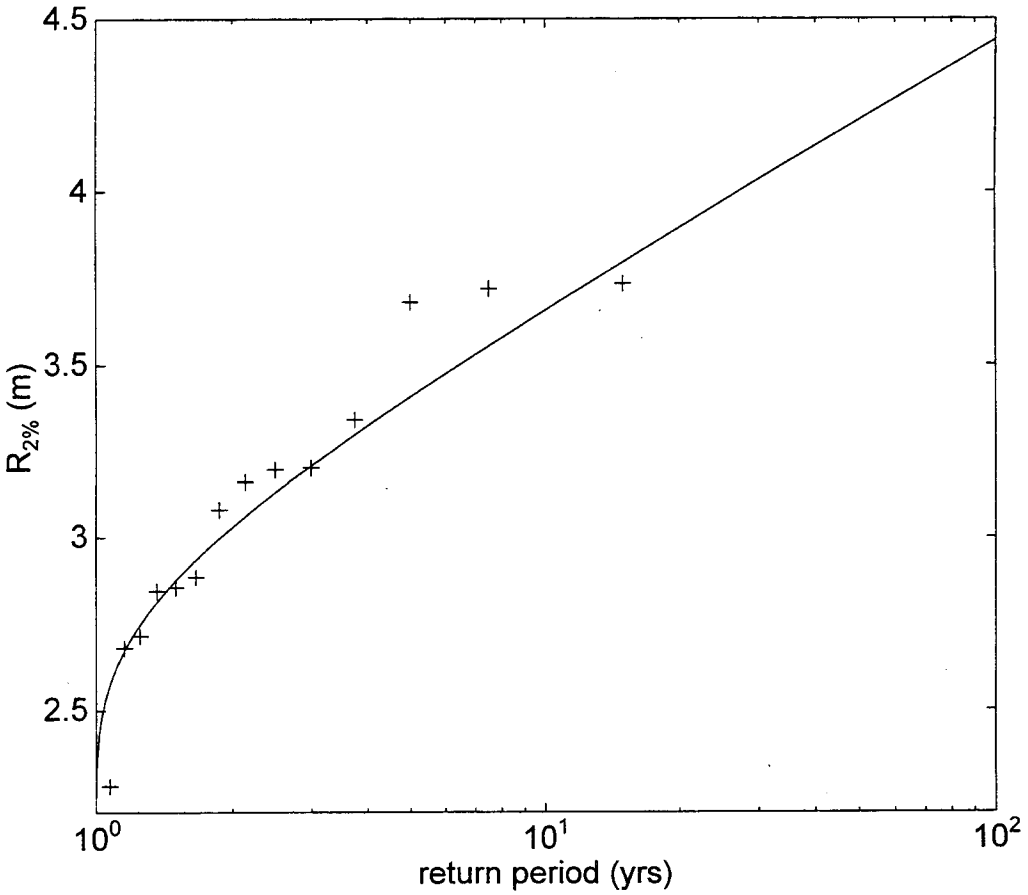

Figure 2.9. Return periods calculated from a Gumbel extreme value distribution of extreme runup levels calculated from Figure 2.8 using runup model (2.4).

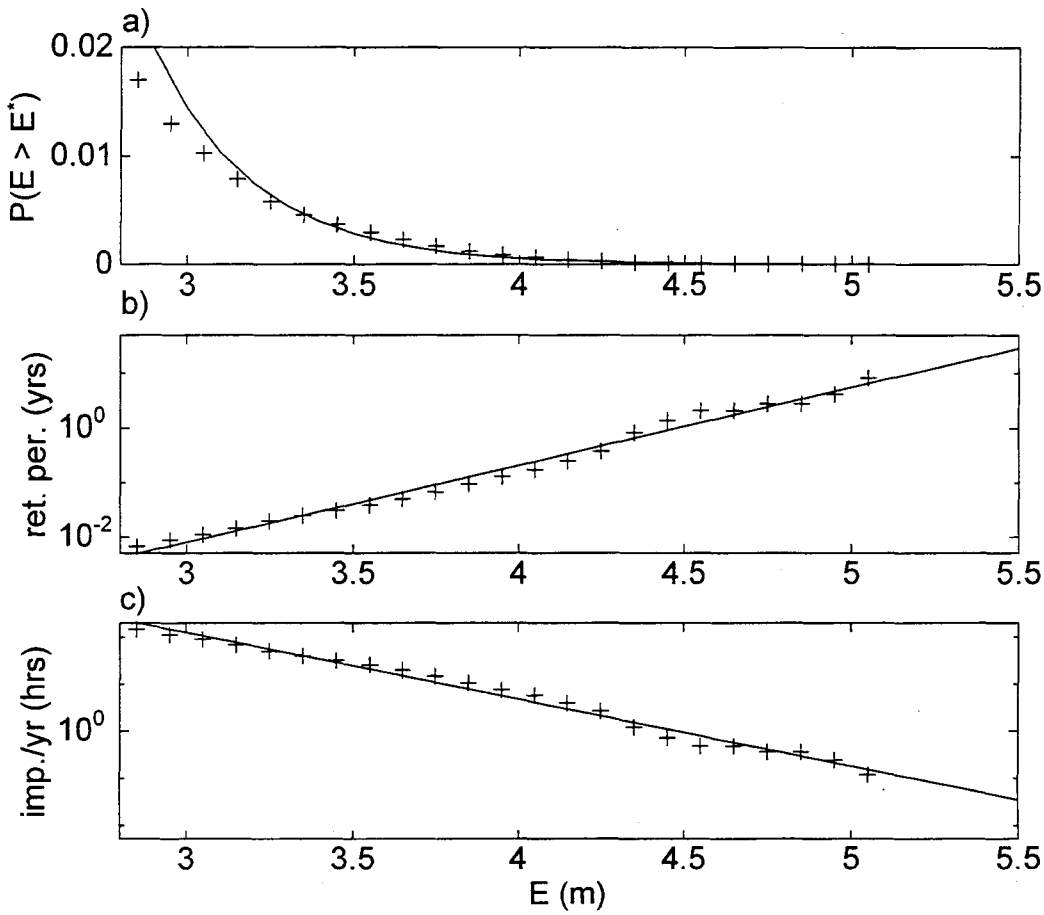

Figure 2.10. a) Gumbel extreme value distribution and b) return periods of simulated total water levels determined by combining both measured tides and runup calculated using runup model (2.4). c) Hours of impact per year in which 2% of runup maxima reach or exceed a particular elevation E.

The two other runup models have also been applied to this direct method of simulating a total water level time series over the period of overlap between the wave and tide measurements. For each of these models, the wave period is needed, in addition to the wave height, in order to determine the deep-water wave length. Also, a beach slope needs to be assumed *a priori* in order to calculate a total water elevation for a particular set of wave height, period and tide measurements. Figure 2.11 gives estimates of hours of wave runup impact per year for the later two runup models for three representative beach slopes, β = 0.01 (pluses), 0.03 (circles) and 0.05 (asterisks). Figure 2.11a, (2.5), and Figure 2.11b, (2.1), show very similar results, with the expected susceptibility to erosion for a particular beach face junction elevation increasing with increasing beach slope. The results from the simple runup model, (2.4), have been overlaid in both figures, as the solid line, and appear to give similar results as the more involved models with a beach slope of between 0.03 and 0.05. This lends confidence to the simple dependence of runup on wave height, as much of the runup data collected in this study were from beaches within this range of beach slopes.

2.4 Beach Elevations and the Erosion of Sea Cliffs and Foredunes

The morphology and size of the fronting beach, and its capacity to serve as a buffer between erosive waves and its backing feature, is another important factor in the occurrence of wave induced property erosion. The Oregon coast is divided into a series of littoral cells, with beaches confined between large headlands. The elevation of the beach-face junction varies considerably between cells due to differences in sediment grain sizes, and the quantities of sand in a particular cell. This elevation can also vary within a cell due to local effects such as the lowering of the beach by rip current embayments (Shih and Komar, 1994). A number of beaches with varying morphologies and buffering abilities are being monitored in Oregon to determine these elevations relative to NGVD 29, as well as to quantify typical summer and winter profiles and long term morphology changes. The erosion

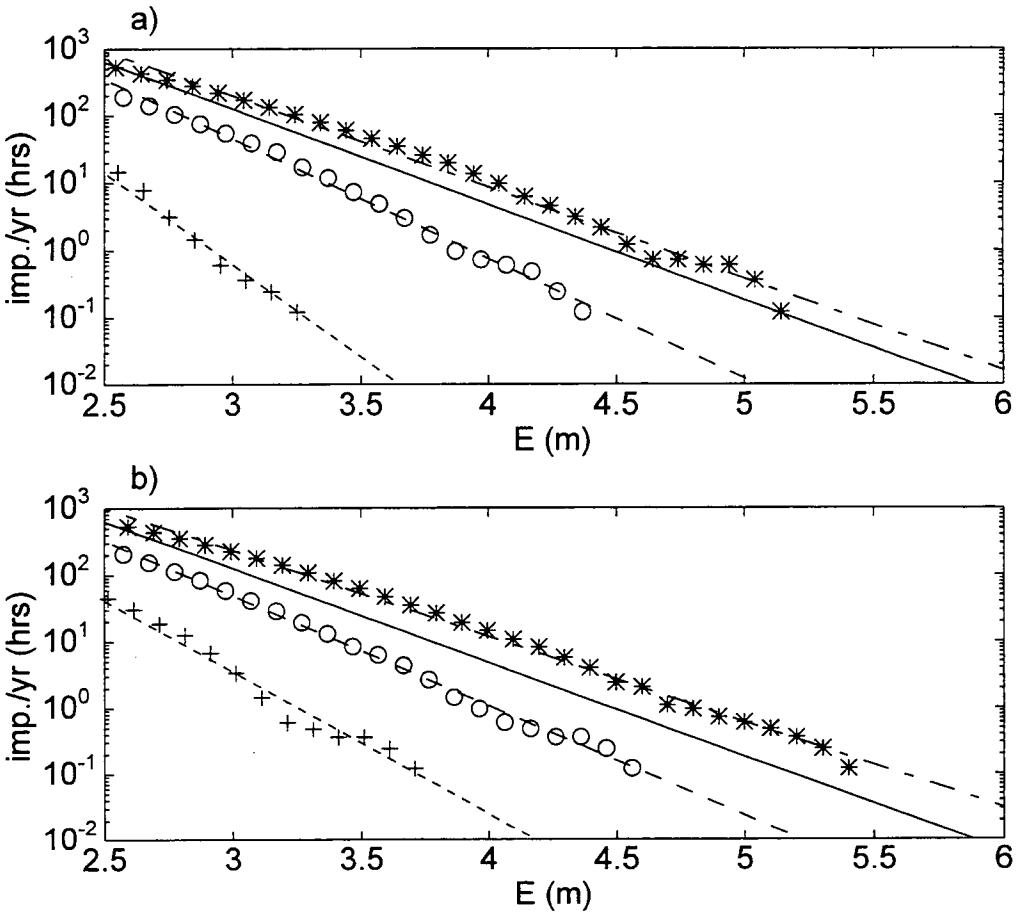

Figure 2.11. Total water level probability curves calculated with runup model (2.5), a), and runup model (2.1), b), for three representative beach slopes, β = 0.01 (data indicated by pluses and the fitted distribution by the dotted lines), 0.03 (circles and dashed lines) and 0.05 (asterisks and dash-dot lines). The solid lines (without data points) indicate results calculated from the simple runup (2.4).

susceptibility model has been applied to 13 sites along the central Oregon coast, accounting for 8 of the 13 littoral cells. More detailed information of the study sites and littoral cells is given in Appendix A of this thesis. The beaches are backed by sea cliffs, dunes and shore protection structures, and all have beach slopes($\beta \leq 0.05$) within the range of applicability of runup models derived from the data collected in this study.

Table 2.3 summarizes the model results as applied to the sites on the Oregon coast. The table lists the average winter beach slopes and the average winter elevations of the junction between the beach face and the respective backing feature. The number of hours per year in which 2% of runup maxima are predicted to reach or exceed E_j are given as compared to field observations concerning the morphologic stability of the particular site. Results have been tabulated for three different runup models, (2.4), (2.1) and (2.5), respectively. The first site, Jump Off Joe, is backed by the remains of a massive landslide which protrudes out onto the active beach profile, hence the very low E_j. The toe of the landslide is actively eroding and is reached by swash during most higher high tides in the winter. Nye Beach, immediately to the south of Jump Off Joe, is relatively stable and backed by a vegetated sea cliff. Figure 2.12 shows beach profile measurements, obtained on 6 June 1995, from these sites. The two lines are separated by only 70 m in the alongshore. The figure reveals that the beach fronting the landslide (pluses) is close to 1 m lower than Nye Beach (circles) over much of the profile. The models predict that the sea cliff at Jump Off Joe will be hit by wave runup much more often than any other site, including the cliff at Nye Beach, agreeing well with observations. The actual number of hours tabulated in Table 2.3, in which runup is expected to impact the property is of less importance than the relative difference between model predictions for various sites.

Figure 2.13a shows the alongshore variations in the elevation of the beach face junction throughout 20 km of the approximately 40 km long Newport littoral

Table 2.3. Wave impacts per year as compared to beach stability observations.

Site	Backing Feature	β	E_j	Impacts per year (hrs)			Observations
				(2.4)	(2.1)	(2.5)	
Jump Off Joe	Sea Cliff	0.034	2.90	173	97	104	severe erosion
Nye Beach	Sea Cliff	0.034	3.70	13	5	4	stable
Beverly Beach	Sea Cliff	0.043	4.02	4	7	5	erosion
Oceanside	Dune	0.023	3.60	18	3	2	stable/erosion
South Beach	Dune	0.026	4.12	3	.3	.2	accretion
Manzanita North	Dune	0.025	4.20	2	.2	.1	stable/erosion
Manzanita South	Dune	0.038	6.30	---	---	---	heavy accretion
Nestucca Spit	Dune	0.046	6.50	---	---	---	heavy accretion
C&L Ranch	Sea Wall	0.030	3.15	77	38	37	severe erosion
Pacific Shores	Sea Wall	0.039	3.65	15	12	10	erosion
San Marine	Sea Wall	0.030	3.75	11	4	3	erosion
Pacific Palisades	Sea Wall	0.052	5.30	---	.3	.2	accretion
Driftwood Shores	Sea Wall	0.033	7.50	---	---	---	heavy accretion

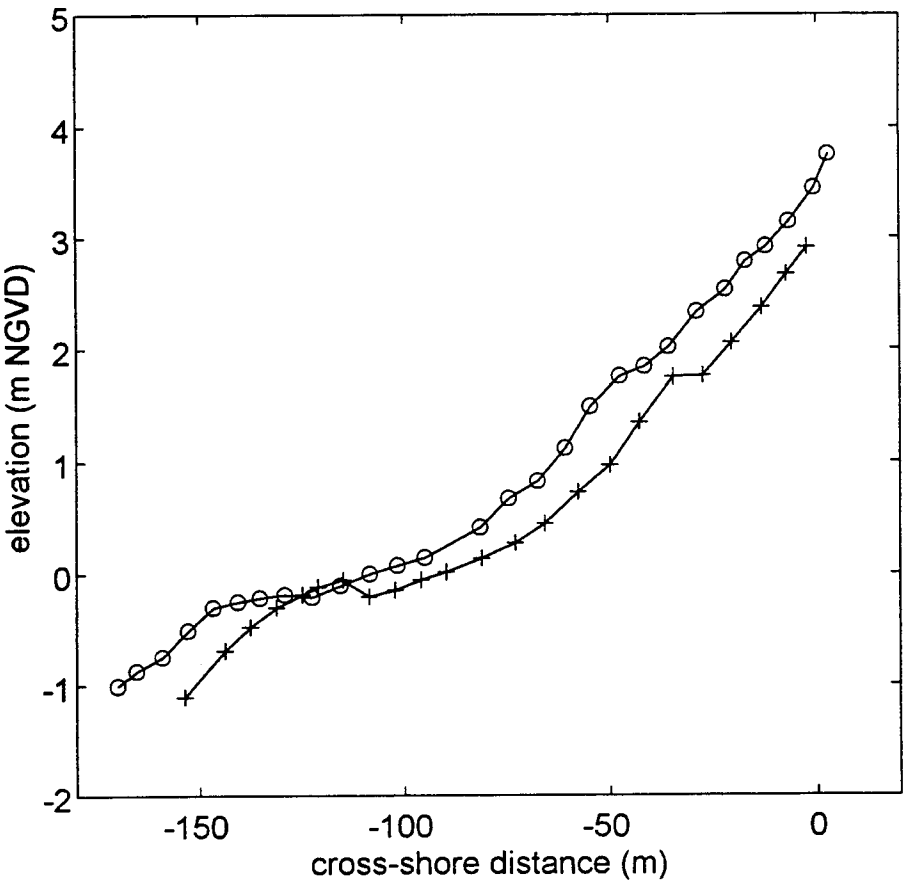

Figure 2.12. Beach profile measurements fronting the Jump Off Joe landslide (pluses) and the sea cliffs of Nye Beach (circles), both within the Newport littoral cell.

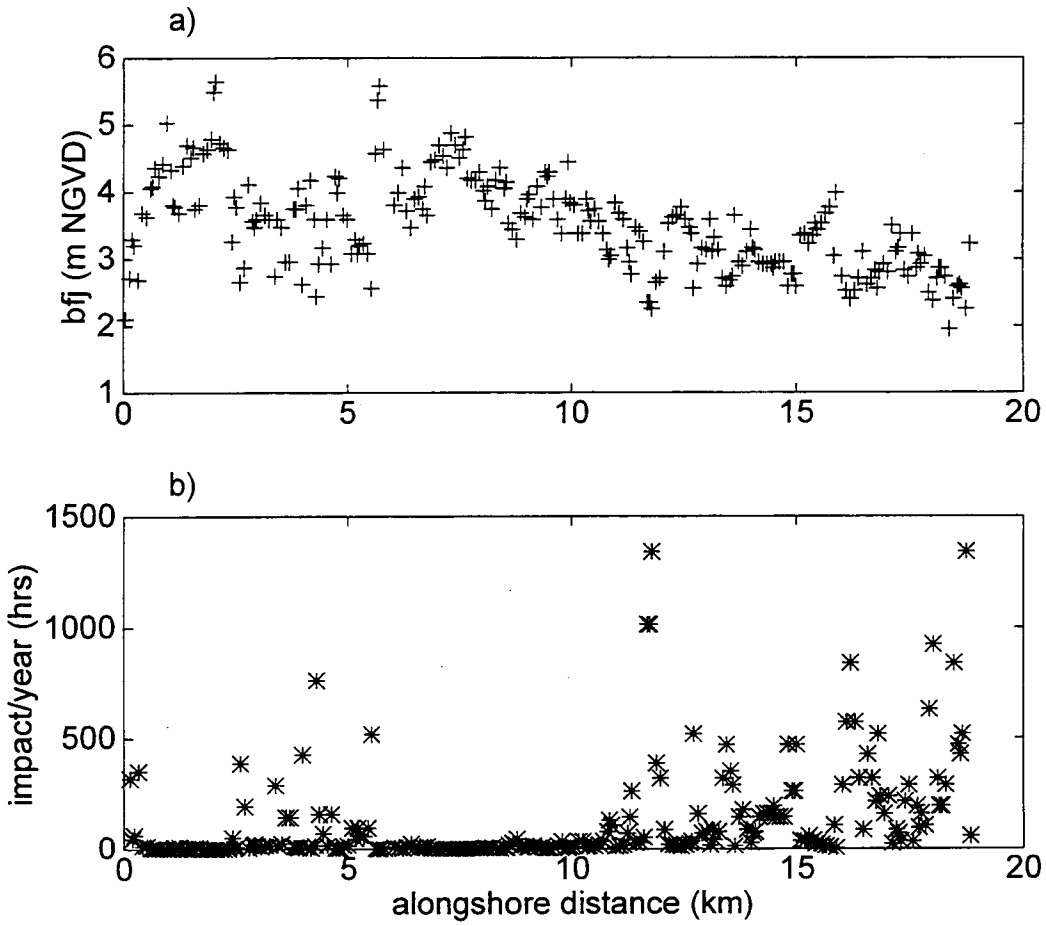

Figure 2.13. a) Elevations relative to NGVD 29 of beach face junctions within the Newport Littoral cell, with increasing distance being to the south. b) Model application (runup model (2.4)) throughout the cell.

cell within which Jump Off Joe and Nye Beach are located. The cell's northern limit, Yaquina Head, is given an alongshore location of 0 km in the figure. The beaches throughout the cell are backed by a variety of features including sea cliffs, dunes and shore protection structures. Foreshore beach slopes also have been measured throughout the cell, all having values less than 0.045 and therefore within the range from which the runup models were derived. However, due to the variability of beach slope, the simple runup model (2.4) is preferred in a littoral cell wide application. Figure 13b shows the results of the model being applied to the beach face junction elevations throughout the cell. The estimates of the frequency of impact reveal the relative susceptibility to erosion along this particular stretch of coastline. For example, the model suggests that the large sand dunes of South Beach, Oregon, located between 6 and 10 km from Yaquina Headland are relatively free from the danger of erosion from wave attack while the beaches further to the south, backed mostly by bluffs and sea cliffs, experience wave attack much more frequently. Again, these results are consistent with long term observations. Although the sea cliffs and bluffs are impacted by waves more frequently than the sand dunes with higher beach face junction elevations, they erode relatively slowly due to their resistance. Sand dunes respond more quickly to erosion events and have thus achieved beach face junctions more in equilibrium with the fronting beach and offshore wave conditions, thereby reducing the frequency with which waves reach the toe of the dunes. However, when waves and extreme water levels do reach the dune toe, the erosional response is rapid.

Model results appear to echo observed differences between littoral cells on the central Oregon coast. Cells that are known to have an abundant supply of sediment such the Umpqua littoral cell, in which Driftwood Shores is located, and portions of both Rockaway and Lincoln City littoral cells, which contain Manzanita South and Pacific Palisades respectively, experience little erosion. This is in agreement with the estimates given for these beaches in Table 2.3. In contrast, the Beverly Beach littoral cell is thought to be deficient in total sand volume and

therefore beaches within this cell have little buffering ability (Komar and Shih, 1993). Model results at this site demonstrate the importance of including morphology information, β, in a runup model. Beverly Beach is known to be more erosive than neighboring Nye Beach in the Newport cell. This difference is revealed in Table 2.3 only for the more complicated runup models (2.1) and (2.5).

2.5 Conclusion and Discussion

Extreme wave runup on high energy dissipative beaches has been characterized under a broad range of offshore wave and beach morphology conditions. Unlike runup on intermediate to reflective beaches, extreme statistics were found to be better parameterized simply by the deep-water wave height rather than by the Iribarren number. Measured extreme water levels on the central Oregon coast can be significantly different than predicted tides, but the extreme events typically do not coincide with extreme runup associated with large storm waves. Extreme total water levels have been predicted by fitting an extreme value distribution to a simulated total water level time-series. These predictions are used to determine the relative susceptibility of properties backing beaches to erosion, and model results agree well with qualitative observations.

With an appropriate model relating runup elevations to deep-water wave conditions, the relative frequency of occurrence of sea cliff or dune erosion can be predicted using historical wave, tide and beach morphology records at any coastal site. Coastal regulators, the anticipated users of the model, will have a quantitative method to determine the susceptibilities of properties to erosion and thus a rationale to establish setback distances for coastal developments. The model can also aid in the development of dune-management plans which balance the role of dunes in reducing future property losses versus development pressures such as those currently being experienced on the Oregon coast. For example, from the data given in Table 2.3 (runup model (2.4)), it appears that shorelines subjected to less than 1 hour of

attack per year tend to be stable, while those with more than 10 hours per year tend to experience erosion. In its present form the model may be used to evaluate the need for shore protection structures and may assist in their design. Future model development will attempt to include impact forces in order to predict erosion rates of both sea cliff and dune backed shorelines. Although not important at the Oregon site, adding the long-term sea level rise to the predicted extreme water levels can be easily accomplished at other sites. For application to beaches which are more reflective than those investigated here, extreme total water levels should be estimated using runup model (2.1) or (2.5). Unfortunately, for erodible beaches, the beach slope itself is a function of the incident wave characteristics and thus the appropriate beach slope needs to be chosen carefully. As we are interested in extreme runup impacting the beach face junction, beach slopes measured in the vicinity of the beach face junction are appropriate as the runup models were developed using local foreshore slopes.

The major weakness of the erosion susceptibility model is the simple relationships between extreme runup statistics and offshore wave conditions. Although runup measurements were taken over a broad range of wave and morphology conditions, the predictive models take no account of the possibility that the functional relationships between runup, wave characteristics and beach slope may change under more extreme conditions than those measured. The models also ignore large-scale morphology, including offshore bars and bathymetry, as well as large-scale alongshore variability. Furthermore, rip current embayments, which serve to greatly reduce the width of the beach fronting properties, are not accounted for. More runup data are needed on beaches between the dissipative extremes presented here, and the more intermediate to reflective systems (particularly with Iribarren numbers between 0.25 and 0.75) to further help in identifying appropriate runup models for a particular beach state.

CHAPTER THREE: LONGSHORE VARIABILITY OF WAVE RUNUP ON A HIGH ENERGY, DISSIPATIVE BEACH

3.1 Abstract

Wave runup data collected on the central Oregon coast during February 1996, stand in strong contrast to the considerable archive of runup data currently available in the literature. These runup data consist of swash elevation time series extracted from video recordings made using 3 cameras mounted on a headland located approximately 2 km from the study site. Overlap in the coverage of the 3 cameras allowed for runup elevations to be analyzed at any alongshore position over a 1.6 km stretch of beach. The significant vertical runup elevation was highly variable, and was found to be dependent on the foreshore beach slope which varied by a factor of 5 over the study area. Runup motions were dominated by low frequency (infragravity) energy with peak periods of swash spectra typically being approximately 200 seconds. Incident band energy levels were 2.5 to 3 orders of magnitude lower than the spectral peaks. A broad saturated region of the runup spectra was observed with a f^{-4} roll off extending to lower frequencies than previously observed. At infragravity frequencies, motions were found to be coherent over alongshore length scales in excess of 1 km. However, due to the low frequency nature of the runup motions, the 1.6 km array was too short to be able to resolve most edge wave modes.

3.2 Introduction

Wave runup, loosely defined as the time-varying location of the shoreward edge of water on the beach face, is of considerable importance in determining the susceptibility of coastal properties to wave induced erosion. Runup (R) is typically expressed in terms of a vertical excursion consisting of two components: a super-

elevation of the mean water level, called setup ($\bar{\eta}$), and fluctuations about that mean, called swash (S). Field investigations of runup dynamics have typically taken place on intermediate to reflective beaches (Holman and Sallenger, 1985; Holman, 1986; Holland, 1995) and low energy dissipative beaches (Guza and Thornton, 1982; Raubenheimer *et al.*, 1995; Raubenheimer and Guza, 1996). The current work extends these analyses to the high energy, dissipative beaches common in the Pacific Northwest of the U.S. It is not uncommon for these low sloping beaches to experience deep-water significant wave heights exceeding 6.0 m. The present investigation summarizes the variability of wave runup statistics and spectral response over a 1.6 km alongshore distance from a 1.5 hour data run on Agate Beach, Oregon. A brief literature review of runup is given in section 3.2, and the study site and experimental methods are described in section 3.3. Results are presented in section 3.4, and are followed by a discussion and summary.

3.3 Wave Runup Dynamics

Based on laboratory observations of monochromatic waves (Hunt, 1959), as well as an extensive set of field observations on the intermediate to reflective beach of the Field Research Facility in Duck, North Carolina (Holman and Sallenger, 1985; Holman, 1986), wave runup has been parameterized by

$$\frac{R_v}{H_s} = c\ \xi_o \tag{3.1}$$

where R_v is the vertical runup excursion normalized by H_s, the deep-water significant wave height, c is a dimensionless constant and ξ_o is the Iribarren number. The Iribarren number is a non-dimensional "surf similarity" parameter which has been found to describe a number of surf zone processes (Battjes, 1974), and is given by

$$\xi_o = \frac{\beta}{(H_s/L_o)^{1/2}} \tag{3.2}$$

where β is the beach slope in radians (assumed small, so that $\tan \beta \simeq \sin \beta \simeq \beta$), L_o is the deep-water wave length given as $L_o = g\,T^2/2\pi$, g is the acceleration due to gravity and T is the peak incident wave period. Low Iribarren numbers, $\xi_o < 1.25$, typically indicate dissipative shorelines (Holman and Sallenger, 1985), while higher values indicate more reflective surf zones. A linear relationship between wave runup and Iribarren number has been proposed by a number of other researchers including Battjes (1971) and van der Meer and Stam (1992). The hypothesis of equivalency, which links monochromatic results and random runup statistics, is often used in association with (3.1) to calculate the distribution of runup maxima from the joint distribution of incident wave heights and periods.

Through non-linear interactions, incident band energy is transferred to both higher and lower frequencies throughout the surf zone (Longuet-Higgens and Stewart, 1962). On dissipative beaches, infragravity energy (with frequencies of roughly 0.05 to 0.003 Hz) tends to dominate the inner surf zone, especially the swash. In contrast to the above linear dependence on ξ_o, Guza and Thornton (1982) found that on relatively low energy dissipative beaches, the infragravity component of R_v varied linearly with the offshore wave height, while the incident band component remained constant. When analyzing a dissipative subset (low Iribarren numbers) of their data, Holman and Sallenger (1985) also showed this difference in behavior between the infragravity and incident bands of runup.

Miche (1951) hypothesized that monochromatic incident waves can be thought of as having both a progressive and a standing component, and that the amplitude of swash oscillations is proportional to the amount of shoreline reflection and thus proportional to the standing wave amplitude. The standing wave amplitude at the shoreline reaches a maxima with waves just large enough to be breaking, and therefore can be termed saturated as a further increase in wave height simply

increases the amplitude of the progressive component, which dissipates through wave breaking and has zero shoreline amplitude. Saturation therefore implies that the swash amplitude does not increase with increasing offshore wave height, a concept used to describe the aforementioned incident band results of Guza and Thornton (1982). Qualitatively, Miche's hypothesis has been confirmed in the laboratory (Battjes, 1974; Guza and Bowen, 1976), in the field (Huntley *et al.*, 1977; Guza and Thornton, 1982; Guza et al., 1984) and more recently in the application of a numerical model based on the one-dimensional depth-averaged nonlinear shallow water equations (Raubenheimer *et al.*, 1995 and Raubenheimer and Guza, 1996). Carrier and Greenspan (1958) analytically solved the non-linear inviscid, shallow water wave equations on a planar beach and showed that a monochromatic, non-breaking standing wave solution exists when

$$\epsilon_s = \frac{a_s \omega^2}{g \tan^2 \beta} \leq 1 \tag{3.3}$$

where ϵ_s is another similarity parameter in which a_s is the vertical swash amplitude at the shoreline and ω is the wave angular frequency. Wave breaking initiates at $\epsilon_s \simeq 1.0$, and the shoreline amplitude has been shown to continue to increase until it reaches a saturation (critical) value ϵ_s^c. Published estimates of this critical value range from 1.25 (Guza and Thornton, 1982) to 3.0 ± 1.0 (Guza and Bowen, 1976). Guza *et al.* (1984) showed that by combining Miche's hypothesis with (3.3) the normalized vertical runup excursion becomes

$$\frac{R_v}{H_s} = \begin{cases} \left(\frac{\pi}{2\beta}\right)^{1/2} & : \xi_o \geq \xi_c \quad : \textit{reflective} \\ \frac{\xi_o^2}{\pi} & : \xi_o < \xi_c \quad : \textit{saturated} \end{cases} \tag{3.4}$$

where $\xi_c = (\pi^3/2\beta)^{1/4}$. Note that in the saturated region of (3.4), R_v is independent of the wave height and has a β^2 dependence rather than the linear relationship with beach slope predicted by (3.1).

In analogy to the above monochromatic results, Huntley *et al.*(1977) suggested that for broad band swash, incident band frequencies in the vertical runup energy density spectrum would become saturated and have the form

$$E(f) = \alpha f^{-4} \tag{3.5}$$

where α is a dimensional constant. Huntley *et al.* (1977) presented field results showing a f^{-4} spectral decay within this band, and by combining (3.3) with (3.5) suggested a universal form for the runup spectrum

$$E(f) = [\epsilon_s^{c^*} g \beta^2/(2\pi f)^2]^2 \tag{3.6}$$

where $\epsilon_s^{c^*}$ is now a dimensional constant related to the bandwidth of the saturated spectrum. Runup energy densities in the saturated band are independent of offshore wave conditions as wave breaking prevents the magnitude of swash oscillations in the saturated band from increasing past a certain level which depends on beach slope. Guza and Thornton (1982) showed similar saturated spectra from field data but with a f^{-3} roll off, a result possibly explained by differences in measurement techniques. Raubenheimer and Guza (1996) presented more runup data with incident band saturation and their field observations, as well as results from the numerical model Rbreak (Kobayashi *et al.*, 1989), both show a f^{-4} roll off. The present results also show this f^{-4} spectral decay over a broad saturated band width, extended to lower frequencies than previously reported. However, the universality of (3.6) is cast into doubt based on multiple realizations of $E(f)$ with similar wave conditions and a strongly variable beach slope.

3.4 Field Experiment

Runup data were obtained during the High Energy Field Experiment at Agate Beach in Newport, Oregon during February 1996 as one component of an investigation into the dynamics of high energy dissipative beaches. Agate Beach

stands in direct contrast to the more reflective Duck, North Carolina, site of many previous runup investigations, as large amplitude, low frequency motions are the dominant forcing within the inner-to-mid surf zone. The field experiment was designed to characterize the temporal and spatial scales of these motions and their role in suspended sediment transport. *In-situ* instrumentation, consisting of current meters, suspended sediment sensors and pressure sensors, were deployed in the inner surf zone in a cross-shaped pattern with cross-shore and longshore arrays of approximately 120 X 324 m. Video monitoring of wave breaking intensity, as well as detailed surveys of the foreshore and offshore bathymetry, were also performed. The environmental conditions during the month of February 1996 are shown in Figure 3.1. The experiment lasted for 11 days, 7 February to 17 February, during which the significant deep-water wave height ranged from 1.4 to 4.1 m (Figure 3.1a), peak wave periods ranged from 5 to 17 s (Figure 3.1b), and the semi-diurnal tide typically had a 2 to 3 m vertical excursion (Figure 3.1c). The wave height and period data were obtained from the Coastal Data Information Program (CDIP) buoy offshore from Bandon, Oregon located in approximately 64 m of water, 100 km to the south of the study site. During the experiment the wave heights from the CDIP buoy compared well with data from the microseismometer system operated by Oregon State University at the Marine Science Center in Newport, Oregon as well as the deep-water buoy of the National Data Buoy Center (NDBC) of NOAA offshore from Newport. Although the latter two data sources are closer to the experiment site, the microseismometer typically provides a poor estimate of wave periods and the NDBC buoy has been found to over predict large wave heights by approximately 10% (Tillotsen and Komar, 1997). The beach sand at Agate Beach has a median diameter of 0.2 mm, and although the foreshore slope varied greatly in the longshore, at any cross-shore transect the foreshore slope (averaging 1:70) changed relatively little throughout the experiment. The definition of foreshore slope in this paper is taken to be the best linear fit of the measured beach surface between $\pm$ two standard deviations from the mean raw runup elevation.

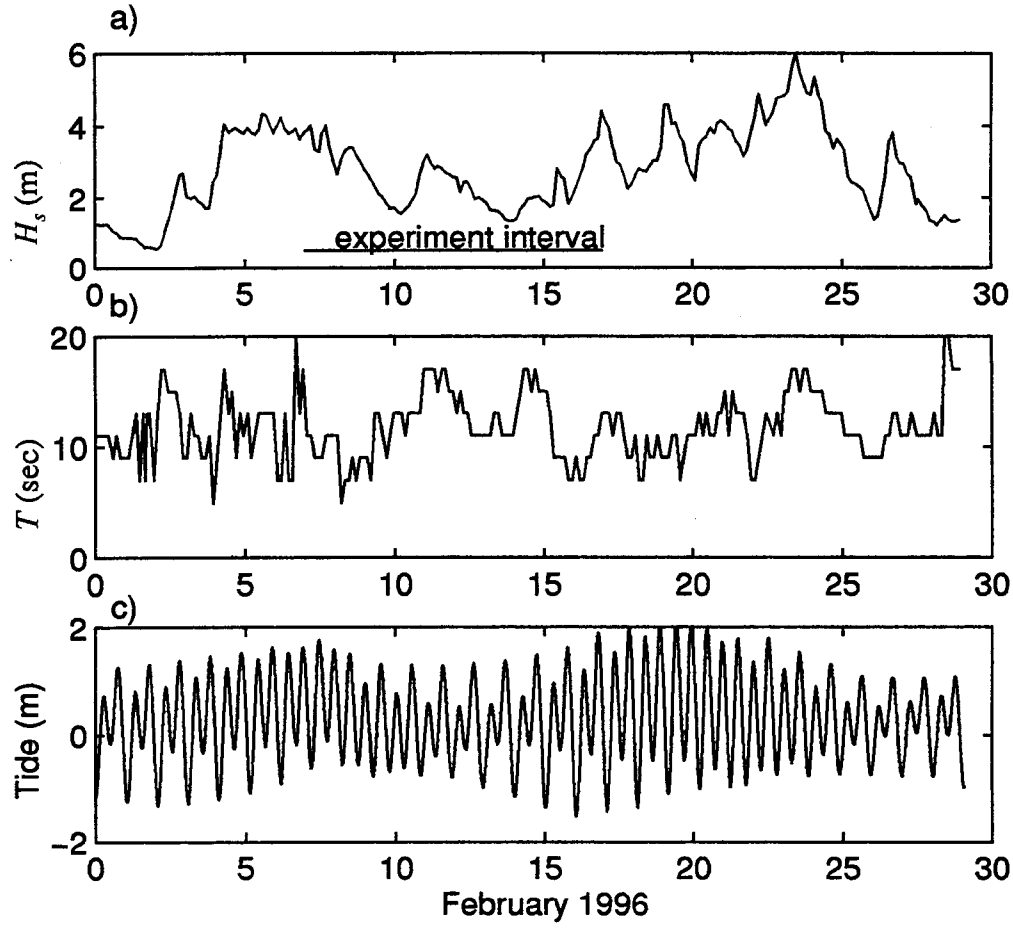

Figure 3.1. Deep-water significant wave height a), peak wave period b) and tide elevation c) during the High Energy Beach Experiment of February 1996.

Figure 3.2 shows an oblique (Figure 3.2a) and plan (Figure 3.2b) view of ten minute time-averaged video exposures taken at Agate Beach at low tide on 11 February 1996. Regions of higher image intensity result from waves breaking preferentially over shallow bathymetric features. The plan view, with the positive x direction being offshore and positive y direction being to the south, reveals two, and possibly three, fairly uniform alongshore sandbars offshore from the study area. The pluses indicate the locations of the *in-situ* instrumentation. One can infer from the location of the instruments, which were submerged at high tide, and the position of the seaward-most sand bar, the extremely large cross-shore length scales O (1 km) typical of this beach.

Video recordings of swash were made using 3 cameras mounted on Yaquina Head, a promontory located approximately 2 km to the north of the *in-situ* instrumentation. Overlap in the field of view of the three cameras allowed for continuous coverage of runup over an alongshore distance of over 1.5 km. The data discussed below consist of 1.5 hour swash elevation time series measured along 33 cross-shore transects spaced every 50 m in the longshore on 11 February 1996 from 15:59 to 17:29 PST. During this data run the deep-water significant wave height was 2.3 m, the wave period was 13 s and the tide was high. Figure 3.3 shows a snapshot from the runup camera aimed furthest north. Overlaid in the field of view are the cross-shore transects at which runup was digitized, for this particular camera, extending from an alongshore position of y=-1200 m to y=-950 m, spaced every 50 m. The middle camera covered from y=-950 m to y=-350 m, and the camera pointed to the south extended the runup coverage to y=400 m. Vertical swash elevation time series were extracted from the video recordings using the "timestack" method as outlined by Aagard and Holm (1989) and Holland and Holman (1993). Using the known geometric transformation between ground and image coordinates, the light intensity of each pixel in the cross-shore transect was digitized. The runup position at each video sample time is the landward-most identifiable edge of water determined via standard image processing algorithms with

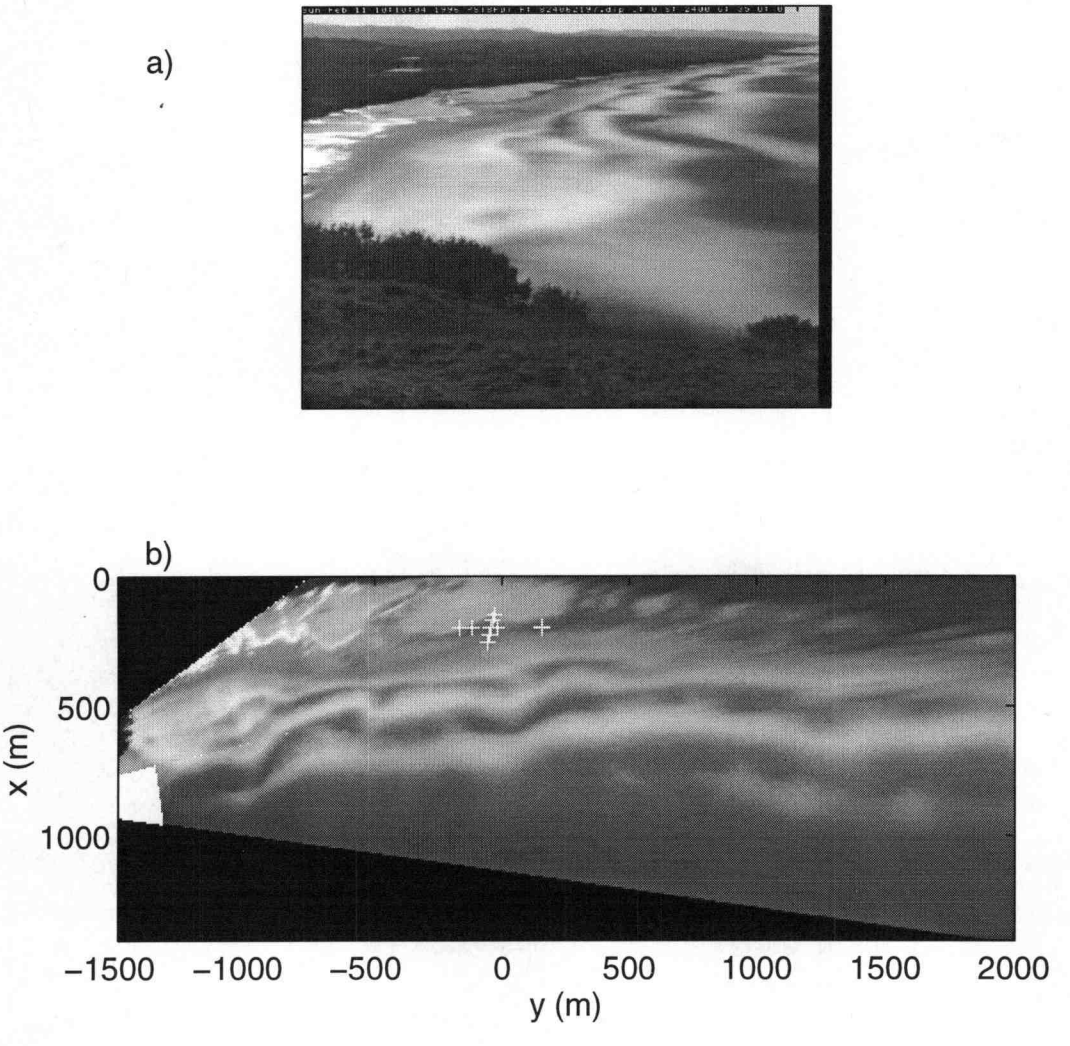

Figure 3.2. Oblique (a) and plan (b) view images from 10 minute time-averaged video exposures of Agate Beach, Oregon on 11 February 1996 at low tide. Pluses in the plan view indicate the locations of *in-situ* instrumentation.

Figure 3.3. "Snap-shot" video image taken from northern most facing runup camera at 16:00 PST on 11 February 1996. Solid lines indicate the locations of cross-shore transects, spaced at 50 m, over which runup was digitized.

manual refinements. Figure 3.4 is an example of a "timestack" showing temporal and spatial runup variability. Holman and Guza (1984) and Holland *et al.* (1995) demonstrated that runup extracted from a video record roughly corresponds to data acquired with resistance wire runup gauges supported less than a few centimeters above the beach face. The vertical resolution of the video technique varies with distance from the cameras but was typically less than 2 cm.

To extract runup elevations along cross-shore transects from video signals using the "timestack" technique, the geometry of the beach is needed in addition to the geometry of the camera. To obtain the beach surface over such large cross-shore and alongshore distances, differential global positioning system (DGPS) surveying techniques were employed. The survey system was installed on a 6-wheeled amphibious "buggy" which by traveling at approximately 5 m/s, yielded a dense mapping of the large beach surface in only a few hours (Plant and Holman, in prep.). Figure 3.5 is a contour map of Agate Beach obtained on 11 February 1996. The dots correspond to the individual survey measurements, and the solid lines reveal the elevation contours referenced to the U.S. National Geodetic Vertical Datum (NGVD) of 1929. The asterisks indicate the locations of the *in situ* instrumentation, and the solid lines perpendicular to the contours give the locations of the 33 transects at which runup time series were extracted and analyzed. The 1600 m runup array has been separated into two sections based on differences in the foreshore beach slope as evidenced by the contour lines and differences in spectra calculated at each of the cross-shore transects. Section I, with a relatively steeper foreshore, consists of both the north, y=-1200 m to y=-850 m, and the south, y=-150 m to y=400 m, regions of the study area, with section II being the middle, y=-800 m to y=-200 m, region. Two typically low flowing drainages from the backing bluff had more substantial flows during the experiment due to heavy rainfall preceding the experiment. These streams deposited sediment in deltas causing the extremely flat beaches in section II.

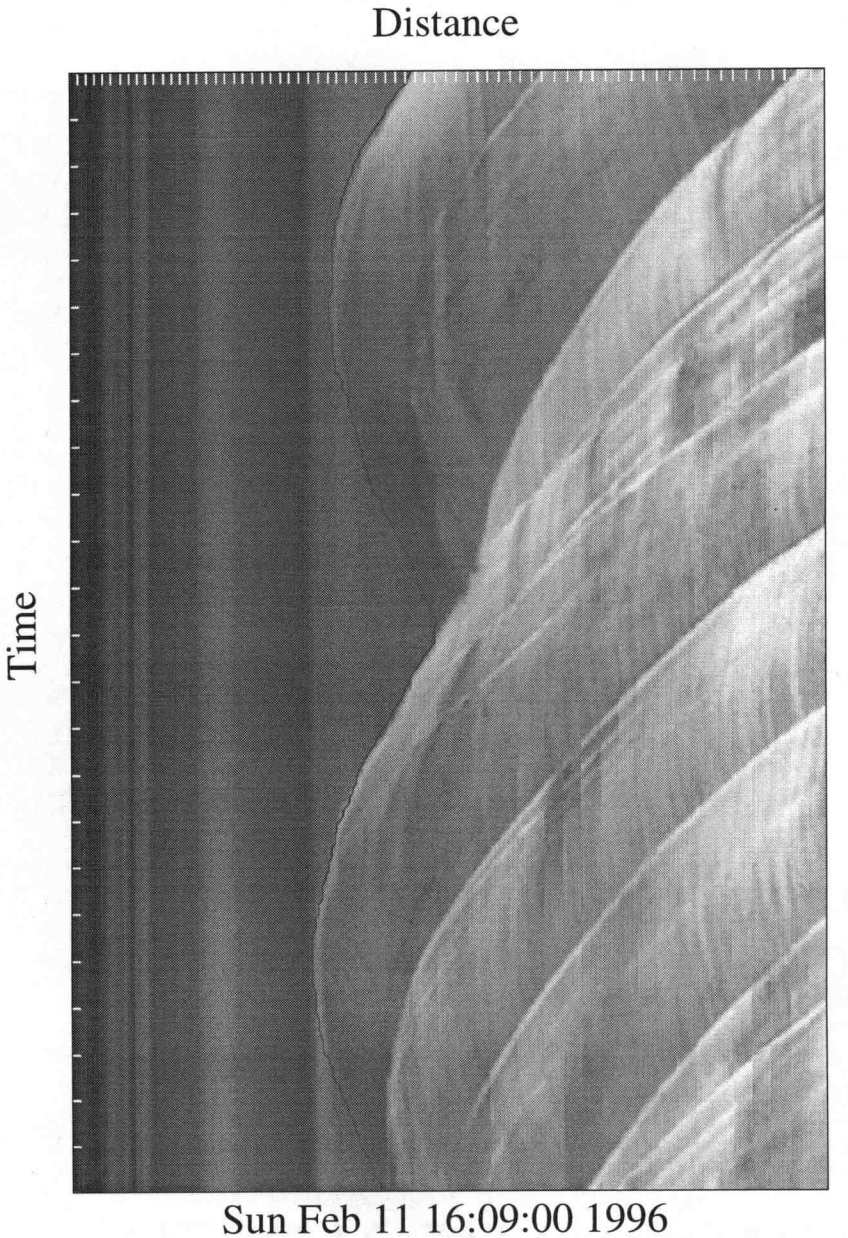

Figure 3.4. Video timestack for the 15:59 PST run at transect y= -1200 m. Intensity patterns vary with time (down the page) and with cross-shore position (across the page). The dark line is the digitized landward edge of runup.

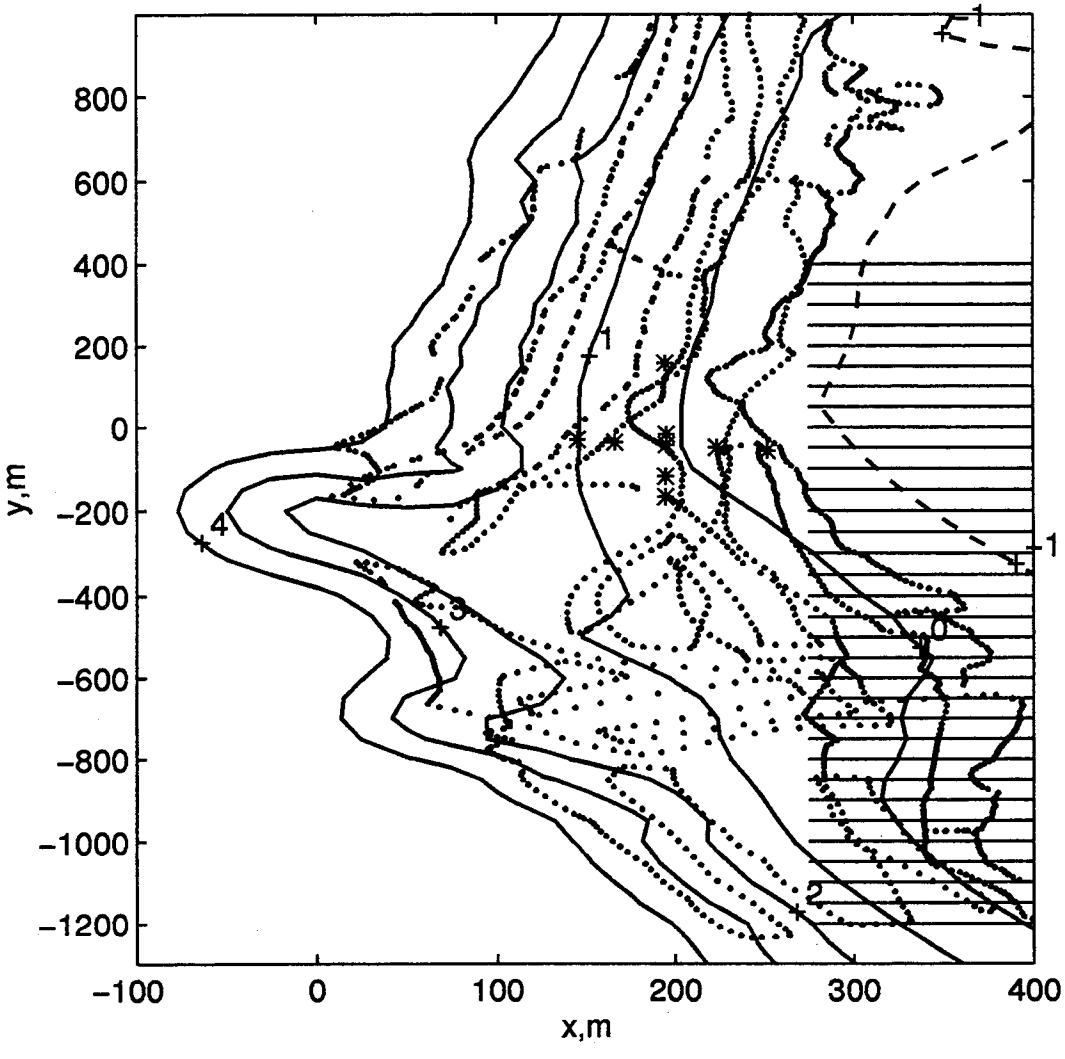

Figure 3.5. Contour map of the foreshore beach survey from 11 February 1996. The dots are the positions of actual survey measurements and contour intervals (solid lines), relative to NGVD 29, are spaced at 1 m. The solid lines perpendicular to the contours indicate the locations of cross-shore transects where runup was measured, at 50 m intervals, with a total alongshore coverage of 1600 m. The asterisks indicate the locations of the *in-situ* instrumentation.

3.5 Results

Analysis of the runup data has been separated into bulk statistics, frequency dependence and alongshore scale and structure. Results for each category are summarized below.

3.5.1 Runup Statistics

In Figure 3.6a the solid line shows the alongshore variability of the significant vertical swash excursion, R_s obtained from the time-series of 33 individual cross-shore transects. R_s, defined as 4σ where σ^2 is the total variance of the runup elevation time series, varies by a factor of two over the 1600 m study region. A clear reduction in R_s is evident section II, y=-800 to y=-200. Also shown in Figure 3.6a as the dash-dot line is the foreshore beach slope, β, as a function of alongshore distance. The foreshore slope varies by a factor of 5 over the study area, ranging from 0.005 to 0.025. The average slope in section I is 0.019 while in section II it is 0.009. The apparent dependence of R_s on β lends credibility to the parameterization of runup with the foreshore slope, defined as above or in a similar fashion. Figure 3.6b shows a power law dependence between the two parameters yielding an exponent of 0.41. The best fit in log-log space is shown as the solid line in the figure. The runup data have been band partitioned to determine the sea-swell (incident band) component (0.05 Hz $< f <$ 0.2 Hz) and the infragravity band component ($f <$ 0.05 Hz) of R_s. For each of the 33 transects, the infragravity band contained over 95% of the total runup variance, and the incident band was saturated. Figure 3.6c reveals a linear relationship between the sea-swell component of the significant runup elevation, R_s^{ss}, and the foreshore slope. This result is in contrast to the squared relationship predicted for saturated runup by (3.4) and results recently published by Raubenheimer and Guza (1996) that also agree with (3.4).

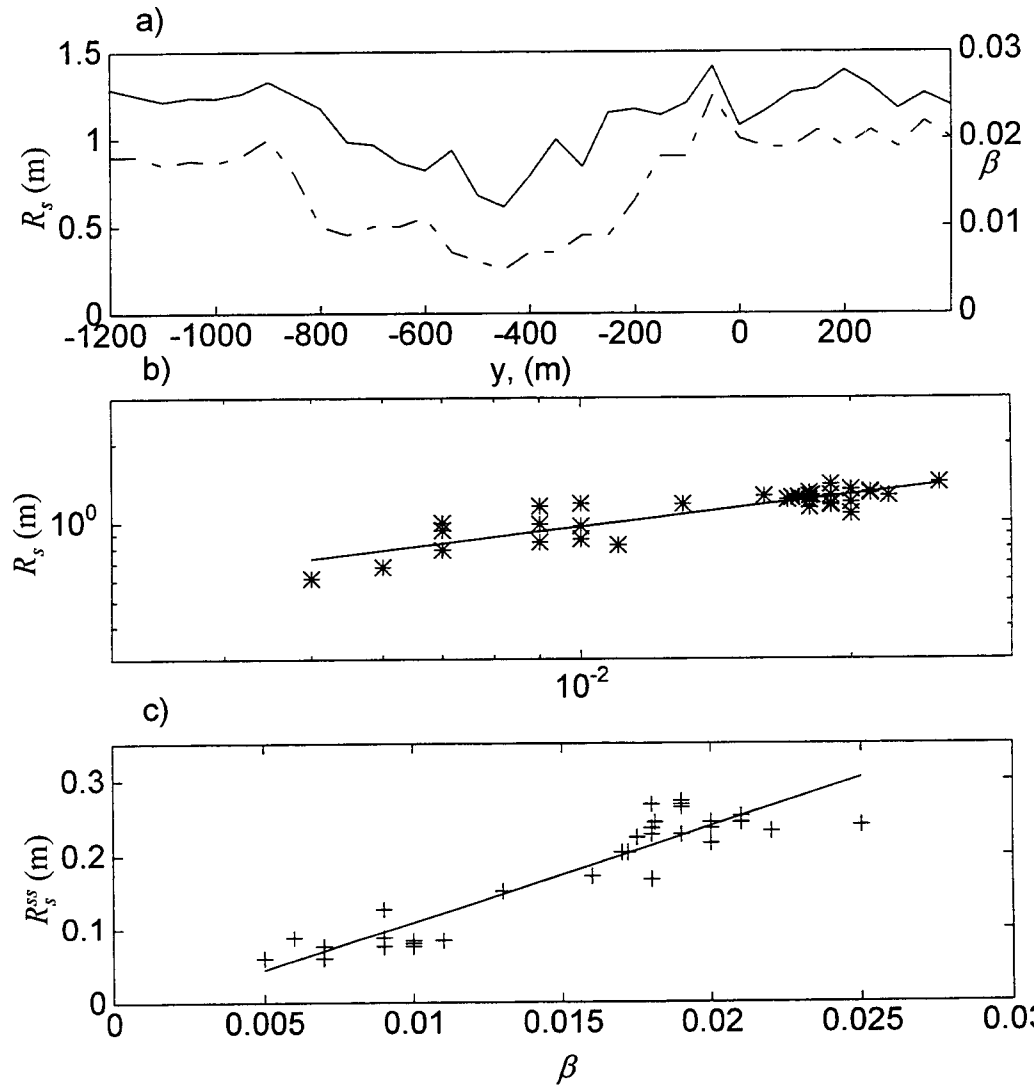

Figure 3.6. a) Significant vertical runup elevation (solid line) and foreshore beach slope (dashed-dot line) as a function of alongshore distance. b) Total significant runup versus beach slope (asterisks) and best fit in log-log space (line). $R_s = 6.2\ \beta^{0.41}$ c) Sea-swell significant runup versus beach slope (pluses) and best fit line. $R_s^{ss} = 13.0\ \beta - 0.02$, $r^2 = 0.87$.

The above results were obtained from a single 1.5 hr data run in which 33 individual cross-shore transects were analyzed. Figures 3.7 and 3.8 show results that include data obtained from other runs during the High Energy Beach Experiment, as well as data from runup experiments on other dissipative Oregon beaches. These data were also obtained utilizing video techniques and are described in Ruggiero *et al.* (in press) and Chapter 2. In Figure 3.7a the band partitioned, normalized significant runup is plotted versus the Iribarren number. The pluses represent the incident band and the circles the infragravity band. All of the data fall in the extremely dissipative range of Iribarren numbers, $\xi_o < 0.5$, and neither frequency band demonstrates a strong dependence on this similarity parameter. In Figure 3.7b it is apparent that a linear relationship between R_s and H_s is more pronounced in the infragravity band than in the incident band, another indication of saturation. The total significant runup, including all frequencies, is shown in Figure 3.8 to have a (weak) linear dependence on wave height. The best linear fit through the data is also shown on the figure, and gives the relationship

$$R_s = 0.37(\pm 0.05)H_s + 0.28(\pm 0.23) \quad r^2 = 0.45 \tag{3.7}$$

In an analysis of extreme runup statistics from the same data (Chapter 2), the two percent exceedence elevation of runup maxima, $R_{2\%}$, was also found to be better parameterized by the deep-water significant wave height than by the Iribarren number. The linear dependence between significant runup elevation and wave height found by Guza and Thornton (1982), $R_s \propto 0.7\, H_s$, was much stronger than found here for the Oregon data, (3.7).

3.5.2 Frequency Dependence

Figure 3.9 shows a sample 5 minute runup time series from two sites: data collected at the FRF during the DELILAH experiment (Figure 3.9a, from Holland (1995)), and data from Agate Beach during the High Energy Field Experiment of 1996 (Figure 3.9b). In each panel, time-series from multiple cross-shore transects

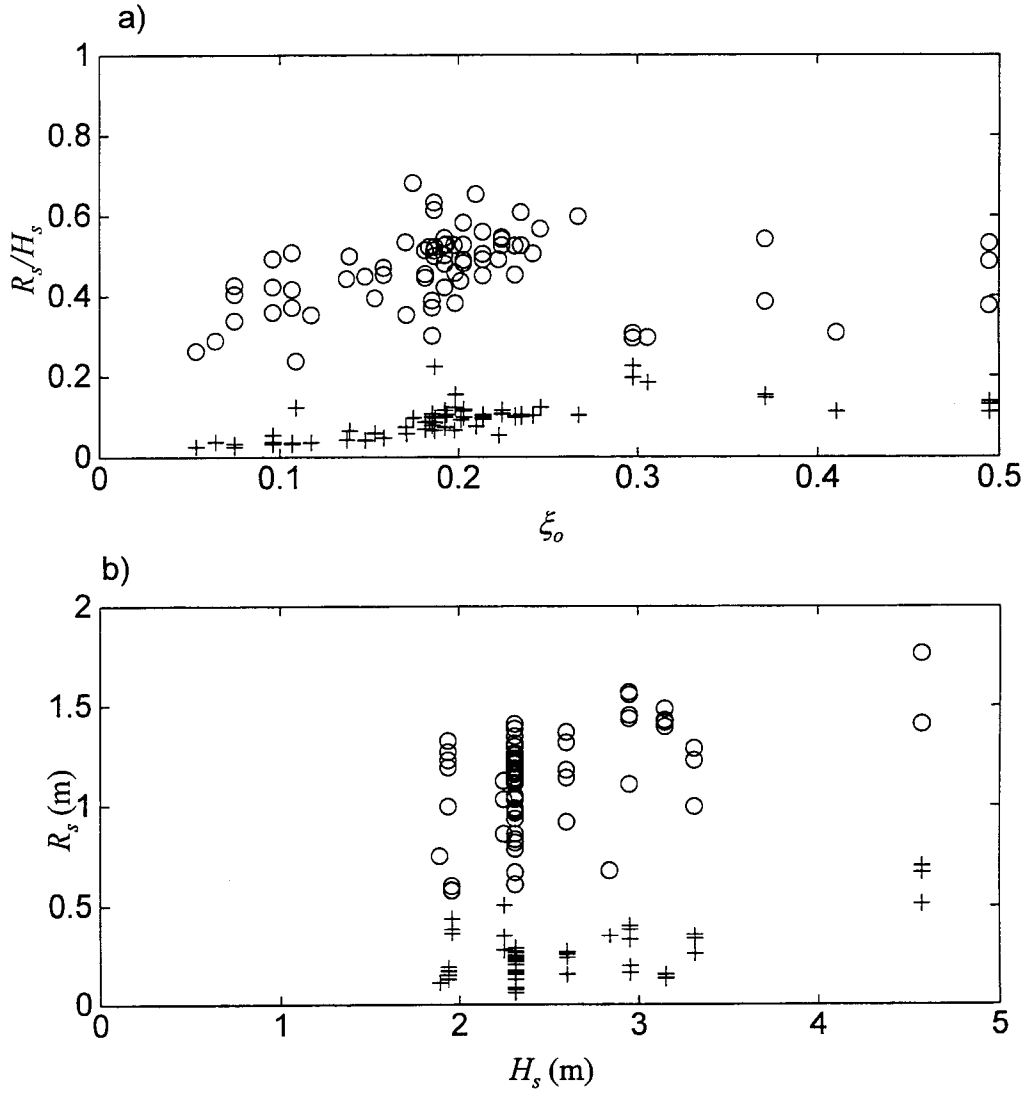

Figure 3.7. (a) Normalized significant runup elevation as a function of Iribarren number obtained from low and high frequency runup variances. Circles represent low frequencies ($f < 0.05$ Hz) and pluses indicate high frequencies ($f >$ 0.05 Hz). (b) Dimensional significant runup elevation versus significant wave height again separated by frequency band.

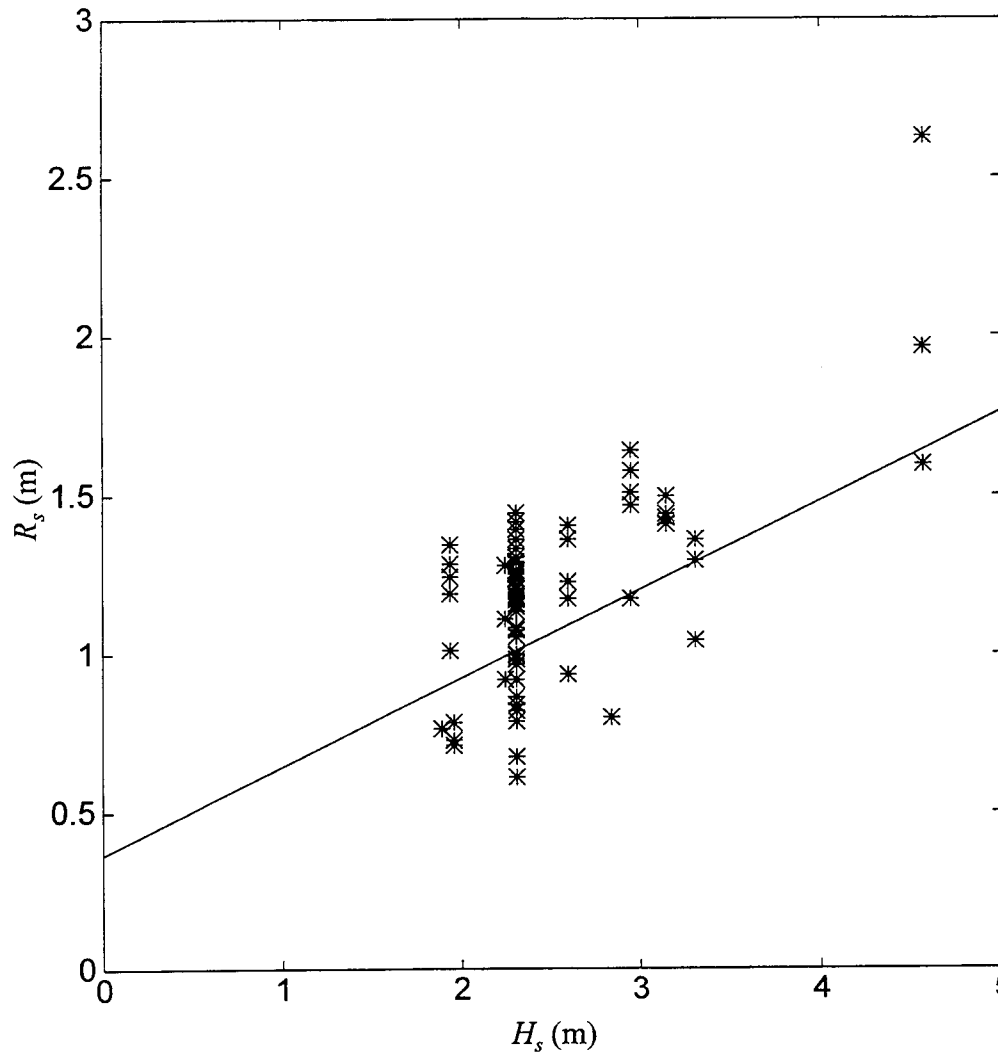

Figure 3.8. Total significant vertical runup elevation versus deep-water significant wave height.

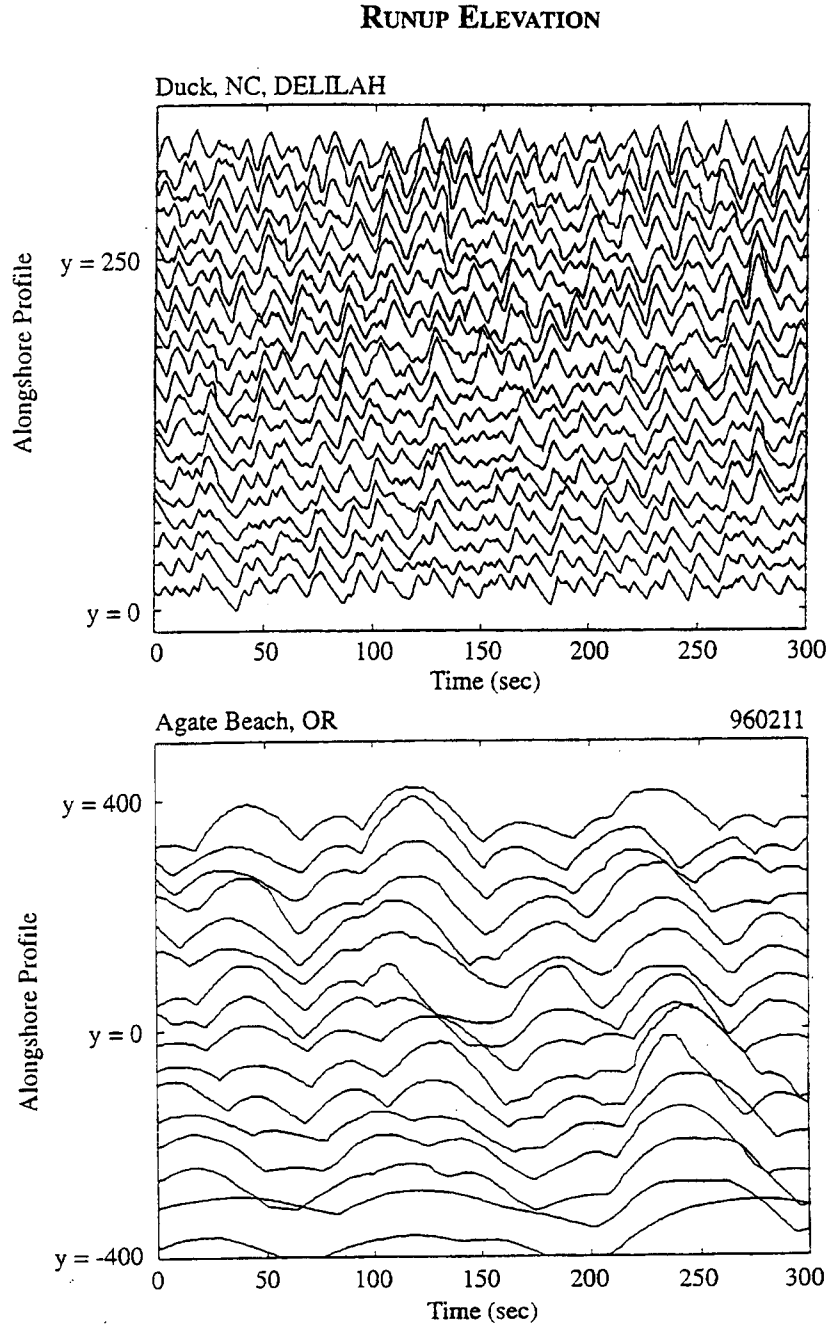

Figure 3.9. Typical 5 minute runup time series from a) the 17 October 1990, 13:38 EST data run of the DELILAH experiment in Duck, NC taken from Holland (1995), and b) the 11 February 1996, 15:59 PST data run from the High Energy Beach Experiment in Newport, OR. Cross-shore transects at which runup was measured are offset vertically. The transects are spaced at 10 m in a) and at 50 m in b).

have been offset vertically to reveal structure in the longshore (the FRF data is spaced at 10 m in the longshore). The FRF data show a dominant incident wave signal having a period of approximately 15 seconds, while the Oregon data show only a few discernible runup maxima over the 5 minute record, clearly indicating the very low frequency infragravity nature of the signal. Individual wave crests can be followed over large alongshore distances at incident band frequencies in Figure 3.9a and at infragravity band frequencies in Figure 3.9b.

Figure 3.10a shows the frequency spectrum for each of the 33 cross-shore transects analyzed from the 15:59 to 17:29 PST data run on 11 February 1996. There appears to be a clear division between spectra from section I, transects with steeper foreshore slopes, and spectra from the shallower sloping section II. Figure 3.10b displays a representative spectrum from each section. Spectra were calculated from runup elevation time series from which both the mean and the tide have been removed. Band averaging resulted in 18 degrees of freedom with a bandwidth of 0.0017 Hz. The most obvious feature in the spectra are the energy peaks at extremely low frequencies, approximately 0.0043 Hz, for both section I and section II. Although the two spectra have energy peaks at similar low frequencies, the spectrum from section I, y = -1100 m, has more energy at all higher frequencies than the spectrum from section II, y = -600 m. There is a sharp roll off in energy beyond the peak frequencies and at the cutoff between the infragravity and incident bands, 0.05 Hz, the spectra have dropped 2.5 to 3.0 orders of magnitude in energy. The asterisks in Figure 3.10a,b indicate the peak frequency of the deep water waves for this particular run.

Figure 3.11 shows averages of the spectra calculated from the transects in each of the two sections in a log-log plot. The average spectra are relatively white at low infragravity frequencies, followed clearly by a red saturated region, approximately proportional to f^{-4}, extending to much lower frequencies, O(0.01 Hz) than previously reported by other researchers. Both Huntley (1977), and

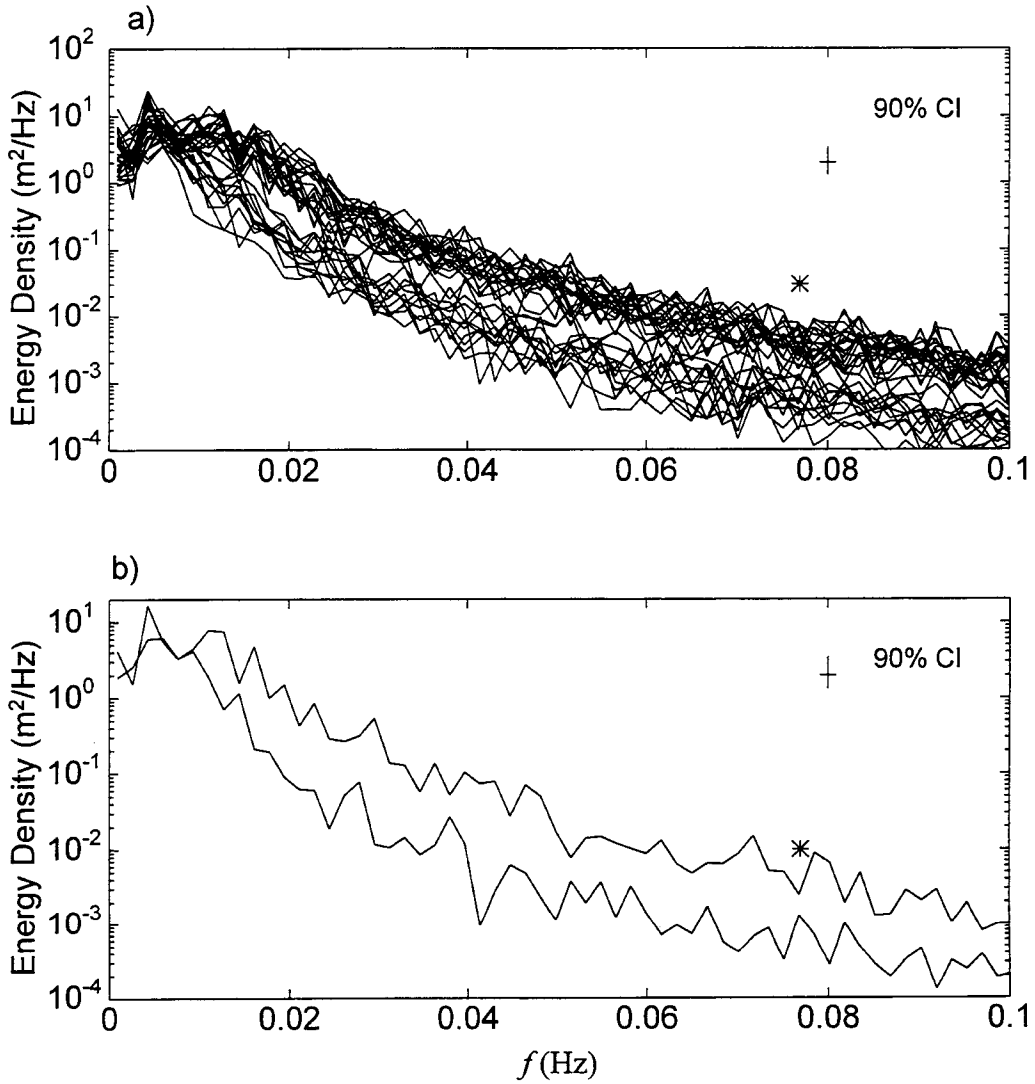

Figure 3.10. a) Observed runup energy density spectra from all 33 transects and b) representative spectra from y = - 1100 in section I (top line) and y= - 600 m from section II. The asterisks indicates the peak period of the deep-water waves.

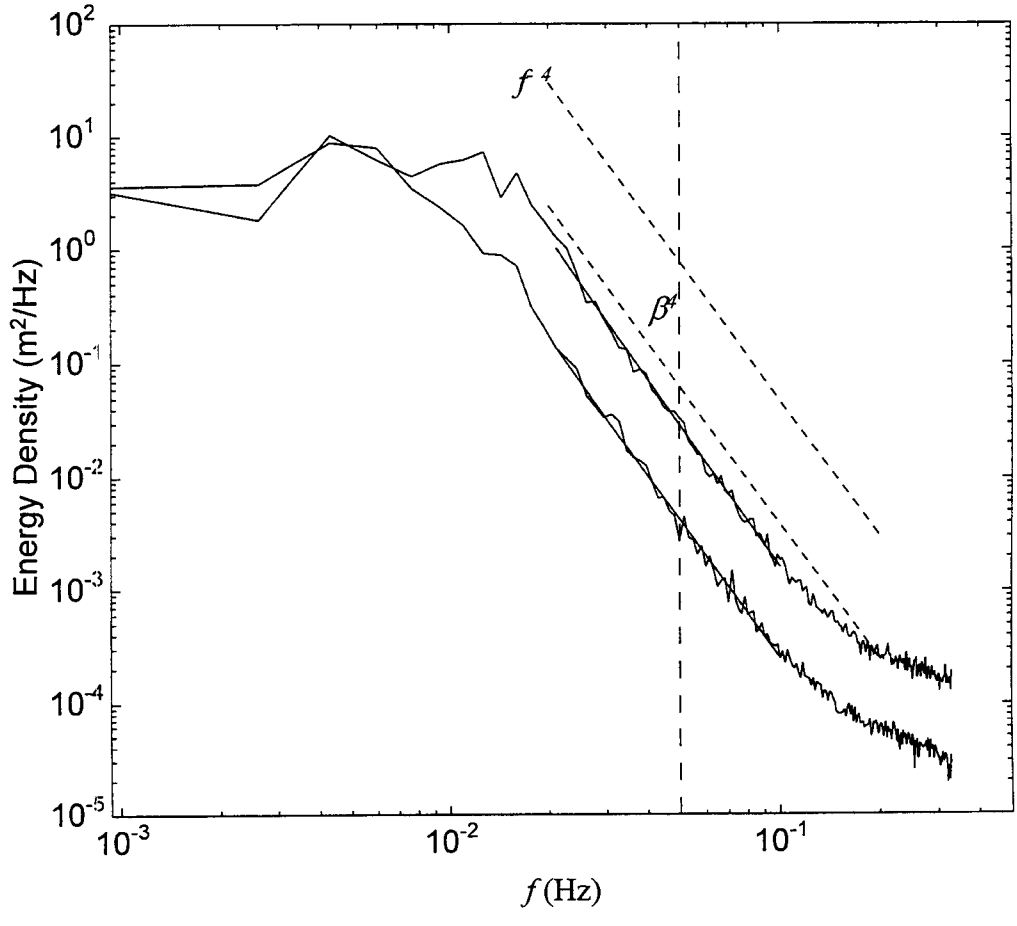

Figure 3.11. Average energy density spectra from section I (top line) and section II. The vertical dashed line at 0.05 Hz indicates the division between the infragravity and the sea swell frequency bands. The dotted lines have a f^{-4} slope and are separated by a distance proportional to β^4. The solid lines through the spectra within the saturated band are the best fits to the estimates in log-log space. The line in section I has the form $E(f) = 1.2 \times 10^{-7} f^{-4.1}$, while in section II, $E(f) = 2.2 \times 10^{-8} f^{-4.0}$.

Raubenheimer and Guza (1996), show saturated runup spectra extending only throughout the incident band. Guza and Thornton (1982) show saturated runup spectra, with an f^{-3} roll off rather than the f^{-4} dependence of the other studies, extending into the infragravity band to approximately 0.04 Hz. Figure 3.11 shows again that the distinction between sections I and II is quite clear, and the saturated region in the spectra from section II, the section with the lower beach slopes, extends to slightly lower frequencies than in section I. The average spectra from the two regions are separated by a distance less than that predicted by the β^4 relationship suggested by Huntley *et al.* (1977) in (3.5) and the observations reported by Raubenheimer and Guza (1996).

3.5.3 Longshore Coherence Length Scales

Agate Beach, Oregon is an extremely dissipative beach due to its low slope. This, coupled with high energy conditions, results in large cross-shore length scales with winter storm waves often breaking at distances greater than 1 km offshore. These large cross-shore length scales and the low frequencies that dominate the surf zone, suggest that alongshore length scales may also be quite large. Measurements of the longshore variability of wave runup have previously been made at the intermediate beach of the FRF by Holman and Sallenger (1984), Holman *et al.* (1990) and by Holland (1995). Holland (1995) defined a simple measure of the longshore structure of runup motions as the length scale over which swash motions of a given frequency are coherent. Squared coherence values were calculated from the cross-spectral matrix of all possible sensor pairs as a function of frequency and sensor separation (alongshore lag). An example can be seen in Figure 3.12 in which the squared coherence (solid line) has been calculated for the peak frequency (0.0043 Hz) from the average spectra in section I. Also shown is the critical squared coherence level (95% significance) which has been calculated individually as a function of lag due to the variable number of corresponding realizations. A coherence length scale, L, is defined as the maximum lag with squared coherence

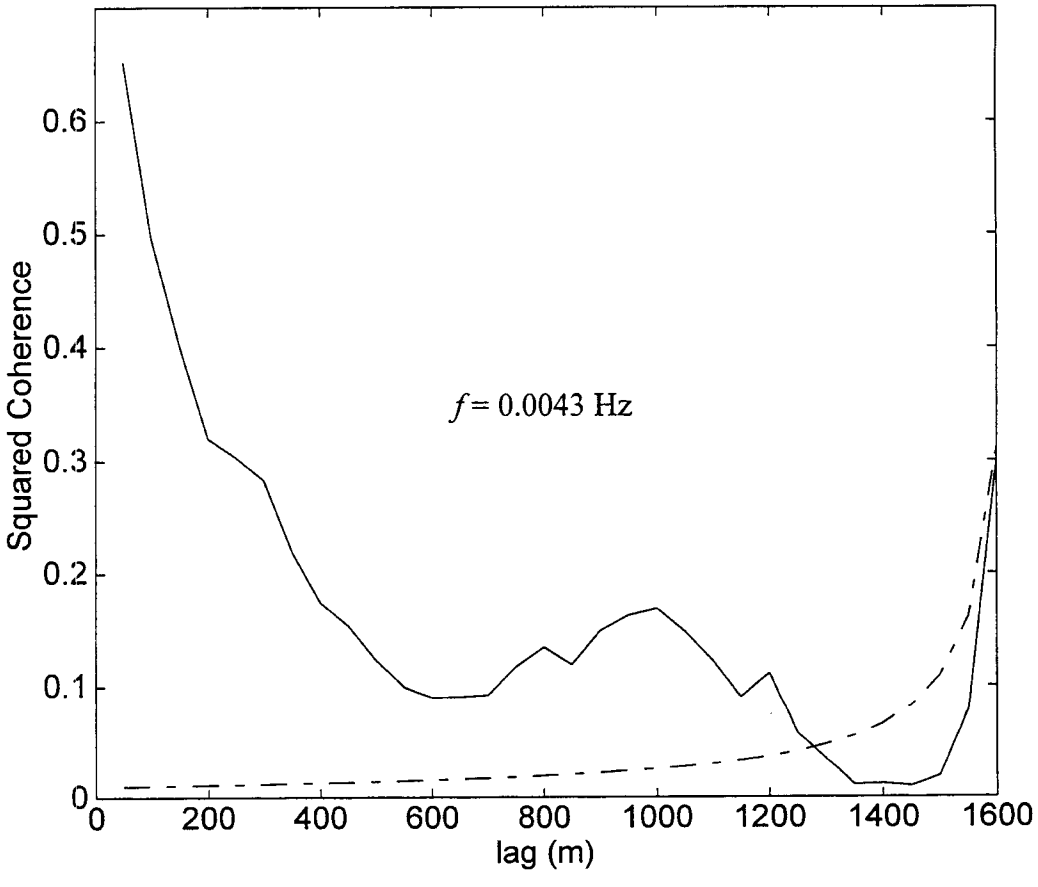

Figure 3.12. Squared coherence (solid line) and critical squared coherence level (95 % significance, dash-dot line) versus alongshore lag for the peak frequency of the average energy density spectrum in section I.

above the critical value, for which all shorter lags have squared coherence levels that were also significant. For the peak frequency shown in Figure 3.12, the coherence length scale is approximately 1250 m. Characteristic longshore length scales have been computed in this manner for all frequencies in the infragravity band and are shown in Figure 3.13a. Consistent with the time-series shown in Figure 3.6b and replays of the video records, the Oregon data is coherent over length scales on the order of 1 km at the peak infragravity frequencies which dominate the runup motions. In contrast, while the multiple time-series in Figure 3.6a reveal alongshore coherence over the length of the array in the incident band, Holland (1995) found that in the infragravity band, swash during DELILAH was coherent only over approximately 100 m as shown in Figure 3.13b.

3.5.4 Wavenumber-Frequency Structure

Potential mechanisms forcing the energetic motions found at low infragravity frequencies include long waves incident from deep water and reflected at the shoreline, forcing by incident wave group structure and edge waves. Measurements of the alongshore variability of runup giving alongshore phase relations can be used to define an alongshore wavenumber, k_y. This wave number can then be used to determine whether or not the infragravity energy consists of edge waves which are trapped to the shoreline or leaky waves which are not trapped. For a particular frequency, ω, these possibilities are distinguished by

$$\begin{aligned} \omega^2 &\leq g k_y \ : \ \textit{edge waves} \\ \omega^2 &\geq g k_y \ : \ \textit{leaky modes} \end{aligned} \tag{3.8}$$

The wave for which the equality holds is called the cutoff mode.

A wavenumber-frequency spectrum was calculated to investigate the dynamics of the runup motions over the length of the array. Figure 3.14 shows the

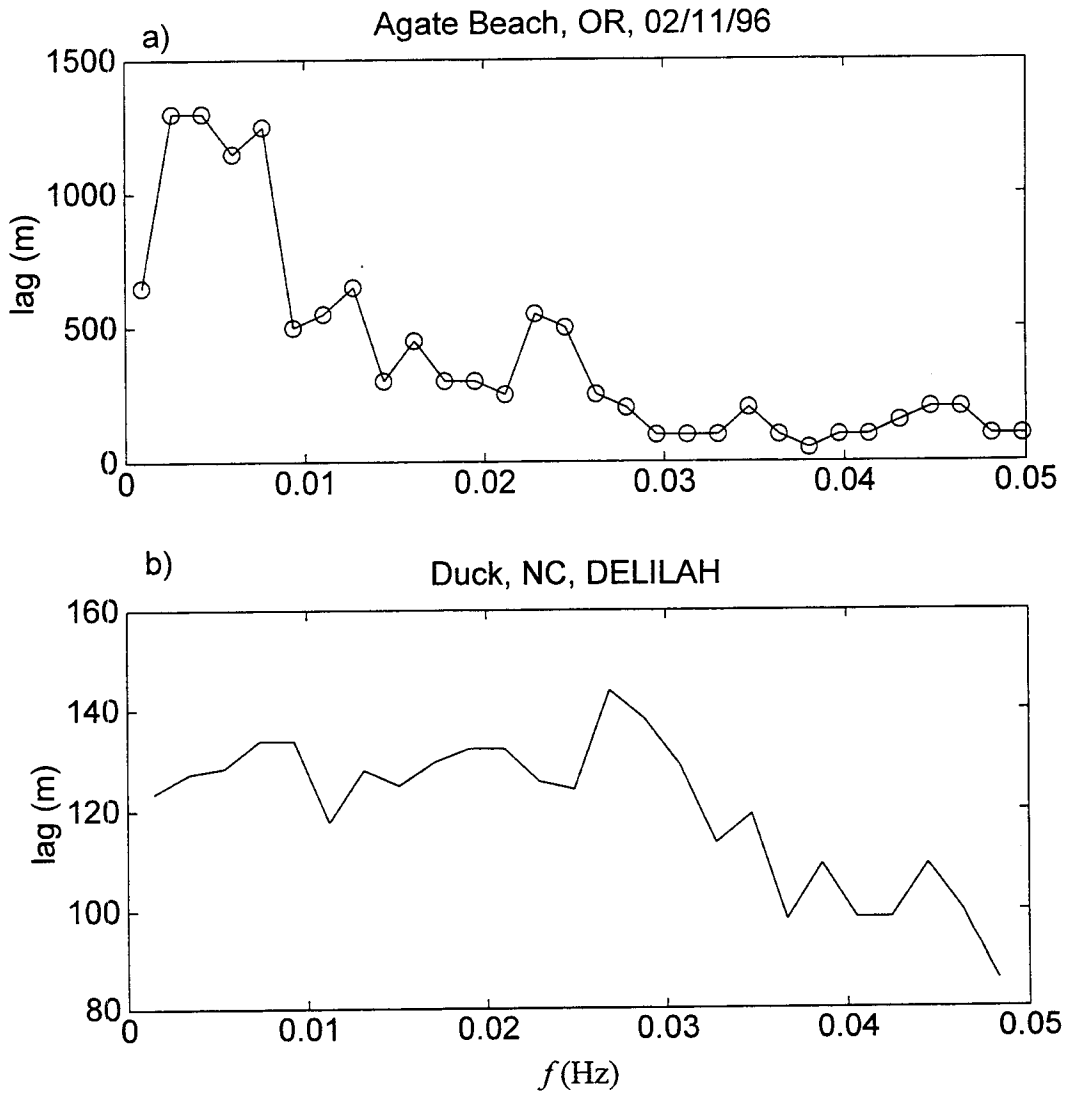

Figure 3.13. Coherence length scale (in the alongshore) within the infragravity band as a function of frequency from a) 11 February 1996, Agate Beach, OR and b) average over all runs during DELILAH experiment in Duck, NC, taken from Holland (1995).

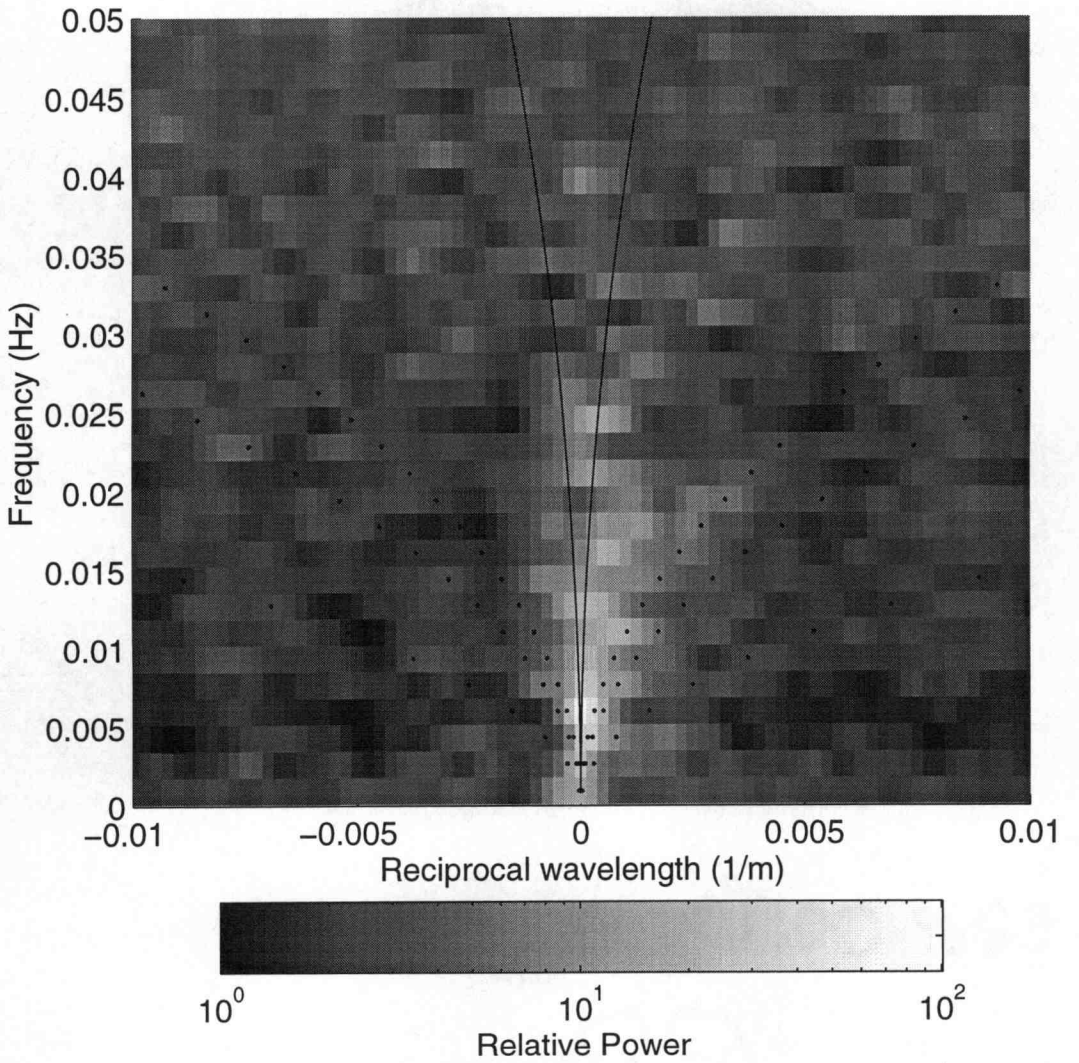

Figure 3.14. The IMLE based wave-number frequency spectra of runup elevation. Dispersion curves for mode 0, 1 and 2 edge waves are indicated by the dotted lines. The solid lines indicate the cutoff between edge waves and leaky modes. Shading intensity is proportional to the measured energy density levels displayed on a log scale.

spectrum, derived from an iterative maximum likelihood estimator (IMLE developed by Pawka (1982)). The IMLE analysis was carried out by designing an alongshore lag array of sensors (runup transects), shifting the array in the longshore for a total of 14 separate realizations, which were then averaged to generate Figure 3.14. Shading intensity is proportional to measured energy density levels displayed on a log scale. For an alongshore homogeneous and temporally stationary wave field, wave energy associated with edge, leaky or shear waves would be expected to lie along ridges in wavenumber frequency space. Dispersion lines for mode 0, 1 and 2 edge waves are indicated on the figure (dotted lines) as are the cutoff between leaky and edge wave modes (solid lines). Only the sub-incident frequencies are shown and wavelengths greater than 100 m. The majority of the energy is concentrated at extremely low wave numbers, and there is no clear evidence of low mode edge waves apparent in the figure. Surprisingly, due to the extremely low frequencies of the motions the 1600 m array length becomes relatively very short. For the peak frequency of the average spectrum from section II (0.0043 Hz), the approximate cutoff wavelength separating the edge wave and leaky mode regimes is 84 km. Therefore, we are unable to resolve the difference between leaky modes and higher edge wave modes.

The alongshore structure in individual frequency bands can be examined using the technique of frequency-domain empirical orthogonal functions or EOF's (Holman and Sallenger, 1984). EOF's are the complex eigenvectors of the cross-spectral matrix and can be expressed in terms of an amplitude and phase. The phase expresses the relative phase amongst the runup transects, with phase jumps of π indicating a wave standing in the longshore, potentially a standing edge wave. Figure 3.15 shows the results of EOF analysis for 3 particular frequency bands centered at 0.0043, 0.0077 and 0.011 Hz, hereafter referred to as band 1, 2 and 3. These frequencies appear as relative peaks in the average energy density spectra from section I in Figure 3.11. The amplitudes and phases of the first two EOF modes are shown for each frequency band. The first mode dominates for each of

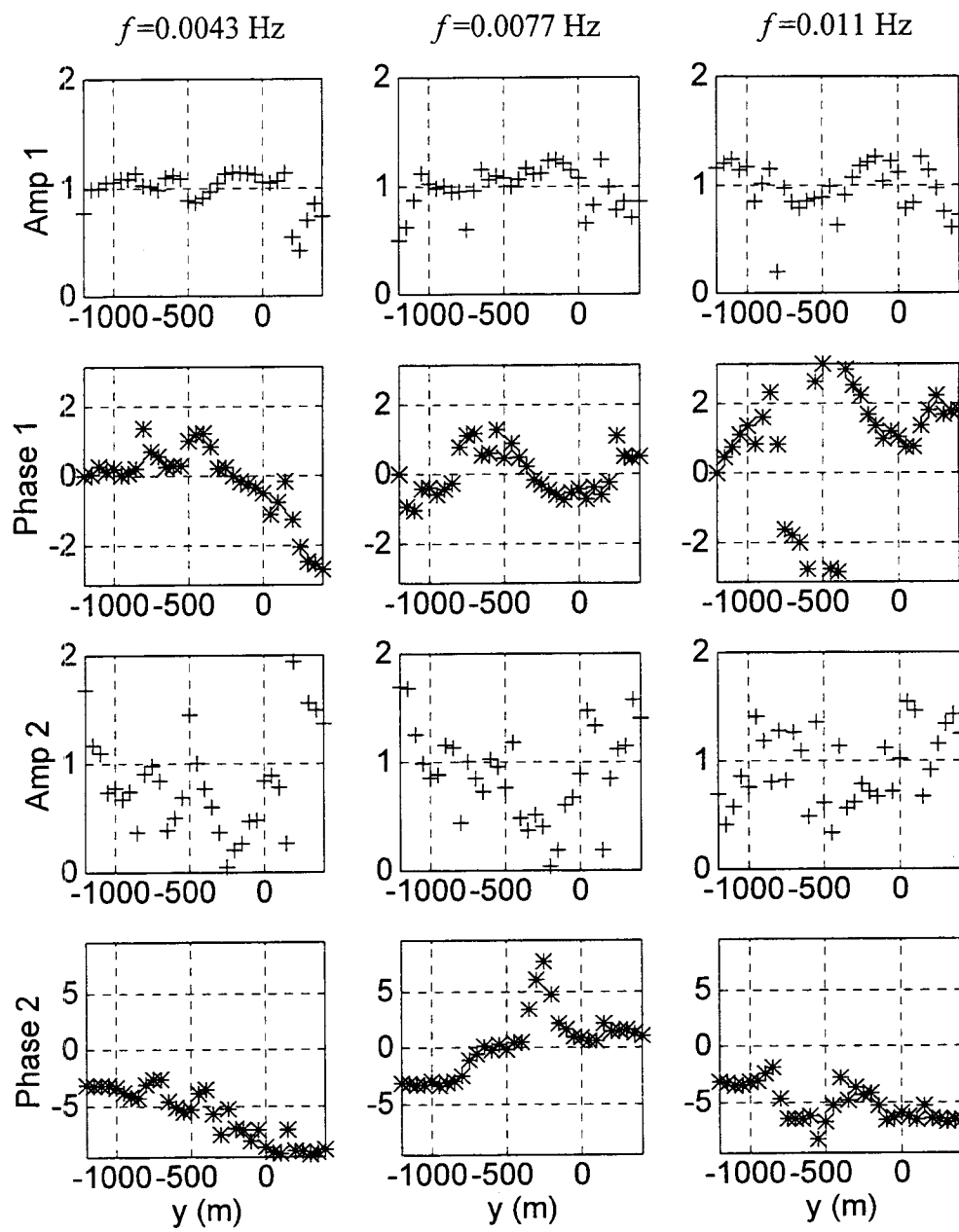

Figure 3.15. Frequency-domain empirical orthogonal functions for three dominant frequency bands, f = 0.0043 Hz, 0.0077 Hz and 0.011 Hz. Amplitude and phase functions are shown for first two modes in each frequency band.

the three frequency bands explaining 72%, 56% and 54% of the total variance respectively. The second EOF mode explains 18%, 26% and 26% respectively.

Both the amplitudes and phases in the first mode of bands 1 and 2 are relatively uniform across most of the 1600 m study area, although there is a drop in phase at the southern end of the beach in the first band. Uniform alongshore phases indicate that the energy within these first two bands are associated with very small longshore wave numbers. The approximate cutoff wavelength separating the edge wave and leaky mode regimes for band 2 is 26 km. The cutoff wavelength would have a 7°, in band 1, and 22°, in band 2, phase shift over the length of the 1600 m array. While the data cannot resolve whether or not there is a high mode edge wave present, it seems likely that the first EOF of these two frequency bands are describing leaky modes. The phase structure of the first mode of band 3 appears to be connected to the morphology of the foreshore. The waves first arrive in the lower sloping region of section II, before either to the north or the south, as waves propagate "down phase" in this analysis. This is probably due to the deeper water in section II relative to section I for a constant cross-shore location (see Figure 3.5).

3.6 Discussion

Guza and Thornton (1982) showed that for a particular beach slope, runup spectra have approximately the same energy level in the saturated frequency range, regardless of incident wave conditions. The dimensional proportionality, α, from (3.5), depends on the foreshore slope and determines what these energy levels will be. This parameter, and the actual power of the roll off of the saturated runup energy density spectrum, can be calculated by fitting spectral estimates within the saturated band to the form of (3.5) in log-log space. For the average spectrum in section I, the top line in Figure 3.11, the energy density spectrum has the form $E(f) = 1.2 \times 10^{-7} f^{-4.14}$. The constant derived for the average spectra in section II is approximately an order of magnitude less and the power dependence is exactly f^{-4}.

These relationships are shown in Figure 3.11 as the solid lines through the spectral estimates within the saturated band. The universal form for the saturated runup spectrum suggested by Huntley *et al.* (1977), (3.6), requires α to be proportional to β^4. To test this dependence, the constant α has been calculated for each of the 33 transects in our runup array. Figure 3.16 shows the estimates from the Oregon data, asterisks, as well as data taken from Huntley *et al.* (1977), circles, from 4 different beaches all with much greater foreshore slopes. The best fit through the data in log-log space is shown as the solid line. The calculated power of the dependence between α and β including both data sets is 2.85. Using just the Oregon data the power of the dependence becomes 2.0, analogous to the linear relationship between the sea-swell significant runup elevation and beach slope shown in Figure 3.6c.

The value of $\epsilon_s^{c^*}$ from (3.6), a dimensional constant with units of $Hz^{-1/2}$, can be determined from the estimates of α using the following relation

$$\epsilon_s^{c^*} = \frac{\alpha^{1/2}\,(2\pi)^2}{g\,\beta^2} \tag{3.9}$$

Note that if α is not proportional β^4, as in the case of the data presented in Figure 3.16, estimates of $\epsilon_s^{c^*}$ will also depend on the beach slope. From arguments of downslope swash accelerations, Huntley *et al.* (1977) define a universal constant, $\epsilon_s^{c^*}$ $(\Delta f)^{1/2}$, approximately equal to 1.0, where Δf is taken as the band width of the saturated runup spectrum. Although the saturated region of the Oregon runup spectra extend to slightly lower frequencies for lower foreshore slopes, the estimated bandwidth for each of the runup spectra is fairly constant. Therefore, for the data presented in this paper, the universal constant, as defined above, is in fact not a constant but a variable depending on β.

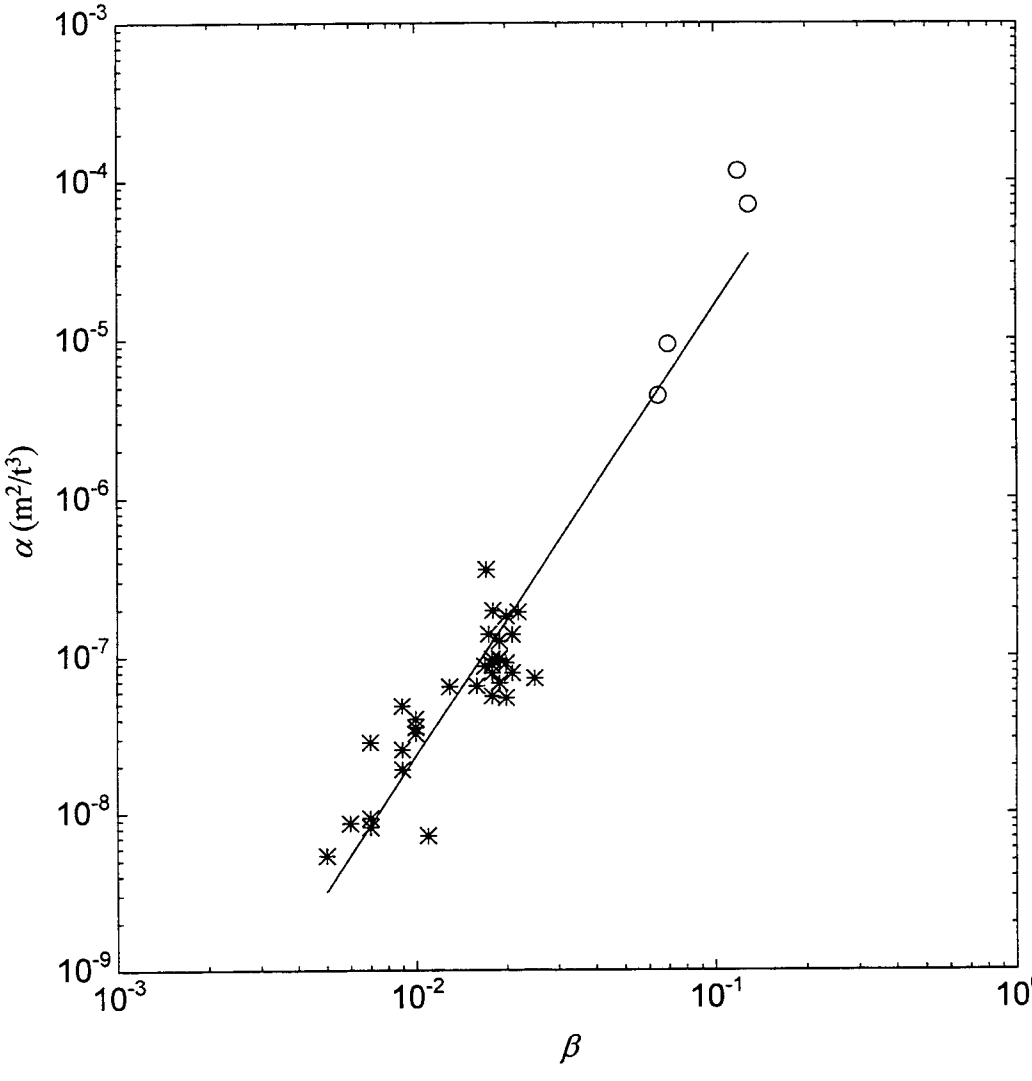

Figure 3.16. Dimensional constant α estimated from the saturated region of runup energy density spectra as a function of foreshore beach slope. Asterisks are from the Oregon data while the circles are taken from Huntley *et al.* (1977).

3.6 Summary

Wave runup on Agate Beach, Oregon is dominated by infragravity energy with spectral peaks at approximately 0.005 Hz. This behavior, on a strongly dissipative beach, contrasts with runup at Duck, North Carolina which is dominated by incident band energy. Significant runup height varied by a factor of 2 over the 1.6 km study area and was dependent on the foreshore beach slope. All calculated runup spectra showed a broad saturated region with an f^{-4} dependence. However, the extension of the universal form for shoreline runup spectra of Huntley *et al.* (1977) to extremely low sloping beaches has been cast into doubt. Runup motions at peak infragravity frequencies were coherent over large alongshore length scales, on the order of 1 km. The cut-off wave length for leaky modes is approximately 84 km at the peak runup frequencies, so even with a 1.6 km array most edge wave modes were under-resolved.

CHAPTER FOUR: LONGSHORE CURRENTS AND SEDIMENT TRANSPORT ON BEACHES WITH SEAWALLS

4.1 Abstract

An analytic model is developed to predict longshore currents and the associated sediment transport on a planar beach backed by a seawall. The model assumes shallow water, small angle of wave incidence, spilling breakers and conservation of reflected wave energy flux. A partial standing wave develops in front of the seawall causing modulations of the bottom stress, radiation stresses and the resulting setup, longshore current and longshore sediment transport. This influence increases as the beach slope decreases because more standing waves develop across the wider surf zone. The total longshore sediment transport is strongly influenced by the cross-shore location of the seawall. On steep beaches, the total transport is less than that for a natural beach. For milder sloped beaches, the modulations become significant and the transport may be either more or less than that for a beach with no wall, depending on the location of the seawall.

4.2 Introduction

The effects of seawalls on beaches has been a topic of study and controversy for many years. Recent reviews of the available literature (Kraus, 1987; Griggs and Tait, 1990; and Kraus and McDougal, 1996) demonstrate the need for still more research. Beaches have been reputed to respond to wave/seawall interactions in many ways, including the formation of scour troughs, deflated beach profiles, end scour, up-coast accretion, down-coast erosion, far down-coast shoals, reflection bars, delayed post-storm recovery, etc. Processes identified as having contributed to these possible responses include sediment impoundment (groin effect), wave reflection, acceleration of longshore currents,

increased sediment mobilization, and so on. Controls on how these processes affect beach change have also been discussed; long term shoreline changes, position of the seawall relative to the surf zone, width of the surf zone, sediment supply as well as wave and seawall characteristics. Confusion and disagreement in the literature is compounded by the lack of sufficient field data and inconclusive physical and theoretical models.

For example, the commonly accepted hypothesis that the reflection of normally incident waves from a seawall is a significant contributor to beach profile change, and to the development of the scour trench located in front of seawalls, has been recently cast into doubt. Several numerical cross-shore profile models have been developed to examine this question, including a modified version of SBEACH which explicitly includes wave reflection from the seawall and its influence on wave breaking and setup (McDougal *et al*, 1996). This study yielded two rather surprising results. The first is that the beach change predictions including reflected waves were not substantially different from those neglecting reflection (*ie*. the standard SBEACH model with a no transport condition at the location of the seawall). The second was that a large scour trench did not develop at the toe of the seawall, even for very energetic waves. These numerical results were confirmed in the large-scale model tests conducted as a component of the SUPERTANK experiments (Kraus *et al*, 1992). The agreement of these two-dimensional numerical and physical models indicate that alongshore processes may be significant in seawall related effects (Kraus and McDougal, 1996).

Unfortunately, there is much less understanding of the alongshore processes in front of seawalls. In an unpublished doctoral dissertation, Jones (1975) theoretically and experimentally examined the effects of a seawall on longshore currents and the response of the fronting beach. He found that the longshore current profiles exhibited maxima and minima in response to a standing wave system, forced by monochromatic waves, which developed in front of the seawall.

Maximum erosion was observed at the toe of the seawall, and the maximum net erosion occurred if the seawall was positioned approximately three-fifths of the distance from the breakpoint to the still water line. Silvester (1977) suggested that oblique wave incidence on a seawall could establish a short-crested wave system which would amplify the transport of material over what would normally occur without the wall. The bed fronting the wall would scour, the immediate down drift section of coast would recede, and further down coast a shoal would develop beyond the influence of wave reflection. In a monitoring project of the effect of structures and water levels on bluff and shoreline erosion in Lake Michigan, Birkemeier (1980) provides one of the few quantitative measurements of longshore currents in front of a seawall. The southward moving current during a small storm was measured with dye tracers to be much larger in front of the wall than the adjacent north and south sections of coast.

In a study based on 20 years of surveys along the Gold Coast, Australia, Macdonald and Patterson (1984) noted that "once the waves impinge on the seawalls for a significant proportion of the time, wave reflections and accelerated longshore currents can lead to increased scour adjacent to the walls." In contrast, Dean (1986) argues that there is no factual data to support the contention that armoring causes increased sediment transport and thus a steepening of the beach profile. He presents a "rational" argument, based on the net longshore thrust including reflection, that wave reflection actually causes a reduction in longshore sediment transport. Plant and Griggs (1992) attempted to test the hypothesis that longshore currents in front of a seawall may be accelerated if the surf zone is sufficiently restricted by the presence of the wall. However, due to the logistics of their study site, they were unable to sample time periods long enough to resolve statistically meaningful variations in the mean current between walled and un-walled sections of beach. In three-dimensional physical model tests, Kamphuis (1992) found that the longshore sediment transport rate in front of a seawall decreased over time as the fronting beach eroded. Two long term field studies

have addressed the effects seawalls have on beaches in California (Griggs et al, 1994) and Oregon (Hearon *et al.*, in press) over time scales of close to a decade. Measurable or significant differences between profiles for seawall-backed and control beaches were not found in the studies, suggesting little long term effect of seawalls on the beaches. Based on the above sometime conflicting results, it has not yet been confirmed in the field or the laboratory whether longshore currents and sediment transport rates will increase or decrease in front of a seawall, as compared to a non-armored section of beach.

This paper presents an analytic model to estimate longshore currents and littoral transport on planar beaches backed by seawalls, the objective being to shed light on the influence of seawalls on nearshore processes. The model is based on the depth and time averaged equations of motion in the nearshore, assuming no longshore gradients. Once the waves, incident and reflected, and the total depth including setup are determined, the longshore equation of motion is used to calculate a mean longshore current, and from this the sediment transport is estimated using a Bagnold-type model (Bagnold, 1963). Attempts have been made, wherever possible, to compare the results of the model with those from a similar beach with no seawall. The behavior of the long wave equation with a seawall as the onshore boundary condition is then used to explain some of the model results.

4.3 Wave Model

As waves propagate toward the shore, they refract, shoal, and break. With a seawall present, they may also reflect, redirecting non-dissipated wave energy back through the surf zone. Figure 4.1 is a plan view which shows the incident and reflected waves relative to the shoreline; θ_i is the incident wave angle, θ_r is the reflected wave angle and the x coordinate is directed positive offshore with an origin landward of the seawall. This mathematically convenient coordinate system will be discussed later. The reflected wave angle is related to the incident wave

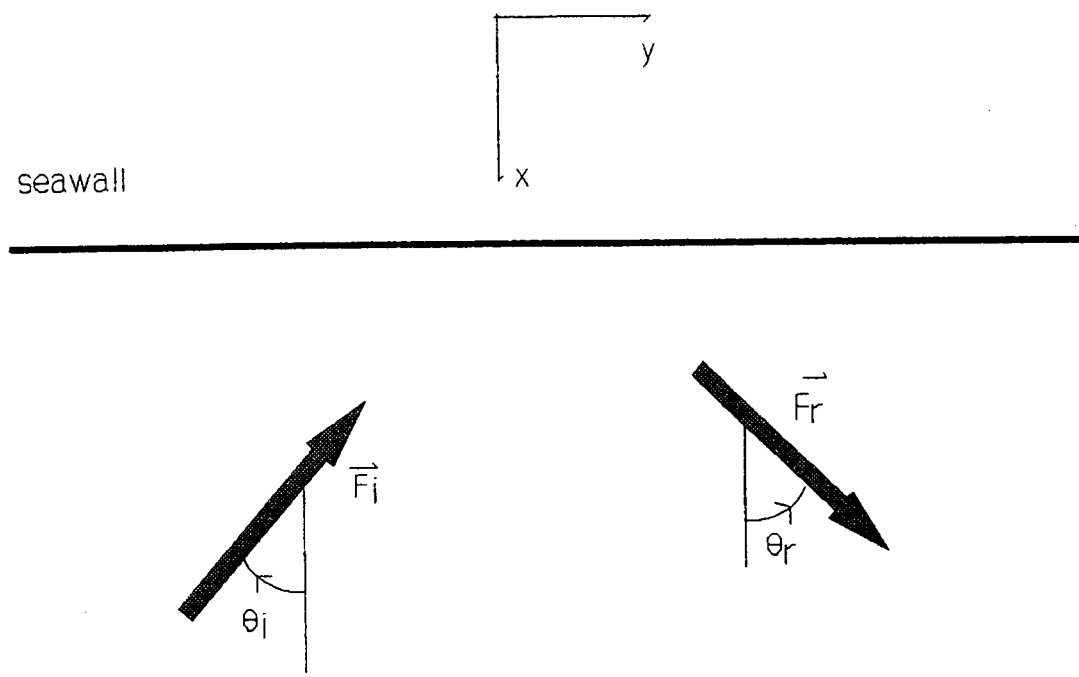

Figure 4.1 Incident and reflected wave coordinate definitions.

angle as, $\theta_r = -\theta_i$, so hereafter the angles will simply be denoted as θ with the appropriate sign. A partial standing wave develops in front of the seawall in which the total velocity potential can be expressed as the sum of the incident and reflected velocity potentials,

$$\Phi = \phi_i + \phi_r = \frac{g\cosh k(d+z)}{\omega\cosh kd}\,(a_i\cos(kx\cos\theta - ky\sin\theta + \omega t) + a_r\cos(kx\cos\theta + ky\sin\theta - \omega t + \epsilon_r)) \tag{4.1}$$

where g is the acceleration due to gravity, k is the modulus of the wave number (k_x and k_y are the components of the wave number in the cross-shore and longshore respectively), d is the total water depth equal to the sum of the still water depth, h, and the mean free surface elevation $\bar{\eta}$, a_i and a_r are the incident and reflected wave amplitudes, ω is the angular frequency, and ϵ_r is the local phase between the incident and reflected waves and is a function of cross-shore location.

4.3.1 Incident and Reflected Wave Amplitude

The change in wave amplitude across the surf zone causes a change in both the cross-shore and longshore radiation stresses. These gradients are balanced by an increase/decrease of the mean water level in the cross-shore, setup/setdown, and by a mean current in the longshore. In the present model, the spilling breaker assumption is employed in the surf zone so that the total breaker amplitude is simply related to the local total water depth as

$$a_i + a_r = \frac{\kappa}{2}(h + \bar{\eta}) = \frac{\kappa d}{2} \tag{4.2}$$

in which κ is a breaker index. The cross-shore variation in the wave amplitude is determined assuming that the reflected wave energy flux, $\vec{F}_r$, is conserved across

the surf zone

$$\vec{F}_r = \frac{1}{2}\rho g a_r^2 C_{gr} = \frac{1}{2}\rho g A \tag{4.3}$$

in which ρ is the water density, C_{gr} is the reflected wave group velocity and A is a constant. This constant is evaluated at the seawall, so let

$$a_r^2 C_{gr} = a^2{}_{r_{wall}} C_{gr_{wall}} = A \tag{4.4}$$

where the subscript $(\,)_{wall}$ denotes values calculated at the seawall. Assuming that the increased energy in the surf zone, due to the reflected wave, is dissipated in the incident wave, (4.2) and (4.4) can be combined to give the cross-shore variation in the incident wave amplitude

$$a_i = \frac{\kappa d}{2} - \frac{A^{1/2}}{C_{gr}^{1/2}} \tag{4.5}$$

The constant A is determined from the reflected wave amplitude at the seawall. This is equal to the incident wave amplitude at the seawall multiplied by a reflection coefficient, K_r. The reflected wave amplitude can now be defined as,

$$a_r = \left(\frac{K_r}{1 + K_r}\right) \frac{\kappa d_{wall}}{2} \left(\frac{C_{gr_{wall}}}{C_{gr}}\right)^{1/2} \tag{4.6}$$

This formulation, along with the assumption that the reflected wave energy is dissipated in the incident wave, is consistent with the work of Jones (1975). However, the present formulation also includes wave setup. Note that as $K_r \rightarrow 0$, $A \rightarrow 0$ and (4.5) collapses to the typical formulation of the incident wave amplitude for spilling breakers, which is used in the classical no seawall derivations of wave setup, longshore currents and longshore sediment transport on planar beaches (*eg.* Bowen *et al*, 1968; Bowen, 1969; Longuet Higgins, 1970a,b; and McDougal and Hudspeth, 1983a,b). The solutions of McDougal and Hudspeth (1983a,b) will be compared with the present model, and will be hereinafter referred to as *MH83*.

4.3.2 Setup/Setdown

Wave setup/setdown is determined from the cross-shore momentum equation, neglecting bottom and surface stresses and assuming no longshore gradients, $\partial(\bullet)/\partial y = 0$,

$$-\rho g(h+\bar{\eta})\frac{d}{dx}\bar{\eta} = \frac{d}{dx}S_{xx} \tag{4.7}$$

where S_{xx} is the onshore component of the onshore directed radiation stress. The present derivation of S_{xx}, including the reflected wave, is slightly different from that of McDougal *et al* (1996). The spatial derivatives of the phase between the incident and reflected wave, ϵ_r', are derived analytically rather than computed via numerical iteration. The present result is written as

$$\begin{aligned} S_{xx} = \; & (E_{ii}+E_{rr})\left[n(\cos^2\theta+1)-\frac{1}{2}\right] + nE_{rr}\frac{\epsilon_r'^2}{k^2} \\ & + E_{ir}\cos(2kx\cos\theta+\epsilon_r)\left[2n\sin^2\theta-1\right] \\ & + n\cos\theta\left[2E_{rr}\frac{\epsilon_r'}{k} - 2E_{ir}\frac{\epsilon_r'}{k}\cos(2kx\cos\theta+\epsilon_r)\right] \end{aligned} \tag{4.8}$$

where E_{ii} and E_{rr} are the incident and reflected wave energies, E_{ir} is

$$E_{ir} = \frac{1}{2}\rho g a_i a_r \tag{4.9}$$

and n is the ratio between group velocity and wave celerity.

At this point, it is necessary to make several simplifying assumptions to develop an analytic solution to the cross-shore momentum equation. First, we assume shallow water in the region of interest such that

$$C = C_g = (gd)^{1/2} \tag{4.10}$$

where C is the wave phase speed. We consider only a planar beach with bottom slope m. In *MH83*, the wave setup is a linear function of cross-shore location for a planar beach, while in the current work there is a spatial oscillation term in the radiation stress which acts to modulate the time averaged total depth. However, we will later show that a linear setup assumption is still valid for the determination of the longshore current and sediment transport in front of a seawall. The present model is developed for a beach backed by a vertical seawall located within the surf zone, such that the elevated mean water level due to wave setup is at a higher elevation than the intersection of the beach with the seawall. The seawall must be landward of the breaker line but can be either landward or seaward of the still water line. The model is valid for three of the six types of seawalls, Type-3, Type-4, and Type-5, according to Weggel's (1988) classification system based on the seawall's location with respect to the shoreline. Figure 4.2 is a profile view of a seawall on a planar beach and geometrically suggests that the total slope, s, is simply the bottom slope, m, less the slope of the wave setup, α, in a coordinate system with an origin at the projected intersection of the wave setup with the planar beach. This choice of coordinate system allows the total depth to be written as $d = sx$, a convenience that greatly simplifies both the cross-shore and longshore equations of motion.

The wave length is the product of the wave celerity and the wave period, so with the above assumptions, the wave number may be written as

$$k = \frac{2\pi}{L} = \frac{2\pi}{CT} = \frac{\omega}{(gsx)^{1/2}} \tag{4.11}$$

in which L is the wave length and T is the wave period. It is assumed that refraction is sufficient to yield small breaking wave angles, and that once inside the surf zone the change in wave angle is also small such that $\theta \cong \theta_B$, a constant evaluated at the breaker line. Separating out the aforementioned spatial oscillation

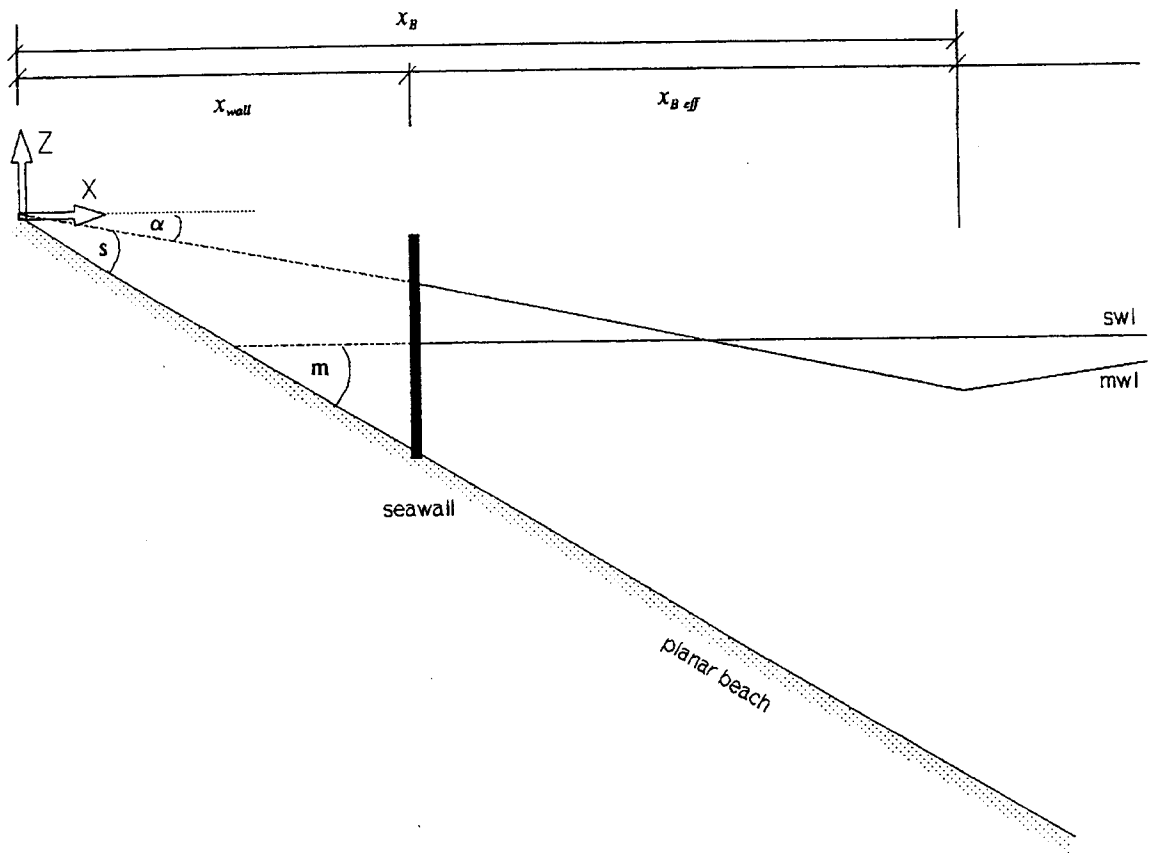

Figure 4.2 Wave setup in front of a seawall, profile view definition sketch.

term, denoted as

$$f = \cos(2kx\cos\theta + \epsilon_r) \tag{4.12}$$

serves to simplify the cross-shore radiation stress term. The phase term can be separated into two parts,

$$\epsilon_r = \epsilon_{rw} + \epsilon_{rg} \tag{4.13}$$

where ϵ_{rw} is determined by the amount of time it takes the incident wave to propagate from an arbitrary offshore location, x_o, to the seawall and back again to x_o

$$\epsilon_{rw} = \frac{4\pi}{T}\int_{x_o}^{x_{wall}} \frac{dx}{C\cos\theta} \tag{4.14}$$

A geometric phase, ϵ_{rg}, arises from the choice of coordinate system and is chosen to ensure an anti-node at the seawall. The radiation stress term can now be simplified and combined with (4.7) to give the dimensional equation for wave setup

$$\frac{d\overline{\eta^*}}{dx^*} = \frac{-3}{4d^*}\frac{d}{dx^*}(a_i^{2^*} + a_r^{2^*} + 2a_i^* a_r^* f) \tag{4.15}$$

where the asterisks, which have been left off until this point for brevity, denote dimensional quantities.

It is convenient to introduce the following dimensionless quantities: $\bar{\eta} = \bar{\eta}^*/d_B^*$, $d = d^*/d_B^*$, $X = x^*/x_B^*$, $A = A^* T^*/(d_B^{*3}(2\pi)^{1/2})$, and $\omega = \omega^* T^*/(2\pi)^{1/2}$. With these definitions, the cross-shore equation of motion can be integrated to give the non-dimensional spatial structure of the wave setup

$$\overline{\eta} = -\frac{3\kappa^2 X}{8} - \frac{A\gamma^{1/2}}{2X} - \frac{9A^{1/2}\kappa\gamma^{1/4}}{4X^{1/4}} + \frac{3A\gamma^{1/2}f}{2X^{3/2}}$$

$$- \frac{3A^{1/2}\kappa\gamma^{1/4}f}{4X^{1/4}} + \frac{3A\gamma^{1/2}}{4}\int X^{-5/2} f dX \qquad (4.16)$$

$$- \frac{3A^{1/2}\kappa\gamma^{1/4}}{4}\int X^{-5/4} f dX + c_1$$

where $\gamma = d_B^*/L_0^*$, $L_0^* = g^* T^{*2}/(2\pi)$ is the deep-water wave length from linear wave theory, and c_1 is a constant of integration. The two integrals in (4.16) have been evaluated and result in lengthy expressions involving special functions which are reported in Appendix B. Wave setdown can be derived and non-dimensionalized in a similar manner to that described for the setup. The constant c_1 is determined by matching the setup and setdown at the breaker line. Again, with no reflection from the seawall, $A \rightarrow 0$ and (4.16) collapses to the no seawall formulation for wave setup on a planar beach.

The seawall, and the partial standing wave that develops in front of it, affect cross-shore surf zone dynamics in several ways. Table 4.1 lists the range of wave and beach conditions which are used to demonstrate the behavior of the model. By varying the position of the seawall across the surf zone, a total of 88 cases were examined. Figure 4.3 shows the influence of the seawall on the width of the surf zone. The ordinate is the ratio of the seawall location, x_{wall}, to the break point location $x_{B\ no\ wall}$, calculated for a beach with the same still water depth slope, m, but with no seawall. This scaling is chosen since it is not *a priori* known where waves will break due to the reflected waves from the seawall. The top curve represents the ratio of the break point calculated for the beach with the seawall, x_B, to $x_{B\ no\ wall}$. The non-dissipated energy that is reflected back through the surf zone causes incoming waves to break further seaward than they would if no seawall was present. For example, a seawall located at approximately 50% of

Table 4.1 Range of wave conditions and beach slopes used in model runs.

Case	a_{iB} (m)	T (s)	m
1 a,b,c,d	0.5	6	1:10, 1:20, 1:50, 1:100
2 a,b,c,d	1.5	10	1:10, 1:20, 1:50, 1:100
3 a,b,c,d	3.5	15	1:10, 1:20, 1:50, 1:100

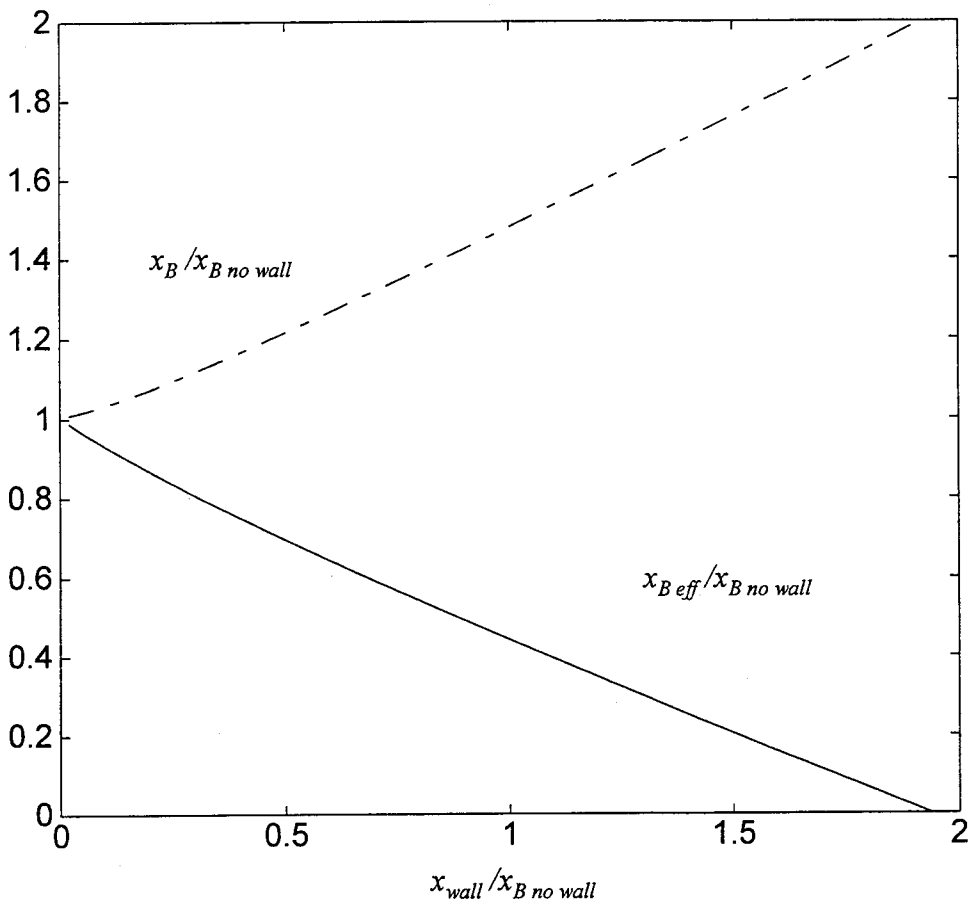

Figure 4.3 Influence of seawall on surf zone width.

the no wall surf zone width causes waves to break 20% further seaward. The bottom curve demonstrates that the seawall does, however, reduce the overall, or effective, width of the surf zone by eliminating the area behind the wall from the surf zone.

Figure 4.4 has three non-dimensional setup/setdown profiles representing three seawall locations, 20%, 40% and 60% of $x_{B\,no\,wall}$. Unfortunately, in the non-dimensionalization of the cross-shore equations of motion, most wave parameters do not drop out as they do in simpler setup/setdown models (*ie. MH83*). Therefore, Figure 4.4 is not general, but represents a specific set of conditions from Table 4.1; case 3d with a_{iB} = 3.5 m, T = 15 s, and m = 1:100. The spatial oscillation term causes the modulation in the wave setup/setdown. The number of oscillations across the surf zone depends on the ratio of the wave length to the surf zone width. Figure 4.4 also demonstrates that the magnitude of the modulations increases as the seawall is moved seaward. This is because the incident wave at the seawall is larger, and therefore the reflected wave is also larger. To further illustrate the seaward extension of the surf zone due to the waves reflected from the seawall, the cross-shore distance in Figure 4.4 has again been scaled by $x_{B\,no\,wall}$, rather than by x_B which would have set each of the scaled break points to a value of 1.

To solve the longshore equations of motion analytically, a simple representation of the total water depth is required. To validate the assumption of a linear total depth slope, 88 setup profiles were calculated and used to determine the corresponding still water depth profiles. Figure 4.5 shows a composite of both the setup and bottom profiles generated from the model. The excellent correlation that a planar bottom slope has with the model results (r^2 = 0.995) confirms that the modulation of the wave setup has only a small effect on the total water depth, thus the approximation of a linear total depth slope is reasonable. The linear regression also gives a relationship between the total slope s, and the bottom slope m,

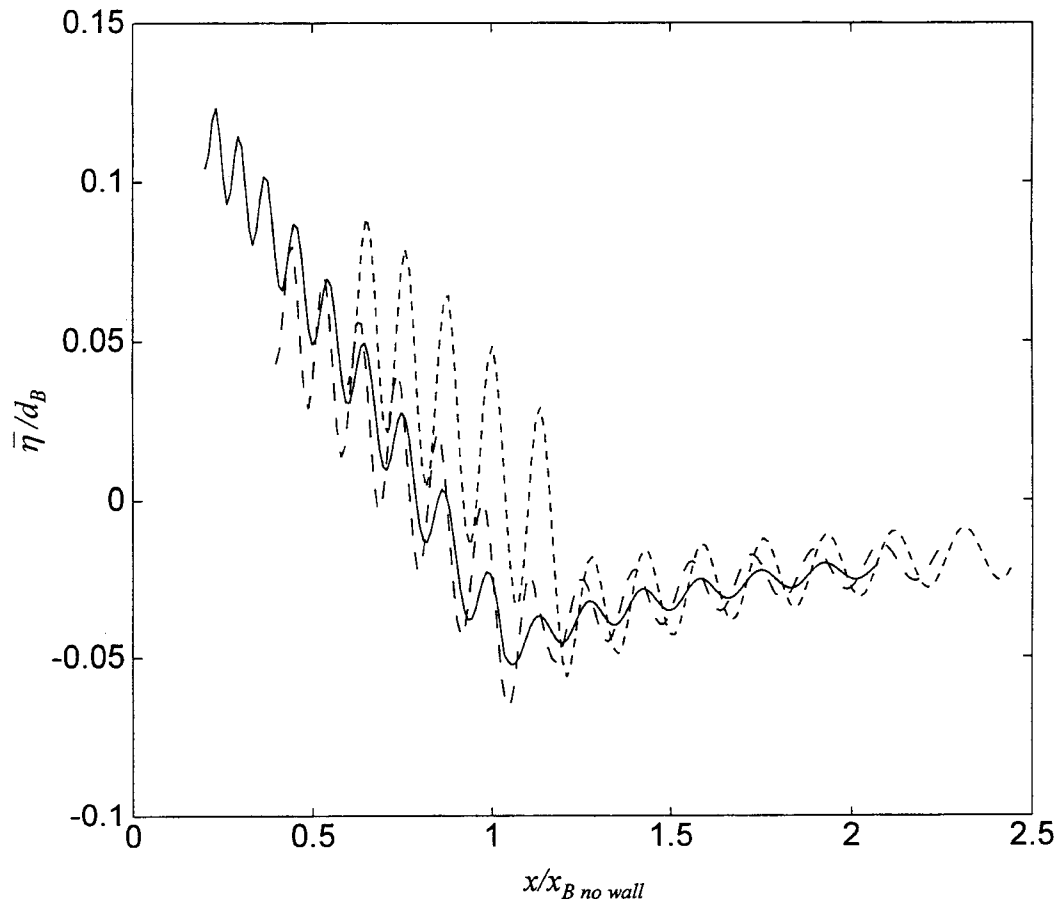

Figure 4.4 Wave setup/setdown in front of seawall for 3 locations of the seawall, $x_{wall}/x_{B\ no\ wall}$ = 0.2 (solid line), 0.4 (dashed line) and 0.6 (dotted line).

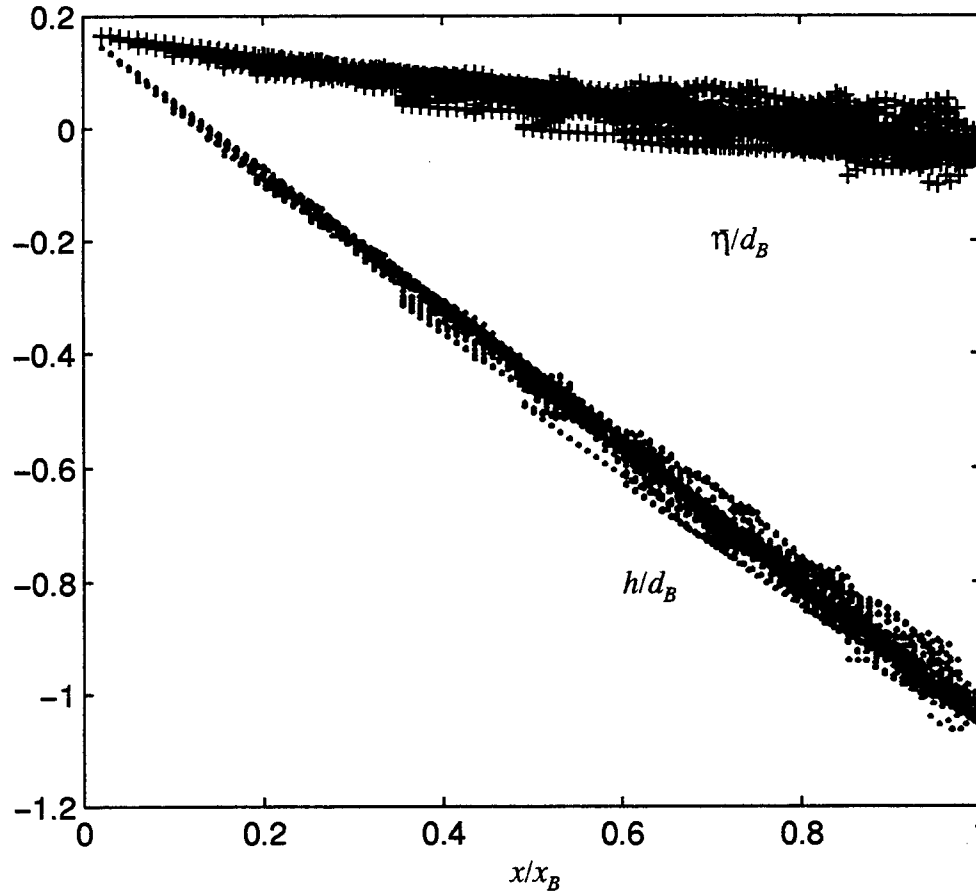

Figure 4.5 Composite of 88 non-dimensional setup and still water depth profiles. Results of linear regression gives $h/dB = 0.156 - 1.197\ X$, $r^2 = 0.995$.

$$s = 0.84\ m \tag{4.17}$$

which is necessary in solving the longshore equation of motion. For comparison, an analytic solution is possible for the no seawall total depth slope and, therefore, a relationship between s_{MH83} and m for a beach with no seawall

$$s_{MH83} = m\ (1 - \frac{3\kappa^2}{8 + 3\kappa^2}) \tag{4.18}$$

For a typical mild slope breaker index of $\kappa = 0.8$ this gives $s_{MH83} = 0.81\ m$. The total depth slope is steeper for a beach with a seawall than for a beach without a seawall.

4.4 Longshore Current

Most theories for mean longshore currents due to oblique wave approach are based on a longshore momentum flux balance (Bowen, 1969; Longuet-Higgins, 1970a,b; Thornton and Guza, 1986 and *MH83*). The present model follows this tradition, but also includes the effect of reflected waves from a seawall. The time averaged equation for longshore momentum can be simplified to a balance between the cross-shore gradient of the longshore radiation stress and the longshore bottom stress. An eddy viscosity term modeling surf zone turbulence is also included, serving to smooth the mean longshore current. The balance becomes

$$\frac{d}{dx}(\mu_e d \frac{d}{dx} v) + \tau_{by} = \frac{d}{dx} S_{xy} \tag{4.19}$$

where μ_e is the eddy viscosity, v is the mean longshore current, τ_{by} is the bottom stress in the longshore direction, S_{xy} is the longshore component of the onshore radiation stress and asterisks are implied, denoting dimensional quantities, but left off for brevity. The eddy viscosity term is necessary for a reasonable longshore current profile when the forcing is from monochromatic waves. Many eddy

viscosity models have been proposed, but the longshore current is rather insensitive to the choice (McDougal and Hudspeth, 1986). We will assume a simple representation of μ_e which increases linearly across the surf zone and is proportional to a characteristic density, velocity and length scale

$$\mu_e = N\rho(gd)^{1/2}x \tag{4.20}$$

where N is a dimensionless constant.

4.4.1 Bottom Stress

The bottom stress is estimated using a quadratic bottom shear stress law, based on the combined wave orbital velocity and mean current velocity

$$\vec{\tau}_b = -\rho c_f |\vec{u}| \vec{u} \tag{4.21}$$

where c_f is a dimensionless coefficient and $\vec{u}$ is the depth averaged velocity vector. For a small angle of wave incidence and weak mean longshore current, the time averaged bottom stress in the longshore direction can be written as

$$\tau_{by} = -\frac{1}{d}\int_{-d}^{\bar{\eta}} \rho c_f \overline{|u_x|(u_y+v)}\,dz \tag{4.22}$$

The longshore component of the wave orbital velocity, u_y, which is easily derived from (4.1), is proportional to $\sin\theta$ and will be neglected from the bottom stress due to the small angle assumption. The onshore component of the wave orbital velocity including the reflected wave is

$$u_x = \frac{gk\cosh k(d+z)}{\omega\cosh kd}(a_i\cos\theta\sin(kx\cos\theta - ky\sin\theta + \omega t) + a_r(\cos\theta + \frac{\epsilon_r'}{k})\sin(kx\cos\theta + ky\sin\theta - \omega t + \epsilon_r)) \tag{4.23}$$

After several trigonometric and algebraic simplifications, (4.23) can be written as

$$u_x = c_2\sin[\omega t + \sigma(x)] \tag{4.24}$$

where the coefficient c_2 is

$$c_2 = g(z)(a_i^2\cos^2\theta + a_r^2(\cos\theta+\frac{\epsilon_r'}{k})2 - 2a_ia_r\cos\theta(\cos\theta+\frac{\epsilon_r'}{k})f)^{1/2} \tag{4.25}$$

in which

$$g(z) = \frac{gk\cosh k(d+z)}{\omega\cosh kd} \tag{4.26}$$

and $\sigma(x)$ is a spatially dependent phase term which will be eliminated during the subsequent time averaging of the bottom stress. The coefficient c_2 can be simplified via a binomial expansion, assuming $a_r/a_i < 1$

$$c_2 \approx g(z)\cos\theta(a_i - a_r(1 + \frac{\epsilon_r'}{\cos\theta})f) \tag{4.27}$$

This assumption is reasonable over most of the surf zone except very close to the wall. At the wall itself, if $K_r = 1.0$, the ratio $a_r/a_i = 1$, and the simplified c_2 would have the greatest error. This maximum error is approximately 14% at the seawall, and much less for the rest of the profile. Making the same set of

assumptions as when determining the total water depth, depth and time averaging, the bottom stress becomes

$$\tau_{by} = -\frac{\rho c_f g}{\pi (gd)^{1/2}}(a_i + a_r f)v \tag{4.28}$$

4.4.2 Longshore Radiation Stress

S_{xy} is the longshore component of the onshore directed radiation stress and is determined from

$$S_{xy} = \overline{\int_{-d}^{\eta} \rho u_x u_y dz} \tag{4.29}$$

The result, again derived accounting for the partial standing wave which develops in front of the seawall, is written as

$$S_{xy} = n((E_{ii} + E_{rr})\sin\theta\cos\theta + (E_{ir}\frac{c_r'}{k}f + E_{rr}\frac{c_r'}{k})\sin\theta) \tag{4.30}$$

Employing Snell's law for wave refraction and making the same set of assumptions as above, the cross-shore derivative of (4.30) is

$$\begin{aligned}\frac{d}{dx}S_{xy} = \quad & \rho g\frac{\sin 2\theta}{4(gd_B)^{1/2}}\frac{d}{dx}(-a_i^2 + a_r^2)(gd)^{1/2} \\ & + \rho g\frac{\sin\theta}{(gd_B)^{1/2}}(-a_i a_r f - a_r^2)(gd)^{1/2}\end{aligned} \tag{4.31}$$

4.4.3 Longshore Current Solution Without Mixing

Due to the complexity of both the bottom stress and the longshore radiation stress, an analytic solution to the differential equation (4.19) is still prohibitively difficult. However, we can determine the longshore current in front of a seawall with no mixing by neglecting the eddy viscosity term in the longshore equation of motion. Figure 4.6 shows the no-mixing longshore current calculated from two possible bottom stresses using case 3d from Table 4.1 and a seawall located at 20% of the no seawall surf zone width. First, the longshore current using the bottom stress formulation in (4.28), which includes the spatial oscillation term, is presented. A second bottom stress, determined by the approximation $a_i + a_r f \approx \kappa\, d/2$, further simplifies the problem. Figure 4.6 shows that this approximation has only a small effect on the longshore current throughout the surf zone, except very close to the seawall where the prediction is non-conservative. For both cases, the longshore current velocity, v, has been non-dimensionalized by the no-mixing, no seawall longshore current evaluated at the breaker line, $v_{B\,no\,wall}$. The no-mixing longshore current profiles shown in Figure 4.6 are questionable not only in magnitude, but also in the large shear developed by the modulations. Including a mixing term to generate a reasonable longshore current profile is more important for a surf zone with a seawall than for one without.

By further simplifying the bottom stress, we have now eliminated the second of the three places where the partial standing wave is encountered. Earlier we showed that the total depth could be approximated as linear, even though the setup is modulated. Here we have also eliminated the spatial oscillation term from the bottom stress to yield

$$\tau_{by} = -\frac{\rho}{\pi} c_f \kappa (g d)^{1/2} v \qquad (4.32)$$

This is the same form of the bottom stress found in many of the no seawall solutions to the longshore equation of motion (*MH83*). The third manifestation of

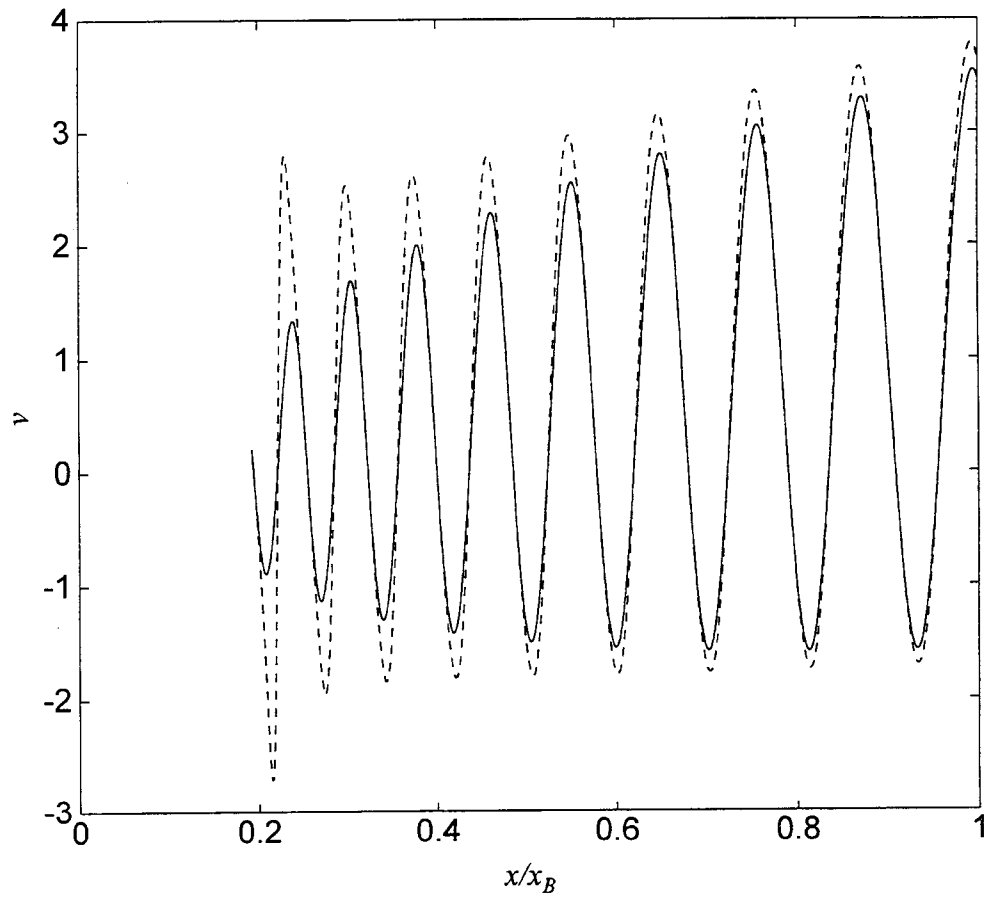

Figure 4.6 Longshore current in front of seawall with no mixing, using model case # 3d and two formulations of the bottom stress, $\tau_{by} \propto (a_i + a_r f)\, v$ (dotted line) and $\tau_{by} \propto \kappa\, d/2\, v$ (solid line).

the spatial oscillation term, which has been retained, is in the forcing of (4.19), dS_{xy}/dx.

4.4.4 Longshore Current Solution With Mixing

We can now simplify the longshore equation of motion (4.19) by using the final form of the bottom stress. The dimensional equation for longshore current in front of a seawall can be written as

$$x^{*2}\frac{d^2v^*}{dx^{*2}} + \frac{5}{2}x^*\frac{dv^*}{dx^*} - \frac{v^*}{P} = \begin{cases} \dfrac{1}{(\rho^* Ns(g^* sx^*)^{1/2})}\dfrac{dS^*_{xy}}{dx^*}; & x^* < x_B^* \\ 0; & x^* > x_B^* \end{cases} \tag{4.33}$$

where the lateral mixing coefficient is

$$P = \frac{N\pi s}{c_f \kappa} \tag{4.34}$$

After non-dimensionalizing (4.33) in the same manner as the cross-shore equation of motion and expanding the radiation stress term, the non-dimensional longshore equation of motion can be written as

$$X^2\frac{d^2V}{dX^2} + \frac{5}{2}X\frac{dV}{dX} - \frac{V}{P} = \begin{cases} c_3X + c_4X^{-1/4} + c_5X^{-1/4}f + c_6X^{3/4}f' + c_7X^{-1/2}f\ ; & X<1 \\ 0; & X>1 \end{cases} \tag{4.35}$$

where

$$c_3 = -\frac{5\sin 2\theta \kappa^2 C_B}{32N} \; ; \qquad c_4 = \frac{5\sin 2\theta \kappa A^{1/2}\gamma^{1/4} C_B}{16N}$$

$$c_5 = -\frac{5\sin\theta \kappa A^{1/2}\gamma^{1/4} C_B}{8N} \; ; \quad c_6 = -\frac{\sin\theta \kappa A^{1/2}\gamma^{1/4} C_B}{2N} \qquad \textbf{(4.36)}$$

$$c_7 = \frac{\sin\theta A\gamma^{1/2} C_B}{N}$$

and $C_B = (g^* d_B^*)^{1/2}/v_{B\,no\,wall}^*$ is a non-dimensional break point celerity. This is the Euler equation and has a homogeneous solution of the form

$$V_h = A_1 X^{\lambda_1} + A_2 X^{\lambda_2} \qquad \textbf{(4.37)}$$

where

$$\lambda_{1,2} = \frac{-3 \pm (9 + \frac{16}{P})^{1/2}}{4} \qquad \textbf{(4.38)}$$

and A_1 and A_2 are integration constants. The particular solution is determined via the method of undetermined coefficients. However, due to the complicated forcing terms in (4.35), P must be chosen carefully to give values of $\lambda_{1,2}$ for which the integrals arising from the solution technique can be solved. This is not a severe limitation in that the longshore current can still be solved over a range of P values consistent with what is usually presented in longshore current discussions. In the subsequent discussion of the model results, solutions with $P = 0.4$ are presented. Once again, note that as $K_r \rightarrow 0$ (4.35) collapses on to the no seawall formulation of longshore currents on a planar beach.

Boundary conditions are introduced to evaluate the integration constants. The velocity must be bounded far offshore and the velocity and the gradient of the velocity must match at the breaker line.

$$V(X \rightarrow \infty) \rightarrow bound \qquad \textbf{(4.39 a)}$$

$$V(1^-) = V(1^+); \quad \frac{d}{dx}V(1^-) = \frac{d}{dx}V(1^+) \qquad \textbf{(4.39 b,c)}$$

Typically, in longshore current models the velocity must also be bound at the shoreline. In the present model, with wave reflection off of a seawall, a mixed boundary condition was chosen which allows for a no-slip wall condition, free-slip wall condition, or a combination of the two

$$\psi_1 V(X = X_{wall}) + \psi_2 \frac{d}{dx} V(X = X_{wall}) = \psi_3 \qquad \textbf{(4.40)}$$

The free-slip condition, with $\psi_1 = 0$, $\psi_2 = 1$ and $\psi_3 = 0$, is the only boundary condition for which results are presented.

With a model for wave setup, and the longshore equation of motion solved, the longshore current in front of a seawall can now be calculated. Non-dimensionalizing does not sufficiently reduce the number of parameters to develop generic plots, so individual cases must be analyzed resulting in rather cumbersome sensitivity analyses. Figure 4.7 shows the longshore current in front of a seawall for case 3d with the seawall located at several positions across the surf zone. As found by Jones (1975), local maxima and minima are evident in the current profiles due to the partial standing waves which develop in front of the seawall. The magnitudes of the longshore currents are sensitive to the position of the seawall, and in the present case the largest current is found when the seawall is approximately three fifths of the way across the surf zone. The *MH83* solution is also shown in Figure 4.7 and the position of the seawall determines whether or not it increases or decreases the longshore current relative to the longshore current on a similar beach with no wall. This dependency on relative seawall location confirms a hypothesis that has been suggested by many researchers (*eg.* Dean, 1986; Weggel, 1988 and Griggs and Tait, 1990).

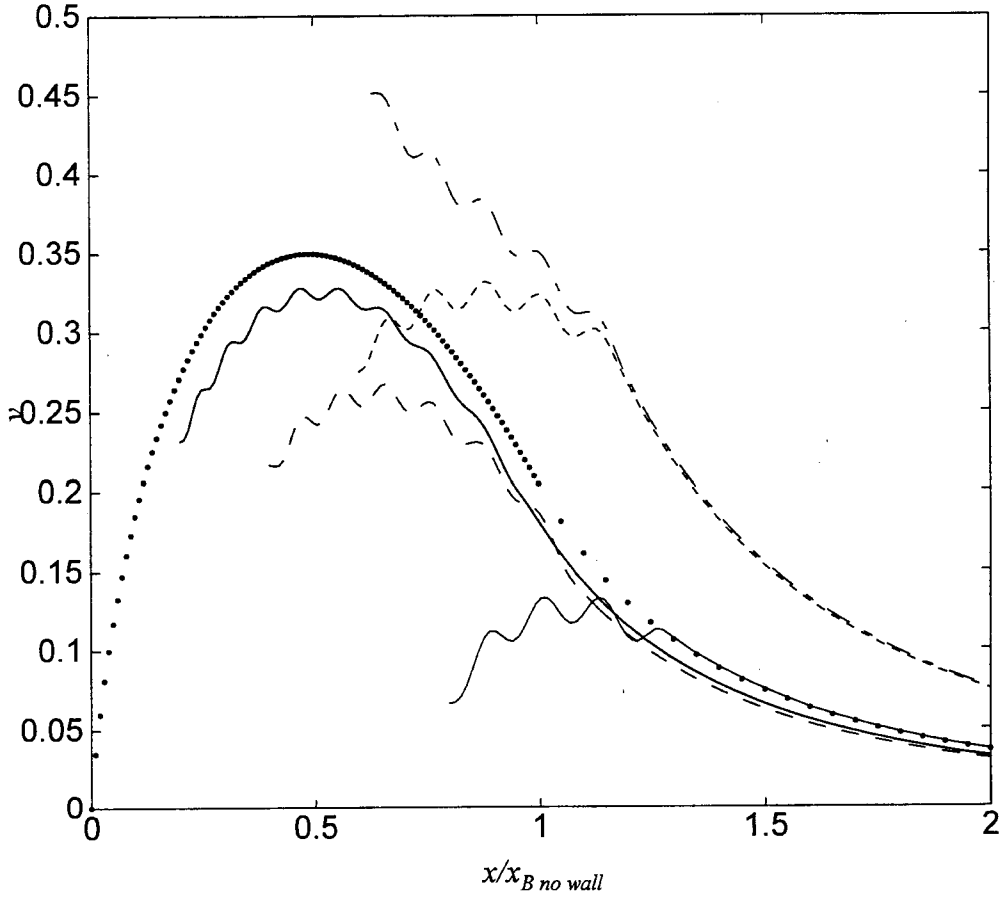

Figure 4.7 Longshore current profiles fronting a seawall for model case # 3d and several positions of the wall, $x_{wall}/x_{B\ no\ wall}$ = 0.2 (thick solid line), 0.4 (dashed line), 0.6 (small dotted line), 0.63 (dashed-dot line) and 0.8 (thin solid line). The large dots represent the longshore current with no seawall (MH83).

Figure 4.7 was generated for a single beach/wave condition and 5 positions of the seawall. Similar results have been generated for many other conditions but are not presented. The model substantiates the observation made by Weggel (1988) that "reflected waves alter radiation stresses and thus affect the cross-shore distribution of longshore current velocity in front of the wall." However, the behavior of the profiles are quite complex. This suggests that integrated quantities across the surf zone might be simpler to analyze. Figure 4.8 shows the results of many model runs in which the longshore current has been integrated from the seawall out to an offshore location of five times the break point to yield the total longshore volumetric flow rate, Q_{tot}. The shallow water assumption is violated in the calculation of Q_{tot} at this distance offshore. However, the velocities are small at these distances so the influence on the total flow is rather small. The total volumetric flow rate from the no wall solution is calculated by integrating the longshore current from the hypothetical seawall location to five times the no wall break point. Each panel in Figure 4.8 represents one beach slope, three offshore wave conditions, and many positions of the seawall ranging from 20% to 80% of the no wall surf zone width. Figure 4.8a, the steepest beach (1V:10H), shows a fairly simple response to the location of the seawall. The total volumetric flow rate decreases as the wall is pushed seaward until the wall is approximately 70% of the way across the no wall surf zone when the flow begins to increase. This steep beach sharply reduces the amount of longshore current as compared to a beach without a seawall. Figure 4.8b reveals that a moderately sloped beach (1V:20H) increases the longshore current relative to a beach with no wall. Interestingly, the larger wave heights and longer wave periods force less total flow than the smaller waves. The next two panels, for mild slopes of 1V:50H (Figure 4.8c) and 1V:100H (Figure 4.8d), have many inflection points. This clearly demonstrates the strong dependence of the longshore current on the cross-shore position of the seawall in the surf zone.

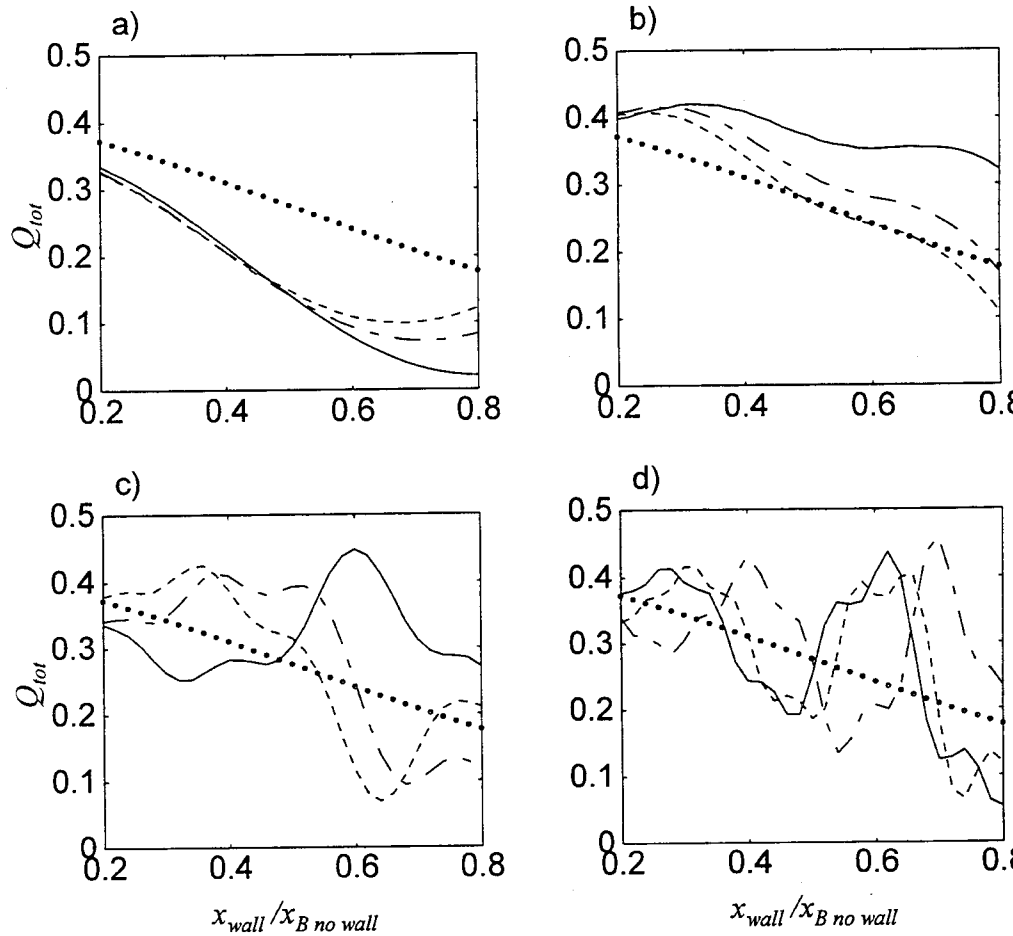

Figure 4.8 Total volumetric flow rate fronting a seawall for 4 planar beach slopes, a) m = 1:10, b) m = 1:20, c) m = 1:50, d) m = 1:100, and several wave conditions, case 1, from Table 4.1, (solid line), 2 (dashed-dot line) and 3 (small dotted line). The large dots represent the total volumetric flow rate with no seawall.

4.5 Longshore Sediment Transport

Once the longshore current in front of a seawall is known, an estimate of the longshore sediment transport profile is possible. A Bagnold-type energetics model (Bagnold, 1963) is used which includes both bed load and suspended load. The model assumes that the orbital wave motion mobilizes the sediment, wave power is expended maintaining the sediment in motion, and the presence of a mean current, regardless of how small, transports the sediment. In calculating the sediment transport, the same set of assumptions are used as when determining the wave setup and the longshore current. Non-dimensionalizing the transport rate by the no seawall, no mixing transport rate evaluated at the breaker line, the dimensionless transport, I, is given as

$$I = \left(\frac{d_B}{d_{B\ no\ wall}}\right)^2 X\ V \tag{4.41}$$

Figure 4.9 shows the non-dimensional sediment transport profile in front of a seawall for case 3d and the same positions of the seawall which were presented in Figure 4.7. Similar to the response of the longshore current model, the magnitudes of sediment transport depend greatly on the position of the seawall. Figure 4.10 reveals the dependency of the total quantity of sediment transport, I_{tot}, as a function of bottom slope, wave conditions, and the position of the seawall. I_{tot} is calculated by integrating the transport from the position of the seawall to the break point. The integration stops at the break point because the sediment transport model is only valid in the surf zone. Due to the simplicity of the sediment transport model, the integrated sediment transport responds similarly to the integrated longshore current. For steep beaches, the total longshore transport is less than that on a beach without a seawall. On moderately sloped beaches, the total transport is greater than a beach without a seawall. For mild sloped beaches, the total transport is generally greater with a seawall, but depends on the surf zone width relative to the number of standing waves within the surf zone. Figure 4.11 demonstrates the effect the reflection coefficient, K_r, has on the total sediment

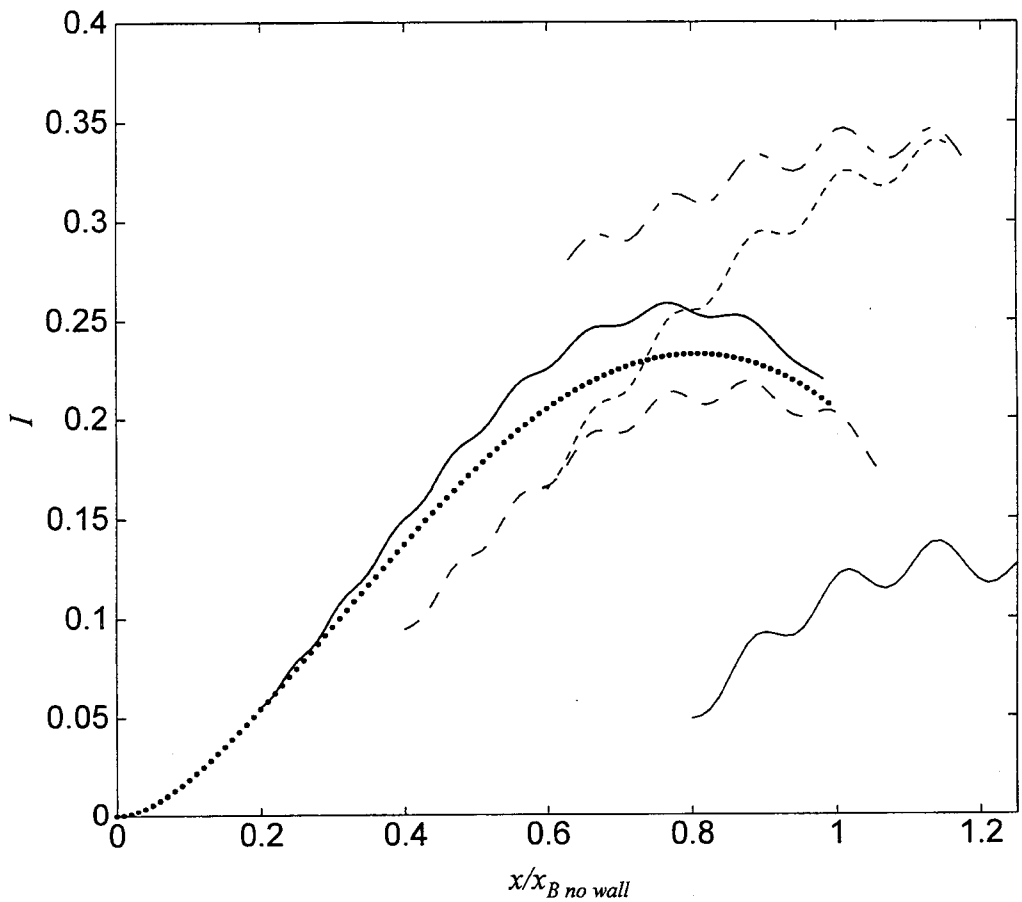

Figure 4.9 Sediment transport profiles fronting a seawall for model case # 3d and several positions of the wall, $x_{wall}/x_{B\ no\ wall} = 0.2$ (thick solid line), 0.4 (dashed line), 0.6 (small dotted line), 0.63 (dashed-dot line) and 0.8 (thin solid line). The large dots represent the sediment transport with no seawall.

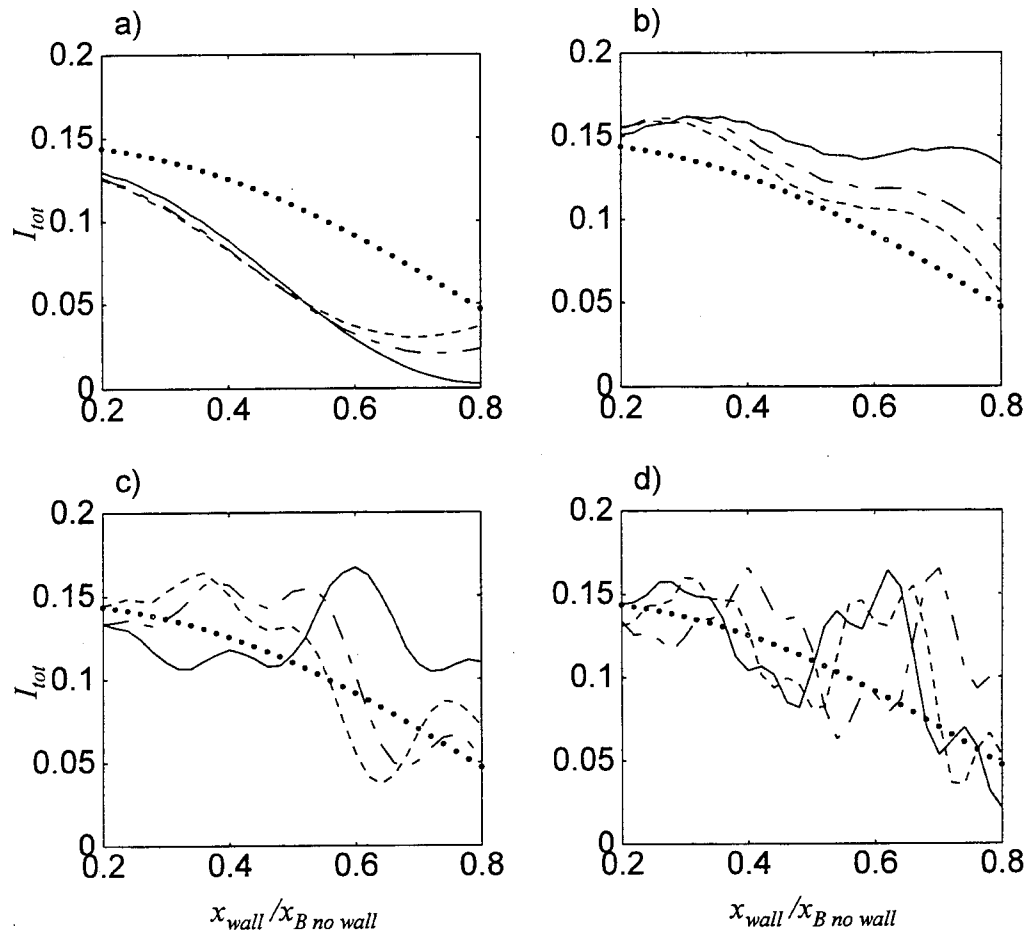

Figure 4.10 Total sediment transport fronting a seawall for 4 planar beach slopes, a) m = 1:10, b) m = 1:20, c) m = 1:50, d) m = 1:100, and several wave conditions, case 1 (solid line), 2 (dashed-dot line) and 3 (small dotted line). The large dots represent the total sediment transport with no seawall.

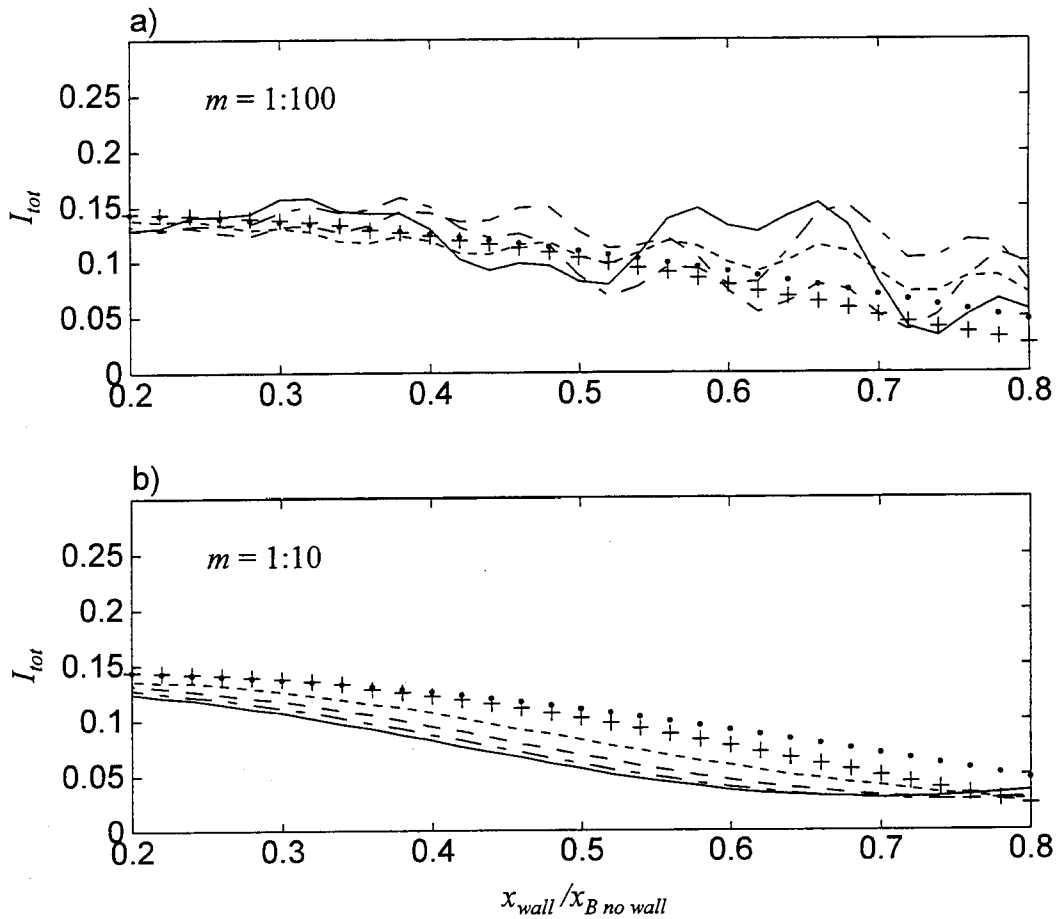

Figure 4.11 Effect of reflection coefficient on total sediment transport for two planar beach slopes a) m = 1:100, b) m = 1:10 and 5 reflection coefficients, K_r = 1.0 (solid line), 0.75 (dashed-dot line), 0.50 (dashed line), 0.25 (small dotted line) and 0.01 (pluses). The large dots represent the total sediment transport with no seawall.

transport. For the mild slope (Figure 4.11a), decreasing the reflection coefficient reduces the oscillations in the response due to a smaller standing wave system in the surf zone. For the steep sloping beach (Figure 4.11b), increasing the reflection coefficient actually decreases the total sediment transport for most positions of the seawall. For both beaches the model shows the total sediment transport tending toward the no wall solution as the reflection coefficient goes to zero.

4.6 Comparison With The Long Wave Equation

Solving the linear long wave equation

$$\frac{d^2}{dt^*}\overline{\eta^*} = \frac{d}{dx^*}(g^* d^* \frac{d}{dx^*}\overline{\eta^*}) \qquad (4.42)$$

with a seawall as the landward boundary condition both confirms some of the results of the present model and sheds light on the complex behavior of longshore processes fronting a seawall. The solution for the free surface profile in front of a seawall, from the long wave equation, is a combination of Bessel functions. In Figure 4.12, a dimensionless amplification factor, $\bar{\eta}/d_{B\ no\ wall}$, from the long wave equation is compared to the solution of the cross-shore equation of motion, (4.15). Although the magnitudes of the two solutions are quite different (note the different scales on the vertical axes) the similarity in the modulations of the free-surface is apparent. The results presented in this figure were calculated for case 3d with the seawall at 20% of the no wall surf zone width, $x_{wall}/x_{B\ no\ wall} = 0.2$. Similar results have been reproduced for all cases. The modulations in the long wave equation can also be compared to the modulations in the longshore current profile. Figure 4.13 shows that there is a one to one correspondence between the modulations of the cross-shore model and the longshore model.

Due to the Bessel function nature of the solution to (4.42), as the seawall is moved seaward the linear long wave equation encounters singularities which result

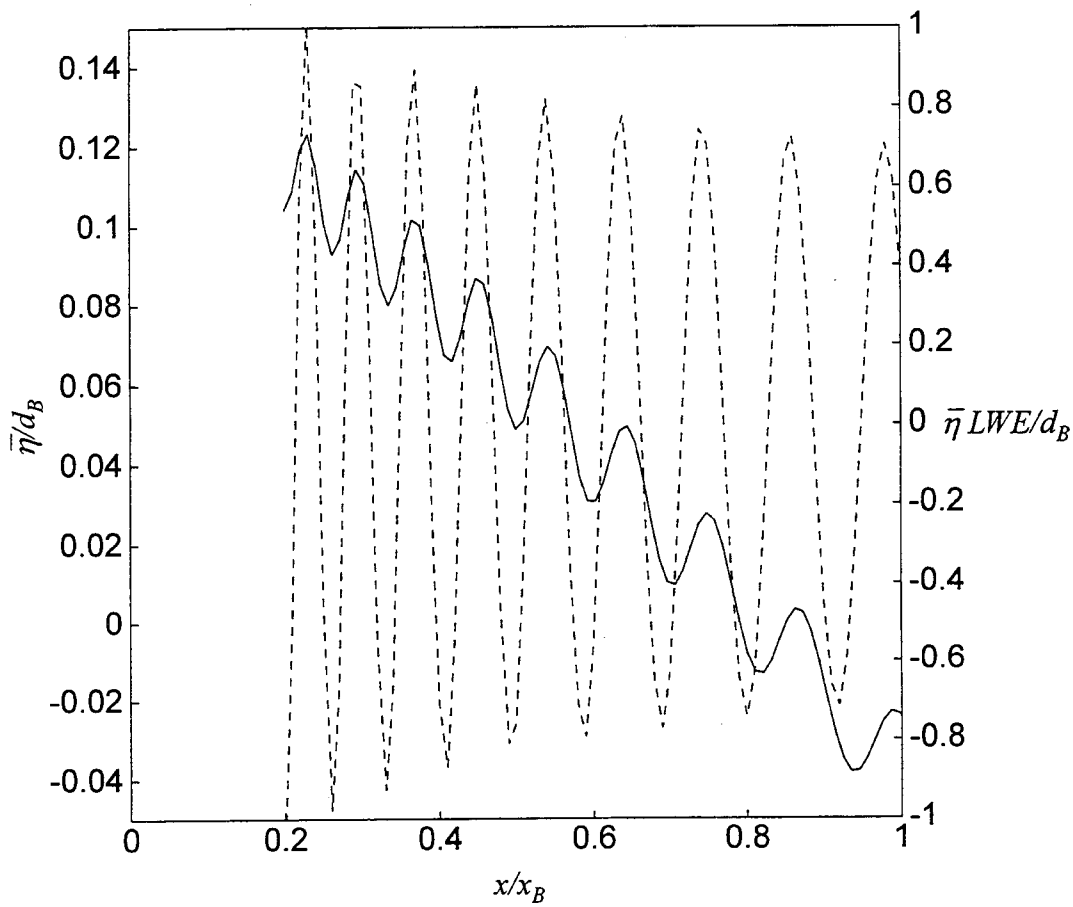

Figure 4.12 Comparison between the wave setup in front of a seawall (solid line) and the linear long wave equation (dotted line).

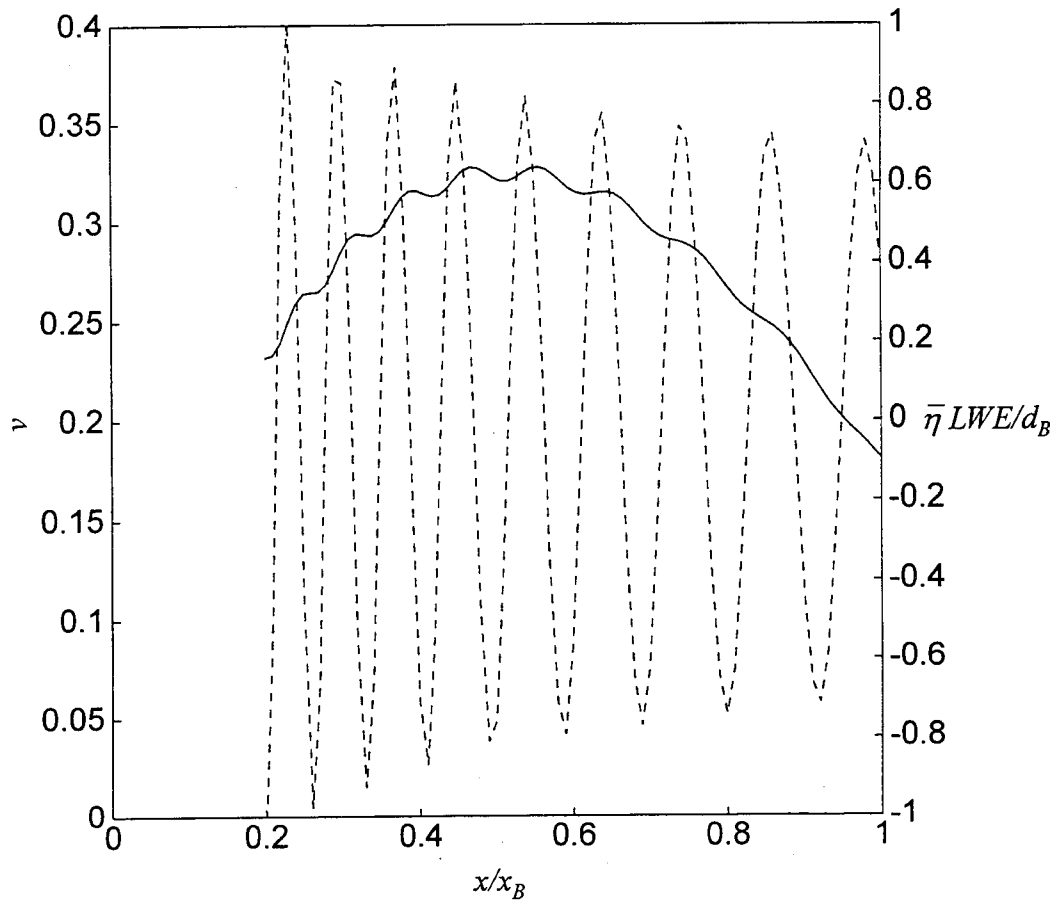

Figure 4.13 Comparison between the longshore current fronting a seawall (solid line) and the linear long wave equation (dotted line).

in free-surfaces with infinite magnitudes. The larger the surf zone width, the more singularities. Figure 4.14 shows the integrated total volumetric flow rate, for several positions of the seawall, for case 3c and case 3d. Superimposed on the figure are the positions of the seawall which cause singularities in the long wave equation for these two cases. Again, there is almost a one to one correspondence between the singularities and each inflection point in the total longshore current. Earlier, it was shown that the maximum longshore current for case 3d occurs when the seawall is at a cross-shore position of three fifths of the no wall surf zone width ($x_{wall}/x_{B\ no\ wall} = .63$). This corresponds almost exactly to one of the singularities in the long wave equation. Figure 4.15 shows the maximum longshore current as a function of the seawall location for case 3c and 3d. The singularities in the long wave equation fall exclusively on or near the local maxima and minima in these curves. These results are somewhat surprising as we are comparing a cross-shore quantity from a fairly simple model with longshore quantities from a much more complex model. It does, however, suggest that the behavior of the longshore current and sediment transport in front of a seawall can be explained in terms of a resonance, which is tuned by the position of the seawall across the surf zone.

4.7 Conclusions

An analytic model has been developed to estimate longshore currents and the associated sediment transport on a planar beach backed by a seawall. The model assumes shallow water, small angle of wave incidence, spilling breakers and conservation of reflected wave energy flux. A partial standing wave develops in front of the seawall causing modulations in the bottom shear stress, radiation stresses and the resulting setup, longshore current and longshore sediment transport. Modulations associated with the total water depth and bottom stress are relatively small and can be neglected. The modulation of the radiation stress is

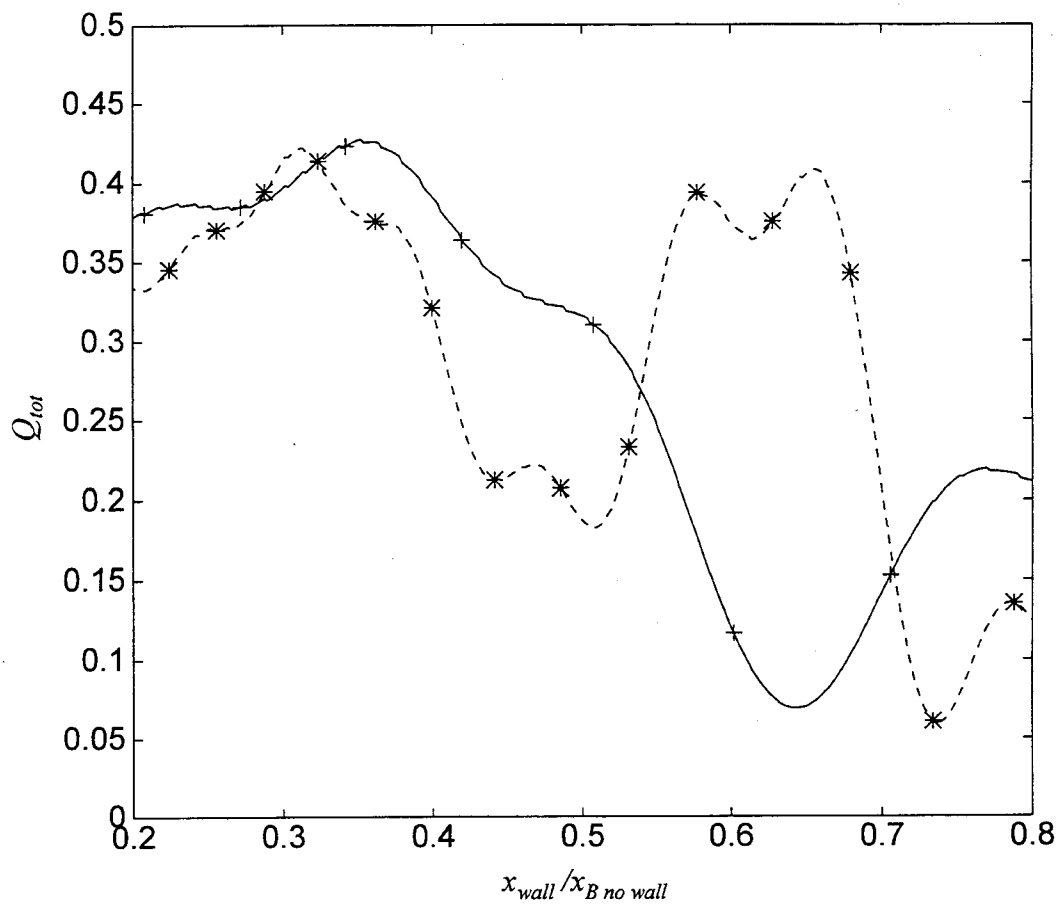

Figure 4.14 Singularities of the long wave equation (pluses and asterisks) superimposed on the total volumetric longshore flow rate fronting a seawall (solid line and dotted line) for cases 3c and 3d respectively, and many positions of the seawall.

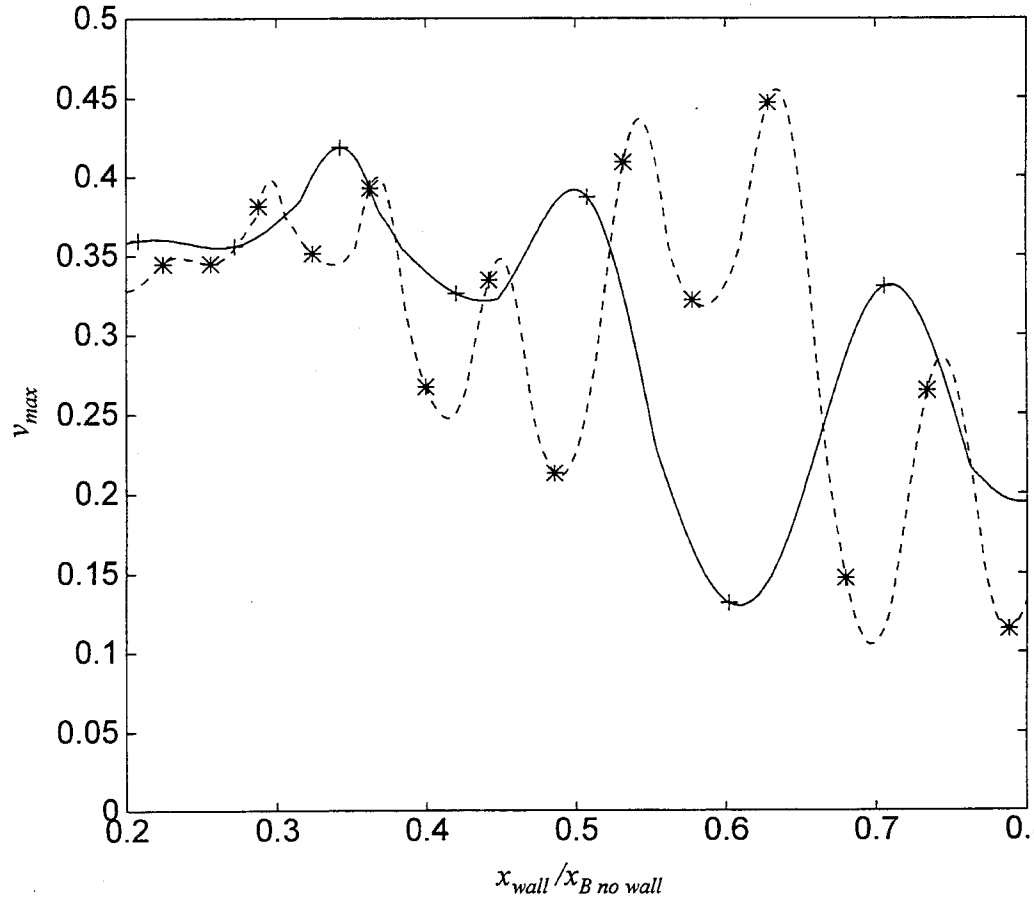

Figure 4.15 Singularities of the long wave equation (pluses and asterisks) superimposed on the maximum longshore current (solid line and dotted line) for cases 3c and 3d respectively, and many positions of the seawall.

retained and forces longshore current and sediment transport profiles which behave quite differently than no wall formulations.

Reflection from a seawall causes waves to break further seaward, resulting in a steeper total depth slope. However, the effective width of the surf zone (the distance from the seawall to the break point) is actually less than the surf zone width without a seawall. As the reflection coefficient goes to zero, the present model collapses to the no wall solutions for wave setup, longshore current and sediment transport on planar beaches. The magnitudes of the longshore current and sediment transport in front of a seawall can be either greater than or less than a similar beach without a seawall, depending on the location of the seawall in the surf zone, the beach slope and the wave conditions. A comparison with the solution to the linear long wave equation suggests that the position of the seawall serves to tune the surf zone with some positions forcing a resonant condition causing local maxima and minima in the behavior of the longshore current and sediment transport.

CHAPTER FIVE: CONCLUSIONS

This thesis characterizes wave runup on high energy dissipative beaches utilizing results from field investigations performed on the central Oregon coast. A methodology is developed to predict the susceptibility of coastal properties to erosion. This model is valid for sea cliffs, sand dunes and coastal protection structures which are intermittently impacted by extreme wave runup events. For vertical structures, whether sea cliffs or sea walls that have toes seaward of the mean water line, longshore processes become increasingly important. Therefore, an analytic model which predicts longshore currents and sediment transport on beaches backed by vertical structures has been formulated. The main conclusions of this thesis can be summarized as follows.

1) Extreme wave runup statistics have been found to have a linear dependence on the deep-water significant wave height on high energy dissipative beaches. Dimensional runup has also been parametrized by $(\beta H_s L_o)^{1/2}$. Measured water levels on the central Oregon coast can be significantly different than predicted tides, but the extreme events typically do not coincide with extreme storms. Predictions of extreme total water levels, including water levels measured by tide gauges as well as water levels due to wave runup, have been used to determine the relative susceptibility to erosion of coastal properties. Model results compare well with qualitative observations, illustrating the application of the model to coastal zone management decision making.

2) Wave runup on high energy dissipative beaches is dominated by very low frequency infragravity energy. Runup spectra show a large saturated region with an f^{-4} roll off extending to lower frequencies than previously reported. Significant vertical runup elevations varied by a factor of 2 over a 1.6 km study area and were found to depend strongly on the local foreshore slope. Runup at Agate Beach, Oregon is coherent over large alongshore length scales, on the order of 1200 m at

peak frequencies. The cut-off wave length for leaky modes is approximately 60 km at the peak runup frequencies, so even with a 1.6 km array of runup measurements, most edge wave modes were not resolved.

3) Partial standing waves develop in front of vertical structures causing modulations in the bottom shear stress, radiation stresses and the resulting setup, longshore current and longshore sediment transport. Modulations associated with the total water depth and bottom stress are relatively small and can be neglected. The magnitudes of the longshore current and sediment transport in front of a vertical structure can be either greater than or less than on a similar beach without a structure, depending on the location of the structure within the surf zone, the beach and the offshore wave conditions. A comparison with the solution to the linear long wave equation suggests that the position of the structure serves to tune the surf zone, with some positions forcing a resonant condition causing local maxima an minima in the behavior of the longshore current and sediment transport.

In addition to the above conclusions, this work identifies the potential for several future directions. The methodology for predicting the relative susceptibility of coastal properties to erosion would benefit from an inclusion of the impact forces associated with wave runup as well as the corresponding erosion rates of sea cliffs and sand dunes. More wave runup measurements would be useful on high energy intermediate beaches with Iribarren numbers higher than those reported here. Also, runup measurements during large storm events would demonstrate whether the functional relationships determined in this study still hold during extreme conditions. Finally, the analytic model developed in Chapter 4 should be verified in both the laboratory and the field.

BIBLIOGRAPHY

Aagard, T., and Holm, J., 1989, "Digitization of Wave Runup Using Video Records," *Journal of Coastal Research*, 5, pp. 547-551.

Aagard, T., 1990, "Swash Oscillations on Dissipative Beaches - Implications for Beach Erosion," *J. of Coast. Res.*, Special Issue No. 9, pp. 738-752.

Bagnold, R.A., 1963, "Beach and Nearshore Processes, Part I. Mechanics of Marine Sedimentation," *In: M.N. Hill (Editor), The Sea*, pp. 507-528.

Battjes, J.A., 1971, "Run-up Distributions of Waves Breaking on Slopes," *ASCE Journal of Waterways Harbor and Coastal Engineering Division*, 92, pp. 91-114.

Battjes, J.A., 1974, "Surf Similarity," *Proceedings 14th Coastal Engineering Conference, American Society of Civil Engineers*, pp. 466-479.

Birkemeier, W.A., 1980, "The Effects of Structures and Lake Level on Bluff and Shore Erosion in Berrigen County, Michigan, 1970-1974," *Miscellaneous Report No. 80-2, Coastal Engineering Research Center*, U.S. Army Corps of Engineers, 74 pp.

Bowen, A.J., Inman, D.L. and Simmons, V.P., 1968, "Wave Set-down and Set-up," *Journal of Geophysical Research*, Vol 73, pp. 2569-2577.

Bowen, A.J., 1969, "The Generation of Longshore Currents on a Plane Beach," *Journal of Marine Research*, 27, pp. 206-215.

Carpenter, D.D., 1995, "Application of Beach and Dune Erosion Models to the Oregon Coast," *Engineering Report, Dept. of Civil Engineering*, Oregon State University, Corvallis, OR, 102 pp.

Carrier, G.F. and Greenspan, H.P., 1958, "Water Waves of Finite Amplitude on a Sloping Beach," *Journal of Fluid Mechanics*, 4, pp. 97-109.

Dean, R.G., 1986, "Coastal Armoring: Effects, Principles, and Mitigation." *Proceedings 20th Coastal Engineering Conference, American Society of Civil Engineers*, pp. 1843-1857.

Douglass, S.L., 1992, "Estimating Extreme Values of Run-up on Beaches," *Journal of Waterway, Port, Coastal and Ocean Engineering*, Vol. 118, No. 2, pp. 220-224.

Gares, P.A. 1990, "Predicting Flooding Probability for Beach/Dune Systems," *Environmental Management*, Vol. 14, No. 1, pp. 115-123.

Griggs, G.B. and Tait, J.F., 1990, "Beach Response to the Presence of a Seawall, A Comparison of Field Observations," *Shore and Beach*, pp. 11-28.

Griggs, G.B., Tait, J.F., and Corona, W., 1994, "The Interaction of Seawalls and Beaches: Seven Years of Monitoring, Monterey Bay, California," *Shore and Beach*, pp. 21-28.

Guza, R.T. and Bowen, A.J., 1976, "Resonant Interactions for Waves Braking on a Beach," *Proceedings 15th Coastal Engineering Conference, American Society of Civil Engineers*, pp. 560-579.

Guza, R.T., Thornton, E.B. and Holman, R.A., 1984, "Swash on Steep and Shallow Beaches," *Proceedings 19th Coastal Engineering Conference, American Society of Civil Engineers*, pp. 708-723.

Guza, R.T. and Thornton, E.B., 1982, "Swash Oscillations on a Natural Beach," *J. of Geophys. Res.*, 87, pp. 483-491.

Hearon, G.E, 1995, "Long-Term Beach Response to Shore Stabilization Structures," *Engineering Report, Department of Civil Engineering*, Oregon State University, Corvallis, Oregon, 176 pp.

Hearon, G.E, McDougal, W.G. and Komar, P.D., (in press), "Long-Term Beach Response to Shore Stabilization Structures," *Proceedings 25th Coastal Engineering Conference, American Society of Civil Engineers*.

Holland, K.T. and Holman, R.A., 1993, "The Statistical Distribution of Swash Maxima on Natural Beaches," *J. of Geophys. Res.*, 98, pp 10271-10278.

Holland, K.T., 1995, "Foreshore Dynamics: Swash Motions and Topographic Interactions on Natural Beaches," *Ph.D. Thesis, Department of Oceanography,* Oregon State University, 119 pp.

Holland, K.T., Holman, R.A., Lippman, T.C., Stanley, J. and Plant, N.G., 1997, "Practical use of Video Imagery in Nearshore Oceanographic Field Studies," *Journal of Oceanic Engineering*, Special Issue on Image Processing for Oceanic Applications, Vol. 22, No 1, pp. 81-92.

Holman, R.A. and Guza, R.T., 1984, "Measuring Runup on a Natural Beach," *Coastal Engineering*, 8, pp 129-140.

Holman, R.A. and Sallenger, A.H., 1984, "Longshore Variability of Wave Run-up on Natural Beaches," *Proceedings 19th Coastal Engineering Conference, American Society of Civil Engineers*, pp. 1896-1912.

Holman, R.A. and Sallenger, A.H., 1985, "Setup and Swash on a Natural Beach," *J. Geophys. Res.*, 90, pp. 945-953.

Holman, R.A., 1986, "Extreme Value Statistics for Wave Run-up on a Natural Beach," *Coastal Engineering*, 9, pp. 527-544.

Holman, R.A., Howd, P., Oltman-Shay, J. and Komar, P.D., 1990, "Observations of the Swash Expression of Far Infragravity Wave Motions," *Proceedings 22nd Coastal Engineering Conference, American Society of Civil Engineers*, pp 1242-1253.

Hunt, I.A., 1959, "Design of Seawalls and Breakwaters," *J. Waterw. Harbors Div.*, 85, pp. 123-152.

Huntley, D., Guza, R.T. and Bowen, A.J., 1977, "A Universal Form for Shoreline Run-up Spectra?," *J. Geophys. Res.*, 82, pp 2577-2581.

Huyer, A., Gilbert, W.E, and Pittock, H.L., 1983 "Anomalous Sea Levels at Newport, Oregon, During the 1982-83 El Niño," *Coastal Oceanography and Climatology News*, 5, pp. 37-39.

Jones, D.F., 1975, "The Effect of Vertical Seawalls on Longshore Currents," *unpublished Ph.D. Thesis, Department of Coastal and Oceanographic Engineering*, University of Florida, Gainesville, FL, 188 pp.

Kamphuis, J.W. Rakha, K.A., and Jui, J., 1992, "Hydraulic Model Experiments on Seawalls," *Proceedings 23rd Coastal Engineering Conference, American Society of Civil Engineers*, pp. 1272-1284.

Kobayashi, N., DeSilva, G.S. and Watson, K.D., 1989, "Wave Transformation and Swash Oscillation on Gentle and Steep Slopes," *J. of Geophys. Res.*, 94, pp. 951-966.

Komar, P.D., 1977, "Beach Profiles on the Oregon and Washington Coasts Obtained with an Amphibious DUKW," *The Oregon Bin*, 39, pp. 169-180.

Komar, P.D. and Enfield, D.B., 1987, "Short-term Sea-level Changes and Coastal Erosion," In *Sea-level Fluctuations and Coastal Evolution*, edited by D. Nummedal et al. Soc. Econ. Paleo. and Mineral., Special Publication No. 41, pp. 17-27.

Komar, P.D. and Shih, S.-M., 1993, "Cliff Erosion Along the Oregon Coast: A Tectonic-Sea Level Imprint Plus Local Controls by Beach Processes," *J. of Coast. Res.*, 9, pp. 747-765.

Komar, P.D., McDougal, W.G. and Carpenter, D.D., 1995, "The Application of Beach and Dune Erosion Models to the High-Energy Oregon Coast," *Report to the Oregon Department of Land Conservation and Development.*

Komar, P.D., Ruggiero, P. and McDougal, W.G., 1995, "Beach and Foredune Erosion Along the Oregon Coast - Data Sources -," *Report to the Oregon Department of Land Conservation and Development.*

Kraus, N.C. and McDougal, W.G., 1996, "The Effects of Seawalls on the Beach: Part I, An Updated Literature Review," *J. of Coast. Res.*, Vol 12:3, pp 691-701.

Kraus, N.C., Smith, J.M. and Sollitt, C.K., 1992, "SUPERTANK Laboratory Data Collection Project," *Proceedings 23rd Coastal Engineering Conference*, American Society of Civil Engineers, pp. 2191-2204.

Kraus, N.C., 1987, "The Effects of Seawalls on the Beach: A Literature Review," *Proceedings Coastal Sediments '87*, American Society of Civil Engineers, pp. 945-960.

Longuet-Higgens, M.S. and Stewart R.W., 1962, "Radiation Stress and Mass Transport in Gravity Waves, with Application to Surfbeats," *J. Fluid Mech.*, 13, pp. 481-504.

Longuet-Higgens, M.S., 1970a, "Longshore Currents Generated by Obliquely Incident Sea Waves, 2" *J. of Geophys. Res.*, Vol 75: pp. 6778-6789.

Longuet-Higgens, M.S., 1970b, "Longshore Currents Generated by Obliquely Incident Sea Waves, 1" *J. of Geophys. Res.*, Vol 75: pp. 6790-6801.

Macdonald, H.V. and Patterson, D.C., 1984, "Beach Response to Coastal Works Gold Coast, Australia," *Proceedings 19th Coastal Engineering Conference*, American Society of Engineers, pp. 1522-1538.

McDougal, W.G. and Hudspeth, R.T., 1983a, "Wave Setup/Setdown and Longshore Currents on Non-planar Beaches," *Coastal Engineering*, Vol 7: pp. 103-117.

McDougal, W.G. and Hudspeth, R.T., 1983b, "Longshore Sediment Transport on Non-planar Beaches," *Coastal Engineering*, Vol 7, pp. 119-131.

McDougal, W.G. and Hudspeth, R.T., 1986, "Influence of Lateral Mixing on Longshore Currents," *Ocean Engineering*, Vol. 13: pp. 4199-433.

McDougal, W.G., Kraus, N.C. and Ajiwibowo, H. 1996, "The Effects of Seawalls on the Beach: Part II, Numerical Modelling of SUPERTANK Seawall Tests," *J. of Coast. Res.*, Vol 12:3, pp 702-713.

Miche, R., 1951, "Le Pouvoir reflechissant des ouvrages maritimes exposes a l'action de la houle," *Ann. Ponts Chaussees*, 121, pp. 285-319.

Muir, L.R. and El-Shaawari, A.H., 1986, "On the Calculation of Extreme Wave Heights: A Review," *Ocean Engineering*, Vol. 13, No. 1, pp. 93-118.

Neilson, P. and Hanslow, D.J., 1991, "Wave Runup Distributions on Natural Beaches, "*J. of Coast. Res.*, Vol. 7., No. 4, pp. 1139-1152.

Pawka, S., 1982, "Wave Directional Characteristics on a Partially Sheltered Coast," *PhD. Thesis, Scripps Institute of Oceanography*, University of California, San Diego.

Plant, N.G. and Griggs, G.B., 1992, "Interactions Between Nearshore Processes and Beach Morphology Near a Seawall," *J. of Coast. Res.*, V.8:1, pp. 183-200.

Plant, N. and Holman, R.A., in prep., "Observations of Alongshore and Cross-shore Beach Variability: Understanding the 2-D Sediment Flux Field," *Marine Geology*.

Pugh, D.T., 1990, Tides, Surges and Mean Sea-Level, *John Wiley & Sons*, New York, 472 pp.

Raubenheimer, B, Guza, R.T., Elgar, S and Kobayashi, N., 1995, "Swash on a Gently Sloping Beach," *J. of Geophs. Res.*, 100, pp. 8751-8760.

Raubenheimer, B. and Guza, R.T., 1996, "Observations and Predictions of Run-up," *J. Geophys. Res.*, 101, pp. 25,575-25,587.

Ruggiero, P., Komar, P.D., McDougal, W.G. and Beach, R.A., in press, "Extreme Water Levels, Wave Runup and Coastal Erosion," *Proceedings 25th Coastal Engineering Conference, American Society of Civil Engineers.*

Ruggiero, P., 1995, "Surveys of Beach Profiles Along the Oregon Coast Obtained in a Study of Sea Cliff and Foredune Erosion," *Engineering Report, Dept. of Civil Engineering*, Oregon State University, Corvallis, OR.

Saville, T., 1962, "An Approximation of the Wave Runup Frequency Distribution," *Proceedings 8th Coastal Engineering Conference, American Society of Civil Engineers*, pp. 48-59.

Shih, S.-M. and Komar, P.D., 1994, "Sediments, Beach Morphology and Sea Cliff Erosion Within an Oregon Coast Littoral Cell," *J. of Coast. Res.*, 10, pp. 144-157.

Shih, S.-M., Komar, P.D., Tillotsen, K.J., McDougal, W.G. and Ruggiero, P., 1994, "Wave Run-up and Sea-Cliff Erosion," *Proceedings 24th Coastal Engineering Conference, American Society of Civil Engineers*, pp. 2170-2184.

Silvester, R., 1977, "The Role of Wave Reflection in Coastal Processes," *Proceedings Coastal Sediments '77*, pp. 639-654.

Thornton, E.B. and Guza, R.T., 1986, "Surf Zone Longshore Currents and Random Waves: Field Data and Models," *Journal of Physical Oceanography*, Vol 16, No 7. pp. 1165-1178.

Tillotsen, K.J. and Komar, P.D., 1997, "The Wave Climate of the Pacific Northwest (Oregon and Washington): A Comparison of Data Sources," *J. Coast. Res.*, Vol. 13, No. 2, pp. 440-452.

US Army Corps of Engineers, 1984, Shore Protection Manual, Vol II. U.S. Army Corps of Engineers Coastal Engineering Research Center, Vicksburg, MS.

van der Meer, J.W. and Stam, C.-J., 1992, "Wave Runup on Smooth and Rock Slopes of Coastal Structures," *Journal of Waterway, Port, Coastal and Ocean Engineering, American Society of Civil Engineers*, 118, pp. 534-550.

Walton, T.L., 1992, "Interim Guidance for Prediction of Wave Run-up on Beaches," *Ocean Engineering*, 19, pp. 119-207.

Weggel, J.R., 1988, "Seawalls: The Need for Research, Dimensional Considerations and a Suggested Classification," In The Effects of Seawalls on the Beach, N.C. Kraus and O.H. Pilkey (Volume Editors), *J. of Coast. Res.*, SI 4, pp 29-40.

Wright, L.D. and Short, A.D., 1983, "Morphodynamics of Beaches and Surf Zones in Australia," *In Handbook of Coastal Processes and Erosion*, ed. P.D. Komar, CRC Press, Boca Raton, Florida, pp 35-64.

APPENDICES

APPENDIX A

A.1 Introduction

This report is the companion volume to a study in which computer models have been used to numerically evaluate ocean processes and sediment transport that cause beach and foredune erosion on the Oregon coast, (Carpenter, 1995; Komar *et al.*, 1995). The goal of this work is to yield quantitative assessments of shoreline stability in the beach/dune environment, information which could be used to determine how oceanfront construction setbacks should be established in dune environments. The test sites to which the erosion models are applied span much of the Oregon coast.

The numerical models require physical information about each test site in order to provide reliable predictions of beach/dune response to storm conditions. Ground surveys of beach profiles, sediment sizes, wave conditions and water levels are necessary for model applications. This report documents an extensive beach profiling database that has been compiled for this study. A more general description of data sources available on the Oregon coast is given in Komar *et al.* (1995). The report also includes data collected for parallel studies undertaken by the same research group, *eg.* runup predictions on beaches backed by sea cliffs (Chapters 2 and 3) and the long term beach response to shore stabilization structures (Hearon *et al.*, in press). Data have been organized by type, *eg.* dune, bluff, or sea cliff backed, and by littoral cell.

A.2 Geologic Setting

Much of the Oregon coast consists of pocket beaches separated by large headlands. These pocket beaches range in size from a few kilometers to over one

hundred kilometers. These pocket beaches are termed littoral cells as sediment within a particular cell tends to stay within that cell. There are differences in the erosional responses of the series of littoral cells, in large part due to different sand volumes of the fronting beach and the varying capacity of the beaches to act as buffers between storm waves and foredunes or sea cliffs.

A.2.1 Littoral Cell Classification

Table A.1 lists the 13 littoral cells on the Oregon coast, from south to north, with the southern and northern boundaries and the approximate length of each cell in kilometers. The littoral cells reported here are similar to those presented by earlier researchers and were determined simply by examining coastal charts for large geographic features, usually headlands. The littoral cells have been named according to the major city located within the cell or after a major feature within the cell. Cell 3 has been split into three sub-cells due to the enormous distance between Cape Arago and Heceta Head. The Umpqua and Siuslaw rivers are natural choices for splitting this large cell into sub-cells, both as geomorphological features and the fact that both rivers have large jetties at their mouths that serve to restrict most longshore sediment transport in the same way as the major headlands do. Morphologic and historical descriptions of the cells on the northern half of the Oregon coast can be found in Komar *et al.* (1995).

A.2.2 Study Sites

Originally, test sites were chosen for this study simply by the constraint that foredunes are present, and that a number of littoral cells are sampled. Of particular interest were sites of past foredune erosion, *e.g.* Pacific City, sites where recent or proposed developments may be in danger from future erosion occurrences, *e.g.* South Beach, and sites where foredune accretion in recent years has resulted in

Table A.1. Oregon littoral cell classification.

#	Cell Name	Southern Boundary	Northern Boundary	Approximate Cell Length (km)
1	Brookings	Crescent City, CA	Cape Blanco	120
2	Bandon	Cape Blanco	Cape Arago	45
3	Umpqua	Cape Arago	Heceta Head	90
3 a	Umpqua (Coos Bay)	Cape Arago	Umpqua River	38
3 b	Umpqua (Reedsport)	Umpqua River	Siuslaw River	33
3 c	Umpqua (Florence)	Siuslaw River	Heceta Head	20
4	Yachats	Heceta Head	Cape Perpetua	18
5	Newport	Cape Perpetua	Yaquina Head	42
6	Beverly Beach	Yaquina Head	Cape Foulweather	10
7	Lincoln City	Cape Foulweather	Cascade Head	30
8	Nestucca	Cascade Head	Cape Kiwanda	14
9	Sand Lake	Cape Kiwanda	Cape Lookout	13
10	Netarts	Cape Lookout	Cape Mears	15
11	Rockaway	Cape Mears	Cape Falcon	28
12	Cannon Beach	Cape Falcon	Tillamook Head	18
13	Clatsop Plains	Tillamook Head	Columbia River	30

public pressure to permit dune regrading, *e.g.* Manzanita and Seaside. During model testing it was subsequently learned that offshore bathymetry data was necessary in accurately modeling beach/dune responses to extreme Oregon storm conditions. This is because low sloping beaches, common in Oregon, can have surf zones extending well over a kilometer in width during major storms. Bathymetric data off of the Oregon coast is almost non-existent, save for work done by Willard Bascom in the 1940's (Komar, 1977), due to the difficulty in gathering data in such a harsh environment. These Bascom sites were re-occupied, ground surveys were obtained, and an attempt was made to patch our "modern" beach profiles onto Bascom's "historical" bathymetric data. As mentioned earlier, other studies have been performed during this same period in which beaches backed by sea cliffs and shore stabilization structures have been monitored. Data gathered during those studies are included in this report for completeness and to provide relevant information on shoreline stability for beaches having a variety of morphological characteristics.

Beach profile and sediment size information is reported here for 23 sites, representing 12 of the 13 littoral cells mentioned above. Beach profiles were obtained with an Omni Total Station. Obtaining survey data with the Omni differs from classical surveying techniques in that the Omni remains stationary and measures the location of the target point with respect to its own location and an azimuth set by the user, usually north equals 0 degrees. The target point is a prism mounted atop a staff which the rod-person holds at the desired place on the beach. The Omni sends an optical signal which is returned by the prism and is then processed internally by the Omni unit. The Omni has the capability of measuring and storing up to 180 data points in Cartesian coordinates. Slope distance, vertical angle, and horizontal angle of a target point with respect to the 0 degree azimuth are measured by the Omni. The X and Y (horizontal position), and Z (elevation) coordinates of the target point are internally calculated by the Omni using these measurements and simple trigonometry. Data have been geometrically transformed

in each individual site for coordinate systems with an ordinate (X-axis) positive onshore and as shore-perpendicular as possible. This choice forces the abscissa (Y-axis) to be positive to the north and nearly parallel with the shoreline. Surveys were performed with temporary bench marks which were later tied in to permanent bench marks, usually of the U.S. Coast and Geodetic Survey or the Oregon Department of Transportation. Therefore, the elevation of a particular survey point is fixed relative to a datum, NGVD 1929, but the horizontal position is arbitrary. Usually one of the temporary bench marks was assigned the horizontal position (0,0) and the rest of the points for a particular site are referenced to this, again with the positive X and Y directions as given above.

The studies reported are concentrated on the littoral cells of the northern half of the coast. Table A.2 lists the 23 sites by name and classifies them by littoral cell, whether they are backed by dunes (D), sea cliffs (C), or bluffs (B), and whether or not there are shore stabilization structures, revetments (R), seawalls (SW), or no structure (NA). The table also gives the median grain size, D_{50}, in millimeters for most of the sites, determined from standard sieve analyses of sand samples obtained during the surveys. An asterisk before a site name means that the elevations of this site are not referenced to NGVD. This occurred either due to a lack of confidence in the permanent bench mark near the site, or due to a lack of a permanent bench mark within a few miles of the site.

A.3 Site Descriptions

The following sections give simple physical descriptions of each of the aforementioned 23 sites reported on in this study. The extensive beach profile data base, given in Appendix A of Ruggiero (1995), is also described on a site by site basis. All descriptions of particular beach profile measurements refer to this report.

Table A.2. Study sites

#	Site Name	Littoral Cell	Type	D_{50} mm	Structure
1	Sport Haven Beach	Brookings	B		N/A
2	Driftwood Shores	Umpqua (Siuslaw River)	D	.21	R
3	San Marine	Yachats	B	.22	R
4	C&L Ranch	Newport	B	.20	R
5	Pacific Shores	Newport	C	.20	R
6	South Beach	Newport	D	.26	N/A
7	Nye Beach	Newport	C	.29	N/A
8	Beverly Beach	Beverly Beach	C	.27	N/A
9	Pacific Palisades	Lincoln City	C	.31	R
10	Gleneden Beach	Lincoln City	C	.45	R
11	Pacific Sands Motel	Nestucca	D	.33	SW
12	Nestucca Spit	Nestucca	D	.44	N/A
13	Sand Lake	Sand Lake	D	.32	N/A
14	*Camp Merriweather	Sand Lake	C	.32	N/A
15	*Camp Clark	Sand Lake	C	.31	N/A
16	Oceanside	Netarts	B	.31	N/A
17	*Nedonna Beach	Rockaway	D	.31	N/A
18	Manzanita S.	Rockaway	D	.33	N/A
19	Manzanita N.	Rockaway	D	.32	N/A
20	*Arcata St. Park	Cannon Beach	C	.25	SW
21	Seaside	Clatsop Plains	D	.22	SW
22	Del Ray Wayside	Clatsop Plains	D	.25	N/A
23	Columbia Beach	Clatsop Plains	D	.29	N/A

A.3.1 Brookings

Sport Haven Beach in Brookings is located just south of the southern jetty protecting the entrance to the Chetco River. The area studied is seaward of a moderately developed port district which includes a R.V. park, a marina and a Coast Guard station. The foreshore is particularly steep and is composed of cobbles and coarse sand, for this reason no D_{50} is given for this site in Table A.2. The developed area backing the beach was previously a dune area before riverine fill material was used to raise the elevation of the RV park and its access road. This beach experienced dramatic erosion during December 1994, at which time the road fronting the R.V. park was partially destroyed, (Komar *et al.*, 1995).

Sport Haven Beach was surveyed just once, 2 February 1995, shortly after the area had experienced the aforementioned erosion. Transect 1 in Appendix A of Ruggiero (1995), a profile view, shows a "natural" portion of this beach, a steep slope backed by a relatively short dune, a 5 meter dune crest above mean sea level, with a low lying area further landward which is finally backed by a higher fill area. Transects 2 through 5 front the more developed portions of this site. The cross-shore coordinate (X=0) corresponds with the center line of the access road for the RV park. Transects 3 and 4 show the large scarp that developed during the erosion event and reveals the extent of the road damage.

A.3.2 Driftwood Shores

A dune backed beach located at Heceda Beach just north of Florence. A low rubble mound revetment measuring approximately 30 m backs this site. For full site description see Hearon (1995).

A.3.3 San Marine

A bluff backed beach between Yachats and Waldport. The bluff line is very irregular, containing several indentations and moderately protruding areas along a lengthy front. There is a rubble mound revetment at this site that measures approximately 150 m in length. For full site description see Hearon (1995).

A.3.4 C&L Ranch

C&L Ranch is located midway between Lost Creek State Park and Ona Beach State Park. There is a 25 m long rubble mound revetment that protects and stabilizes the backing bluff of C&L Ranch. For full site description see Hearon (1995).

A.3.5 Pacific Shores

A sea cliff backed beach approximately three miles south of the Yaquina Bay jetties. Two rubble mound revetments, one 20 m and the other 140 m with a 15 m gap between, front the sea cliff. For full site description see Hearon (1995).

A.3.6 South Beach

This study site is just south of the southern Yaquina Bay jetty in Newport. This is an area that accreted due to the construction of the jetties and is characterized by large dunes and a wide dissipative beach. There is a proposal to develop this site. This site was surveyed twice, with winter and summer profiles both taken in 1995. A single profile line was sufficient at this site due to the lack of three dimensionality in the foreshore. The profiles reveal little change in the

foreshore between summer and winter. The beach is backed by an extensive dune network which crests at approximately 8 to 9 meters above NGVD 29, followed by a low lying hummocky area and finally another higher crest further landward.

A.3.7 Nye Beach

This study site is just north of the parking area for Nye Beach in Newport. The site extends from the natural cliff backed portion of the beach towards the north to include portions of the historical "Jump Off Joe" landslide. The beach is relatively flat and backed by large sea cliffs. The beach face junction, the intersection of the sandy beach and the steeper sea cliff or bluff, is at a lower elevation in front of the landslide than on the adjacent beach, thus the landslide experiences wave attack more frequently. Wave runup measurements have been obtained at this site as part of the sea cliff erosion study. The cliff in the southern portion of the site consists of loosely consolidated sandstone and is heavily vegetated. This suggests that it is relatively stable. The bluff fronting the landslide is both mudstone and sandstone with no vegetation due to the movement of the slide itself and because of erosion resulting from waves frequently impacting the base of the bluff.

This site has been occupied 10 times from September 1993 to May 1996, with 31 profiles representing both winter and summer conditions. The landslide area begins approximately at the longshore coordinate, Y = 65 meters, which can be located on any of the plan view diagrams for Nye Beach in Appendix A of Ruggiero (1995). A close look at the profiles reveals a natural seasonal variability in the amount of sand on the beach face. The winter profile has upwards of 60-70 cm less sand than the summer profile. This can be seen in Figure A.1 in which transects 1 from four surveys, 3 September 1993, 22 February 1994, 21 July 1994, and 24 January 1995 have been overlaid. Figure A.2 shows 3 additional surveys at this same cross-shore transect from 24 January 1995, 29 June 1995 and 11 October

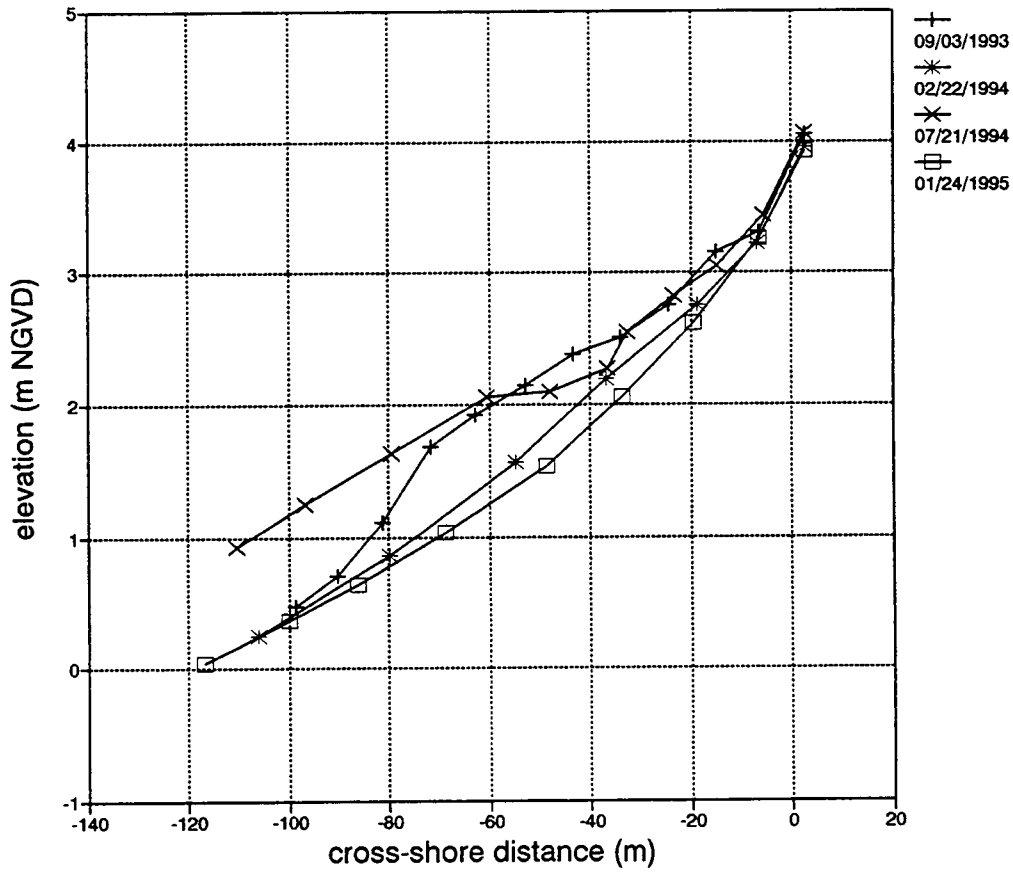

Figure A.1. Summer vs winter beach profile comparison, Nye Beach, Oregon.

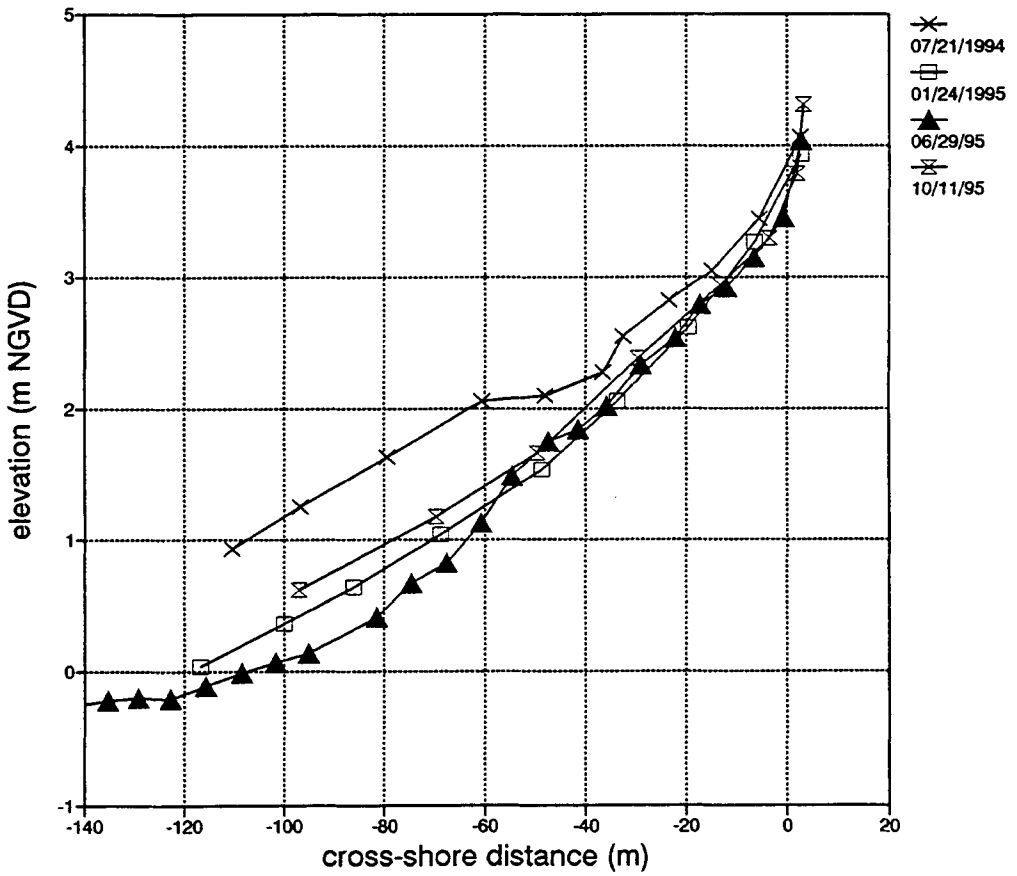

Figure A.2. Lack of summer accretion, Nye Beach, Oregon.

1995. Interestingly, by June 1995 the beach had not yet fully recovered from the previous winter, and even by October 1995 sediment had not fully returned to form the summer upper profile, suggesting that the winter of 1994/1995 transported sediment far enough seaward to prohibit the natural accretionary cycle of the beach.

A.3.8 Beverly Beach

This study site is just to the north of Beverly Beach State Park, and south of Otter Rock. The extremely flat beach is backed by very high cliffs. Of all the littoral cells on the Oregon coast, this cell is one of the most deficient in total sand volume. Therefore it has the least ability to form a beach which serves as a buffer between the waves and the sea cliff (Komar and Shih, 1993). Beverly Beach also has a relatively low beach face junction, on average 4.02 m, which also contributes to the substantially greater susceptibility to wave attack as compared with other locations on the Oregon coast. For this reason, runup measurements have been performed at this site. The cliffs are made of resistant mudstone, and have little vegetation.

Winter and summer profiles have been collected at this site for both 1994 and 1995. Again, the trend is more sand on the profile during the summer. Transect 3 from the 13 July 1995 (Ruggiero, 1995), survey shows the classic dissipative summer profile found on many Oregon beaches. From seaward moving landward, the profile is characterized by a wide, flat, low-tide terrace followed by a series of well developed berms separated by a fairly steep slope. The upper profile has some ephemeral bumps probably caused by eolian processes, as waves do not reach this high in the summer months, and the profile is backed by a steep sea cliff. The winter profiles at this site often approach a planar beach.

A.3.9 Pacific Palisades

A sea cliff backed beach north of Fogarty Creek State Park, just south of Lincoln Beach. A rubble mound revetment follows the curve in the cliff for approximately 300 m. For full site description see Hearon (1995).

A.3.10 Gleneden Beach

A sea cliff backed beach with a revetment just to the north of Gleneden Beach Wayside State Park. A 40 m long rubble mound revetment fronts the sea cliff. For full site description see Hearon (1995).

A.3.11 Pacific Sands Motel

A dune backed beach with a seawall, located near the Neskowin Beach Wayside State Park. A 70 m timber seawall fronts the Pacific Sands Motel. For full site description see Hearon (1995).

A.3.12 Nestucca Spit

The study site is just seaward of the parking lot in Bob Straub State Park which is within Pacific City near the mouth of the Little Nestucca River. There are large, well developed, and heavily vegetated dunes. This site is located within a cell that has an abundance of sediment. Less than a mile to the north is the area of Pacific City where a large area of foredunes have been regraded and planted with beach grass. Unfortunately, a winter profile has not been obtained for this site, but the summer profiles demonstrate the amount of protection the dunes give the backshore with crests reaching up to 14 m. The profiles show a fairly steep

foreshore backed by a pronounced berm and then a smoothly sloping beach reaching the dunes.

A.3.13 Sand Lake

The study site is a several kilometers to the south of Cape Lookout and is within the ATV (All Terrain Vehicle) recreation area. The area is abundant with sand and large dunes. This site was chosen for this study because Bascom performed bathymetric surveys here in 1946, (Komar, 1977; Carpenter, 1995). Only a single summer survey was performed at this site, revealing a well defined berm and extremely large dunes with crest heights on the order of 15 m.

A.3.14 Camp Merriweather

Another Bascom site, this beach fronting a Boy Scout camp is between Sand Lake and Cape Lookout. The beach, backed by a large bluff, is quite remote. Only a single summer survey is available. Unfortunately the elevations of this site have not been tied into a known datum as there is no permanent bench mark within the vicinity. The profiles reveal a convex backshore fronted by a fairly planar beach and a flat low tide terrace.

A.3.15 Camp Clark

The third Bascom site within close proximity, Camp Clark is just south of Cape Lookout. The bluff gets taller as the beach meets the Cape. Again, elevations are not secure for this site.

A.3.16 Oceanside

This bluff backed beach fronts the wayside on the northernmost edge of the town of Oceanside. There is a small headland at the northern edge of this beach, followed by Cape Mears further to the north. This beach is backed by a natural cobble rampart which is seasonally covered and uncovered. Two summer surveys are available for this site. The remnants of a rip current embayment were observed on 28 July 1994, lowering portions of the beach face upwards of a meter. This feature can be seen in the individual profiles but is more striking when plotted as a three dimensional surface or contour plot, also given in Appendix A of Ruggiero (1995). The beach face junction at Oceanside is approximately 4.5 m and the loosely consolidated bluff is heavily vegetated.

A.3.17 Nedonna Beach

The study site is just to the south of the south jetty on the mouth of the Nehalem River. The beach is backed by relatively low-lying dunes. The community here has previously developed a dune management plan. Winter and summer profiles were obtained in 1995. The permanent bench mark used to tie this site in to NGVD was suspect, so there is little confidence that the elevations are correct.

A.3.18 Manzanita South

This study site is south of the seaward end of Oceancrest Lane (what used to be 7th street) in the southern portion of Manzanita. This site has an extremely wide beach at low tide and is backed by large dunes. The dunes at this site reach crest elevations of up to 14 m. Comparing transect 1 from the 10 August 1994, survey with transect 1 from the 7 February 1995, survey demonstrates the classic difference

between summer and winter profiles on the Oregon coast, Figure A.3. The summer profile is relatively bumpy with ephemeral dune features, and a slight berm is evident. The winter waves smooth the entire profile into a classic concave form. The home owner at the end of Oceancrest Lane attempted dune regrading, as the property was being inundated with sand (apparently a common occurrence in this area). Cross-section 1 and transect 3 from the 10 July 1994 survey (Ruggiero, 1995) quantifies how the beach has been modified. This regrading leaves the property much more susceptible to wave attack than its neighbors, as the highest sand elevation is some 3 to 4 meters below the dune crest to either side.

A.3.19 Manzanita North

This study site is near the end of Beulah Reed Road just to the south of Mt. Neahkanie in the northern portion of Manzanita. The backing dunes are fairly stable with dense vegetation near the dune crest. Similar to the Oceanside site, a natural cobble rampart lies at the base of the dunes due to the rocky headland just to the north. The cobbles serve to protect the dune from wave undercutting and are seasonally covered and uncovered. Two sites were chosen in Manzanita as this community has been in the process of developing a dune management plan. The survey's reveal dunes with crests from 7 to 10 m, and the typical variations between summer and winter profiles.

A.3.20 Arcata State Park

This site is just south of the city of Cannon Beach and is characterized by high sea cliffs. The beach is very flat with an exceptionally wide summer profile. The permanent bench mark near this site was suspect, so the reported elevations may not be correct.

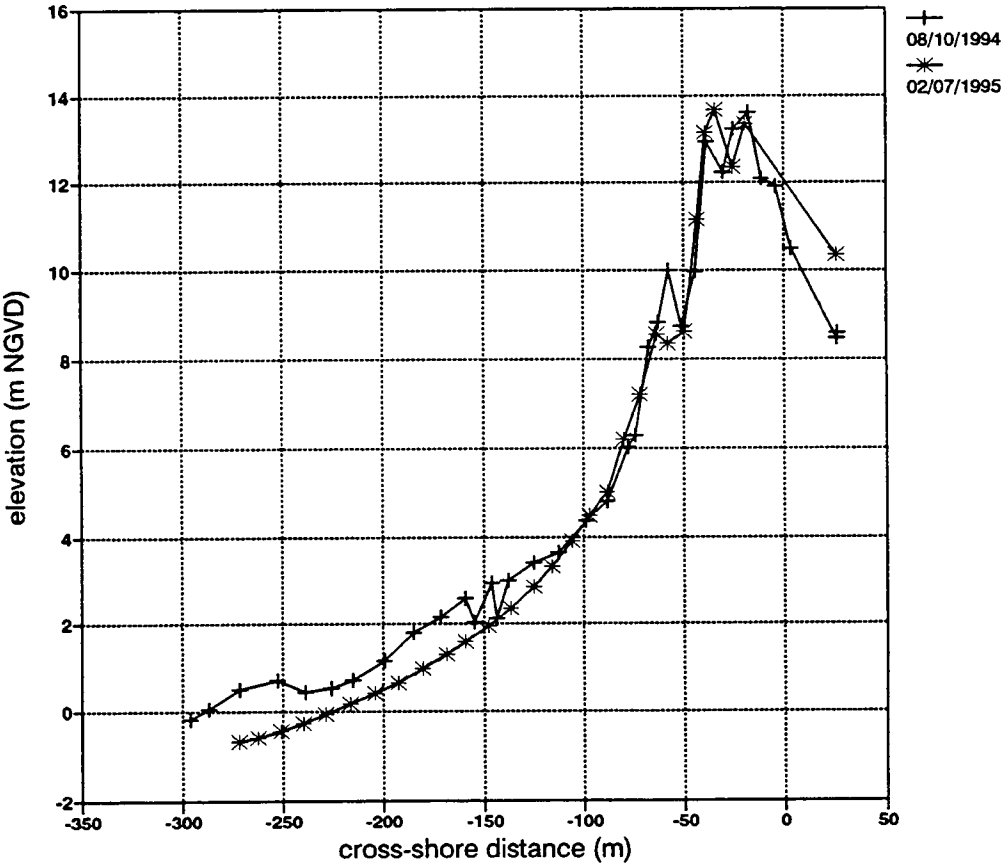

Figure A.3. Summer vs winter beach profile comparison, Manzanita, Oregon.

A.3.21 Seaside

The study site is the beach and backing dunes which front the "Prom" in the heavily developed Seaside community. Transects were performed in front of 8th and 10th avenues as well as further north in the "natural" area between the north end of the prom and the riprap revetment which protects the banks of the Necanicum River. The community has previously developed a dune management plan. A single summer survey is available for this site with transect 1 fronting 8th Avenue, transect 2 fronting 10th Avenue, and transect 3 being a "natural" section of beach. The dunes are relatively low, cresting at less than 8 m, and the beach just seaward of the dunes is slightly convex. Transect 3 reveals the steep scarp fronting the dunes to the north.

A.3.22 Del Ray Wayside

This site is north of the town of Gearhart between two developments, Highlands to the south and Surf Pines to the north. A single summer profile was obtained at this site. Currently there are large well developed and heavily vegetated dunes here which crest at approximately 12 m.

A.3.23 Columbia Beach - Clatsop Spit

This Bascom site is located at the end of Delaurah Beach Road which is south of Fort Stevens and just to the north of the military reservation. The beach is backed with large well vegetated dunes, however vehicular traffic is heavy at this site with tire tracks locally lowering portions of the beach/dune interface. The crests of the dunes range from approximately 11 to 13 m.

APPENDIX B

Integral 1, equation (4.16)

$$b_1\{\frac{(Cos[b_5b_3X^{1/2}](-2Cos[b_4b_3]+b_5^2b_3^2XCos[b_4b_3]-b_5b_3X^{1/2}Sin[b_4b_3]))}{3X^{3/2}}$$
$$+\frac{((b_5b_3X^{1/2}Cos[b_4b_3]-2Sin[b_4b_3]+b_5^2b_3^2XSin[b_4b_3])Sin[b_5b_3X^{1/2}])}{3X^{3/2}}$$
$$+\frac{(b_5^3b_3^3(-(CosIntegral[b_5b_3X^{1/2}]Sin[b_4b_3])+Cos[b_4b_3]SinIntegral[b_5b_3X^{1/2}]))}{3}\}$$

Integral 2, equation (4.16)

$$b_2\{-\frac{(4Cos[b_4b_3]Cos[b_5b_3X^{1/2}])}{X^{1/4}}$$
$$+b_5^{1/2}b_3^{1/2}(32\pi)^{1/2}(-(Cos[b_4b_3]FresnelS[b_5^{1/2}b_31/2(2\pi)^{1/2}X^{1/4}])$$
$$Sin[b_4b_3]FresnelC[b_5^{1/2}b_3^{1/2}(2\pi)^{1/2}X^{1/4}])$$
$$-\frac{4Sin[b_4b_3]Sin[b_5b_3X^{1/2}]}{X^{1/4}}\}$$

where

$$b_1 = \frac{3A\gamma^{1/2}}{2}$$

$$b_2 = \frac{-3A^{1/2}\kappa\gamma^{1/2}}{4}$$

$$b_3 = \gamma^{1/2}$$

$$b_4 = \frac{2\omega x_{wall}^{1/2}}{s}$$

$$b_5 = \frac{2\omega}{s}$$

APPENDIX C

α	dimensional constant (Chap 2), slope of setup (Chap. 4)
β	foreshore beach slope
γ	non-dimensional ratio of depth at breaker line to deep water wave length
ϵ_r	phase between incident and reflected wave
ϵ_r'	cross-shore derivative of phase between incident and reflected wave
ϵ_{rg}	geometric component of phase
ϵ_{rw}	wave component of phase
ϵ_s	swash surf similarity parameter
ϵ_s^c	critical swash similarity parameter
ϵ_s^{c*}	dimensional constant
ζ	measured tide elevation
ζ_o	mean sea level
ζ_p	predicted tide
ζ_r	non-tidal residual
$\bar{\eta}$	wave setup
η	free surface elevation
θ	wave angle
θ_i	incident wave angle
θ_r	reflected wave angle
κ	breaker index
$\lambda_{1,2}$	exponents in solution to Euler equation
μ_e	eddy viscosity
ξ_c	critical similarity parameter
ξ_o	Iribarren number
π	pi
ρ	mass density of water
$\sigma(x)$	spatially dependent phase term
σ^2	variance of runup elevation time-series
τ_b	bottom stress
τ_{by}	longshore component of bottom stress
Φ	total velocity potential
ϕ_i	incident velocity potential
ϕ_r	reflect velocity potential
ψ_1	boundary condition coefficient
ψ_2	boundary condition coefficient
ψ_3	boundary condition coefficient
ω	wave angular frequency
A	constant proportional to reflected wave energy flux
$A_{1,2}$	integration constants
a_i	incident wave amplitude

a_r reflected wave amplitude
a_s vertical swash amplitude
b_1 dimensionless constant
b_2 dimensionless constant
b_3 dimensionless constant
b_4 dimensionless constant
b_5 dimensionless constant
c dimensionless constant
C wave celerity
c_1 constant of integration
c_2 orbital velocity coefficient
c_3 non-dimensional coefficient
c_4 non-dimensional coefficient
c_5 non-dimensional coefficient
c_6 non-dimensional coefficient
c_7 non-dimensional coefficient
C_B non-dimensional break point celerity
C_f dimensionless bottom stress coefficient
C_{gr} reflected wave group velocity
d total water depth
E total water elevation
E_{ii} incident wave energy
E_{ir} cross wave energy
E_j beach-face junction elevation
E_{rr} reflected wave energy
f wave frequency (Chap. 2 and 3), spatial oscillation term (Chap. 4)
F_i incident wave energy flux
F_r reflected wave energy flux
g acceleration due to gravity
$g(z)$ depth dependent coefficient
h still water depth
H_s deep-water significant wave height
I sediment transport rate
I_{tot} total sediment transport
k wave number
K_r reflection coefficient
k_x cross-shore component of wave number
k_y longshore component of wave number
L runup coherence length scale
L_o deep water wave length
m planar beach slope
n ratio between group velocity and celerity
N dimensionless constant
P lateral mixing coefficient
Q_{tot} total volumetric flow rate

R	wave runup
$R_{2\%}$	two-percent exceedence elevation of runup maxima
R_{max}	maximum vertical runup
R_s	significant vertical runup excursion
R_s^{ss}	sea swell significant runup elevation
R_v	vertical runup excursion
s	total slope
S	swash
s_{MH83}	total depth slope of no wall solution
S_{xx}	cross-shore component of onshore radiation stress
S_{xy}	longshore component of onshore radiation stress
T	wave period
u	total depth averaged velocity vector
u_x	cross-shore component of wave orbital velocity
u_y	longshore component of wave orbital velocity
v	mean longshore current
V_h	homogeneous solution to Euler equation
x_o	offshore location

Subscripts

$(\,)_B$	values calculated at breaker line
$(\,)_{B\ eff}$	values calculated at the effective breaker line
$(\,)_{B\ no\ wall}$	values calculated at no wall breaker line
$(\,)_{wall}$	values calculated at location of seawall

Superscripts

$(\,)^*$	dimensional quantity